Response to comments by Anonymous Referee #1

Thank you very much for your review.

In this manuscript, Fujiwara and co-authors present observational data from two lidars in Japan indicating the presence of aerosol particles from the Asian Tropopause Aerosol Layer (ATAL) over the stations just above the tropopause in August and September 2018. The origin of these particles from inside the Asian monsoon anticyclone is indicated by trajectory analyses as well as CAMS reanalysis data of CO and MLS satellite observations of water vapor. Further, the authors exclude the influence of volcanic eruptions and forest fires by inspecting the global condition of aerosols in the UTLS through space borne limb-scatter (OMPS LP) and lidar (CALIOP) observations.

A central point of this work is the depolarization of the observed particles of around 5%. This indicates that at least a part of the aerosols was non-spherical (i.e. not liquid) but solid, however, not as strongly depolarizing as cirrus particles.

In general, the manuscript is well written and logically organised with clear figures. It presents a novel dataset on aerosols from the ATAL embedded in the interpretation of the general atmospheric situation. To my knowledge it is also the first one of an eastward shedding event over Japan and explicitly including the particle depolarization. Therefore, I recommend publication in ACP after taking into account the comments below.

Thank you very much for your evaluation.

Specific comments

L97-L110, Lidar error estimation:
In L98 the BSR uncertainties are stated as 2-3%, but in L106, additional BSR errors are discussed. I would suggest to clearly state first all error terms for the BSR (random and possible systematic ones) and then include those in the discussion on PDR.

This sentence has been revised as follows:
"The BSR uncertainties were estimated as follows. The random component was estimated from the photon counts of the backscatter signals at 532 nm after temporal and vertical averaging by assuming Poisson statistics. Other sources of BSR uncertainties (biases) were estimated by assuming the uncertainty of the normalization value of BSR with 8.5×10^{-3} (Russell et al., 1979, 1982) and that of the extinction-to-backscatter ratio with 30 sr (Jäger and Hofmann, 1991; Jäger et al., 1995). The total uncertainty of BSR were then estimated to be 2–3 % typically around the tropopause."

References:

Jäger, H., and Hofmann, D.: Midlatitude lidar backscatter to mass, area, and extinction conversion model based on in situ aerosol measurements from 1980 to 1987, Appl. Opt., 30(1), 127, https://doi.org/10.1364/ao.30.000127, 1991.

Jäger, H., Deshler, T., and Hofmann, D. J.: Midlatitude lidar backscatter conversions based on balloonborne aerosol measurements, Geophys. Res. Lett., 22(13), 1729–1732, https://doi.org/10.1029/95GL01521, 1995.

Russell, P. B., Swissler, T. J., and McCormick, M. P.: Methodology for error analysis and simulation of lidar aerosol measurements, Appl. Opt., 18(22), 3783, https://doi.org/10.1364/ao.18.003783, 1979.

Russell, P. B., Morley, B. M., Livingston, J. M., Grams, G. W., and Patterson, E. M.: Orbiting lidar simulations 1: Aerosol and cloud measurements by an independent-wavelength technique, Appl. Opt. 21(9), 1541, https://doi.org/10.1364/ao.21.001541, 1982.

L135, 'in this data product, clouds and Polar Stratospheric Clouds (PSCs) have been removed':
Please add the information, how cirrus clouds have been removed.

The algorithms to classify the CALIOP backscatter signals into various types of clouds and aerosols, presented by Young and Vaughan (2009), are quite complicated, but in short, they are based on the particulate extinction-to-backscatter (lidar) ratio and the multiple-scattering factor profile. At the end of the sentence, we have added:
"based on the information of particulate extinction-to-backscatter (lidar) ratio and the multiple-scattering factor profile". Also, we will add more recent publication by Kim et al. (2018).

Reference:
Kim, M.-H., Omar, A. H., Tackett, J. L., Vaughan, M. A., Winker, D. M., Trepte, C. R., Hu, Y., Liu, Z., Poole, L. R., Pitts, M. C., Kar, J., and Magill, B. E.: The CALIPSO version 4 automated aerosol classification and lidar ratio selection algorithm, Atmos. Meas. Tech., 11, 6107–6135, https://doi.org/10.5194/amt-11-6107-2018, 2018.

L145:
Please discuss also the event around Aug, 9th, over Tsukuba since there has been a clear eastward shedding as can be seen in Figs. 7 and 8. It is not clear to me if the particles were above or below the tropopause since there is quite a strong change in tropopause height visible by the red dots in Fig. 1.

We have added the following sentence just after describing the 18–26 August case:
"We also observe another strong event around 9 August at 15–17 km, although missing observations before and after this date prevent from characterizing the temporal scale of the event; furthermore, the tropopause height was highly variable around this date and was located at 17 km on that date, situating the aerosol enhanced layer temporarily in the troposphere."

We have also added this information to Section 3.2 in the discussion for Figure 7 as:
". . . in the fact that only the 20–25 August event was relatively well observed, with the 5–15 August event being captured only on 9 August."

L181, 'PDR values of 1%–3%':
The difference between the PDR values between Tsukuba, showing clearly enhanced signals, and Fukuoka is tentatively explained by the different measurement periods. In case of Tsukuba, quasi no event has been shown with values of PDR less than 2 (see Fig. 2), while there are many above Fukuoka. Please discuss whether this might hint to some unidentified bias in one of the instruments. It would e.g. be informative to present some observations before June or after September where both instruments show consistently low/high values of PDR.

The reason why PDR values less than 2% were rare in the plot for Tsukuba (Fig. 2) is that we do not plot the data with "relative" uncertainty of PDR larger than 30%; this treatment resulted in removing data points with BSR values lower than ~1.05 where background spherical sulphate particles (with PDR values of <2%) were presumably predominant. We have noted this treatment for Tsukuba data in the revised manuscript.

Figures R1-1 and R1-2 below show the lidar profiles at Tsukuba on some days in May 2018 and in October 2018, respectively. These figures show that BSR in these months did not show enhancements of >1.1 like those found in August and September (Figs. 2c, e). However, we note that TDR slightly increased below 20 km, suggesting a possibility of presence of minute amount of non-spherical particles. The origins of the particles are unknown and a subject of our future study.

Figure R1-3 below shows the lidar profiles at Fukuoka on some days in May-June 2018 and in October-November 2018. Again, we did not detect depolarization enhanced layers (with depolarization ratio higher than 2%) in these months.

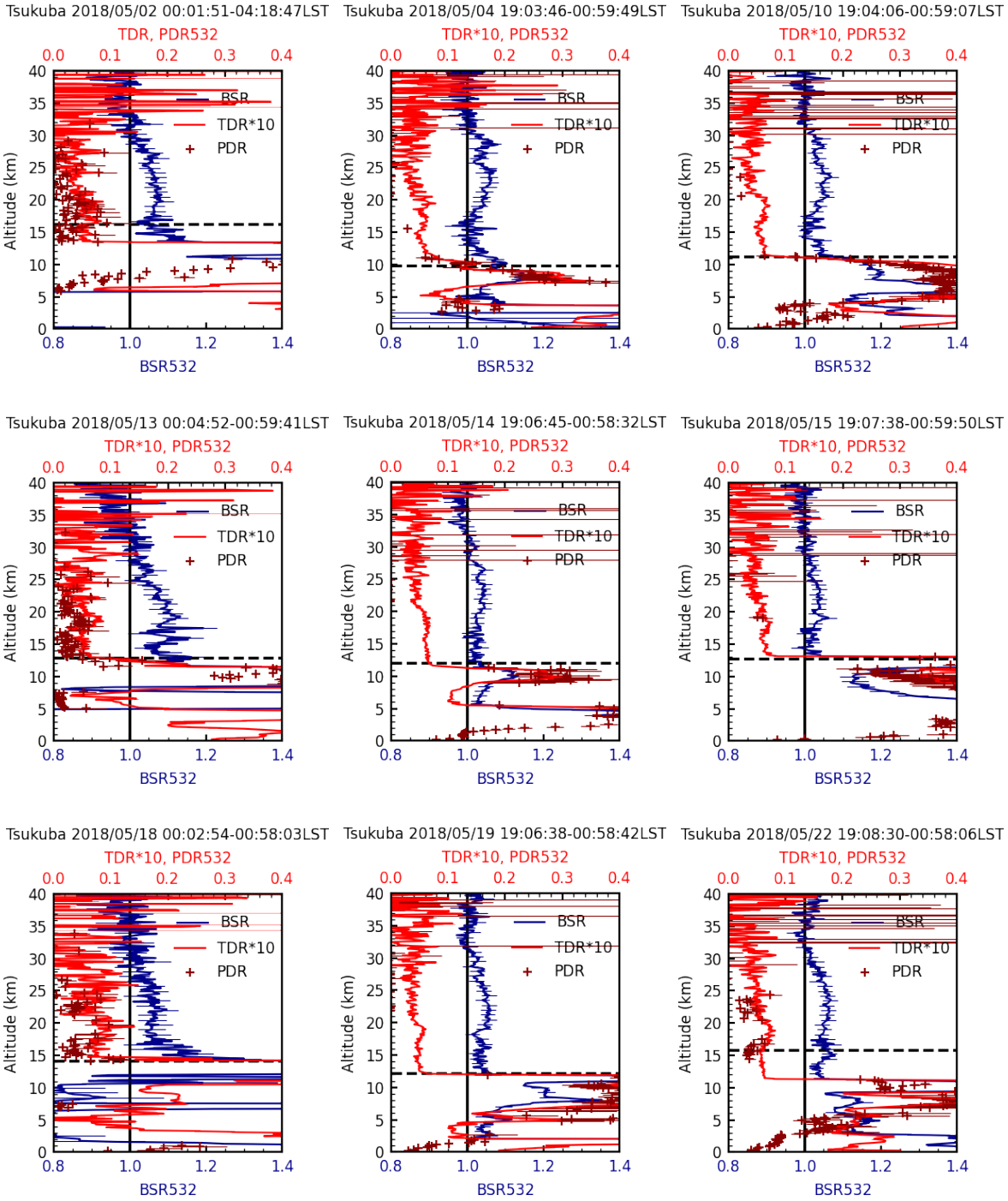
Tsukuba 2018/05/02 00:01:51-04:18:47LST
Tsukuba 2018/05/04 19:03:46-00:59:49LST
Tsukuba 2018/05/10 19:04:06-00:59:07LST
Tsukuba 2018/05/13 00:04:52-00:59:41LST
Tsukuba 2018/05/14 19:06:45-00:58:32LST
Tsukuba 2018/05/15 19:07:38-00:59:50LST
Tsukuba 2018/05/18 00:02:54-00:58:03LST
Tsukuba 2018/05/19 19:06:38-00:58:42LST
Tsukuba 2018/05/22 19:08:30-00:58:06LST
TDR, PDR532
TDR*10, PDR532
BSR
TDR*10
PDR
Altitude (km)
BSR532

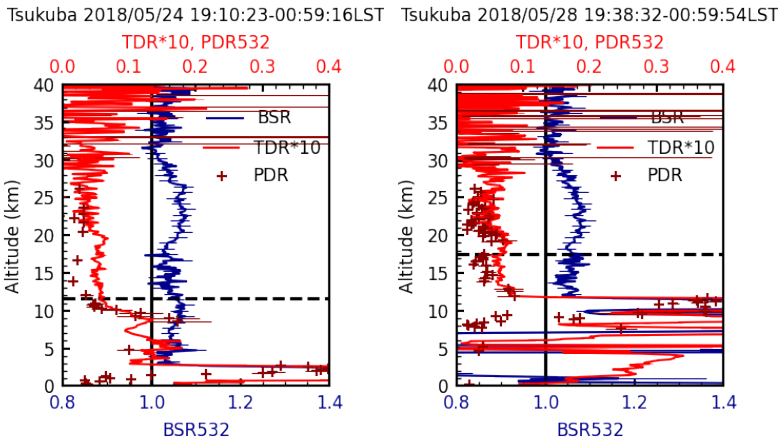

Figure R1-1. Lidar profiles taken at Tsukuba on May 2, 4, 10, 13, 14, 15, 18, 19, 22, 24, and 28, 2018. The horizontal dashed line in each panel indicates the location of the first lapse rate tropopause. It is noted that for "TDR*10" = 0.05 means TDR = 0.05/10 = 0.005, i.e., 0.5%TDR. This is close to the depolarization ratio value, 0.366% for air molecules.

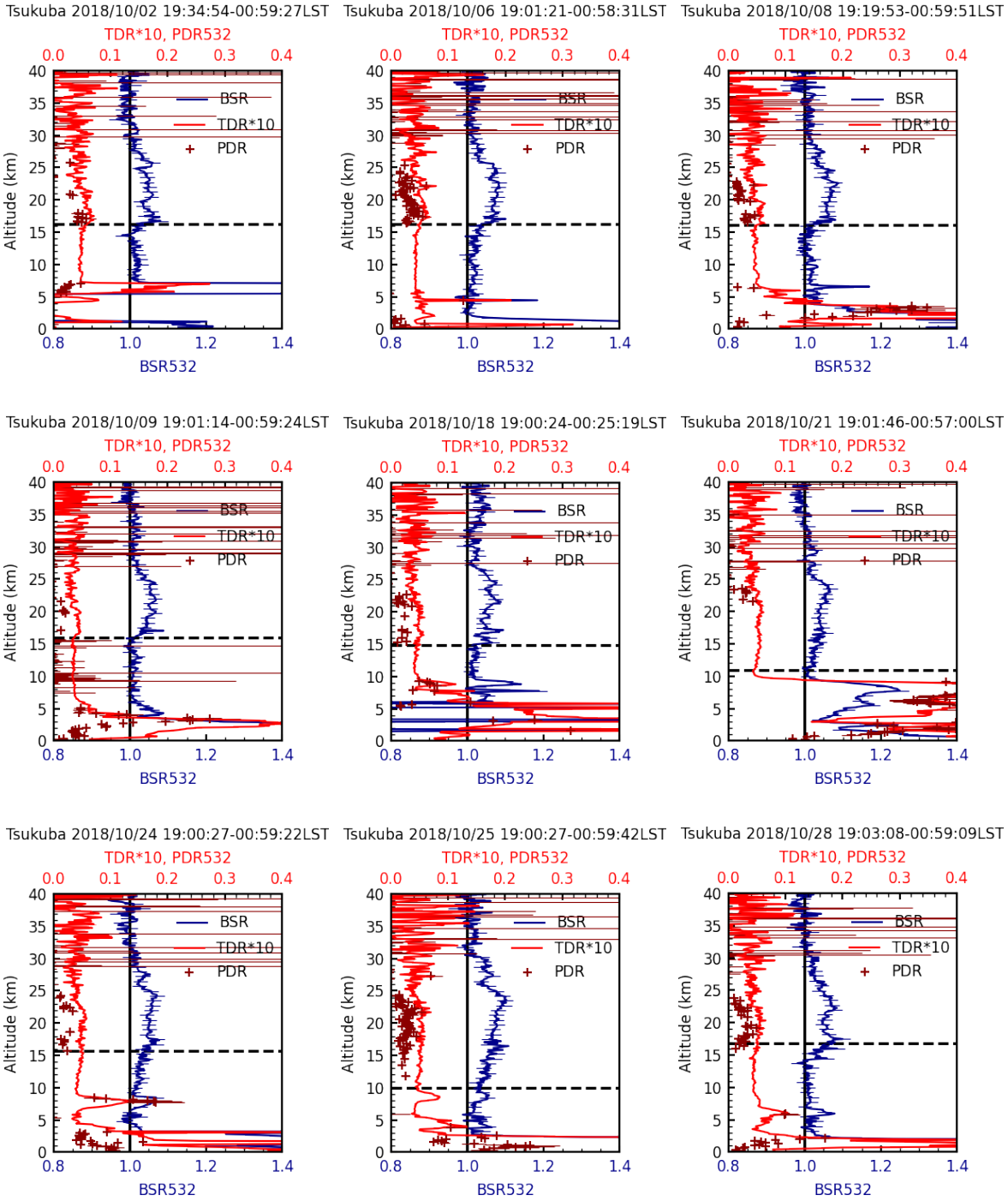
Tsukuba 2018/10/02 19:34:54-00:59:27LST
Tsukuba 2018/10/06 19:01:21-00:58:31LST
Tsukuba 2018/10/08 19:19:53-00:59:51LST
Tsukuba 2018/10/09 19:01:14-00:59:24LST
Tsukuba 2018/10/18 19:00:24-00:25:19LST
Tsukuba 2018/10/21 19:01:46-00:57:00LST
Tsukuba 2018/10/24 19:00:27-00:59:22LST
Tsukuba 2018/10/25 19:00:27-00:59:42LST
Tsukuba 2018/10/28 19:03:08-00:59:09LST
TDR*10, PDR532
BSR
TDR*10
PDR
Altitude (km)
BSR532

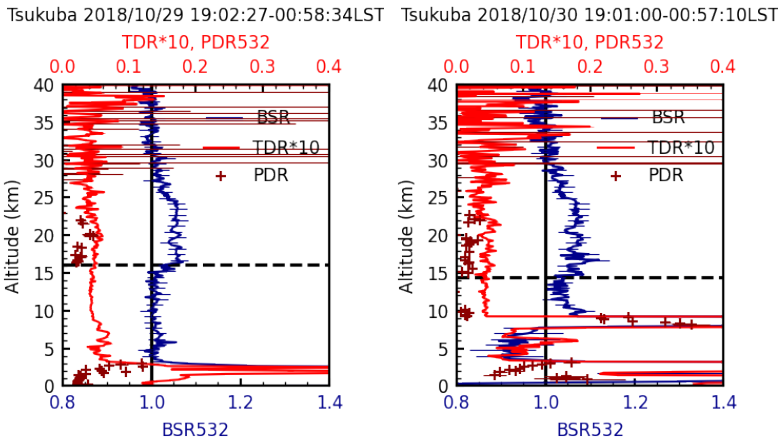

Figure R1-2. As for Figure R1-1, but for October 2, 6, 8, 9, 18, 21, 24, 25, 28, 29, and 30, 2018.

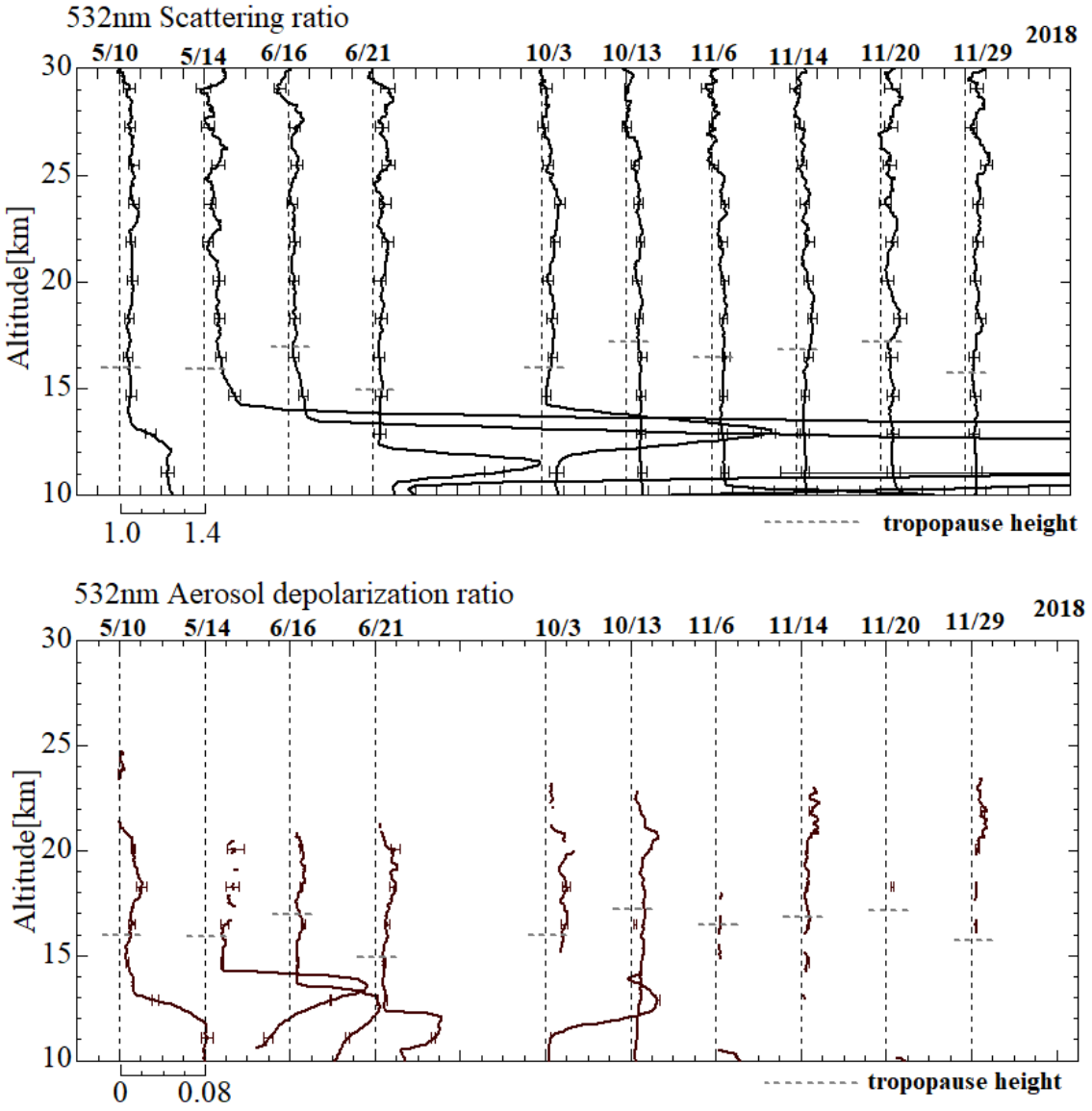

Figure R1-3. Lidar profiles taken at Fukuoka on the days in May-June 2018 and in October-November 2018 when the lidar was operated.

L196, '3.2 Trajectories and airmasses':

From the trajectories shown, it is not clear if they reach altitudes below the tropopause. Could you provide any discussion on this point?

Following the comments by other reviewers, the colored geopotential height range of Figures 4 and 5 has been changed (narrowed).

We have revised the original sentence,

"They also indicate that airmasses with enhanced aerosol particles at this height tend to originate in regions within the ASM anticyclone, whereas those without enhanced aerosol particles tend to originate from edge regions surrounding the anticyclone."

as:

"They also indicate that airmasses with enhanced aerosol particles at this height tend to originate in regions within the ASM anticyclone at the altitudes 16.5–18 km, i.e., around or just below the tropopause, whereas those without enhanced aerosol particles tend to originate from edge regions surrounding the anticyclone." (i.e., the underlined part has been added.)

L240:

I would be interested if the CAMS CO data could be supported by MLS measurements of CO. This should be easy by providing a figure similar to Fig. 8 but for MLS CO.

Thank you for this suggestion. Please see Figure R1-4 below. We see that CAMS CO data are roughly ~10 ppbv greater than MLS CO over Japan during August–September 2018, but also that eastward extension signals coming over Japan agree fairly well qualitatively within the differences in spatio-temporal sampling of the two data sets. We have added this note to Section 2.2.

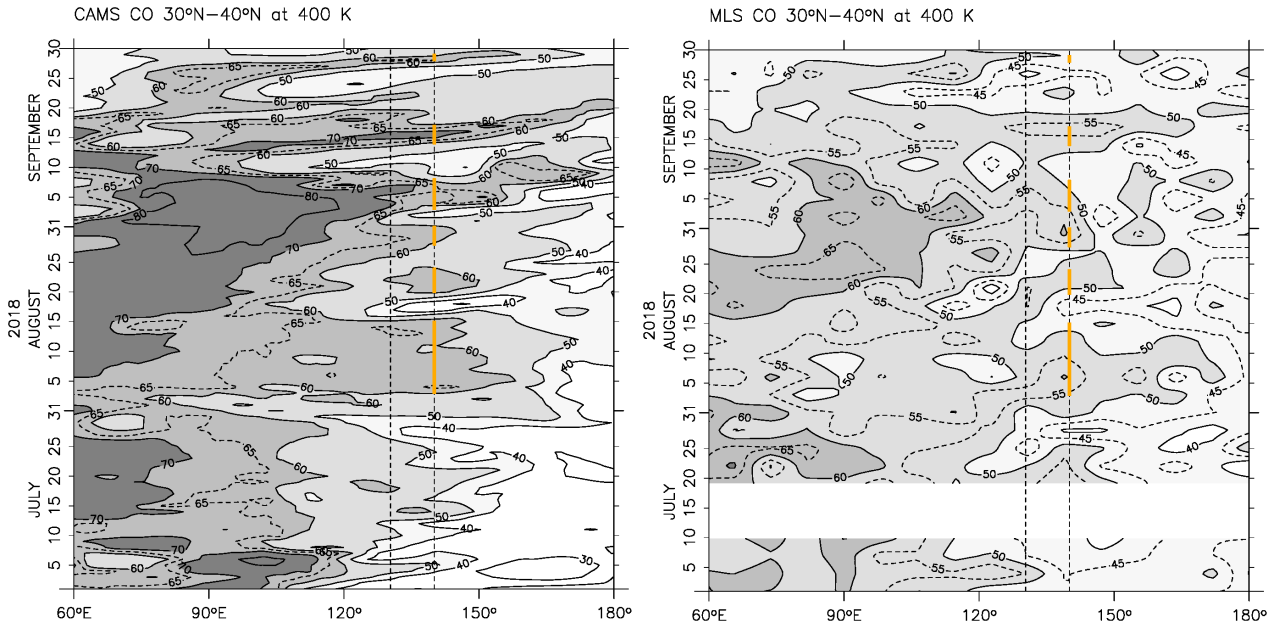

Figure R1-4. (Left) Same as Figure 7 (the revised version following Referee #2's suggestion: Coloured line segments have been added for the periods when CO concentration was ≥~60 ppbv along the longitude of Tsukuba (i.e., 3–15, 20–24, and 28–31 August, and 3–8, 14–17, and 28–29 September)). (Right) Same as left but for MLS CO data. Data for the 30°N–40°N region have been aggregated into 3-day and 8°-longitude bins, each constituting about 10 individual data points. The contours for 45 ppbv and 55 ppbv as well as 65 ppbv are added as dotted lines.

L283:

Is any direct comparison/match of the ground based lidars with the CALIOP lidar possible during the relevant time period?

We have looked at the CALIOP lidar data on 21 August 2018 when the lidar at Tsukuba (36.1°N, 140.1°E) observed the strong signal and when the CALIPSO flew over the region relatively close to Tsukuba: https://www-calipso.larc.nasa.gov/products/lidar/browse_images/show_v4_detail.php?s=production&v=V4-10&browse_date=2018-08-21&orbit_time=03-36-39&page=3&granule_name=CAL_LID_L1-Standard-V4-10.2018-08-21T03-36-39ZD.hdf

As you see from the above link, we do not observe the corresponding signals around the orbital track (31.71°N, 139.38°E) to (37.78°N, 137.66°E) around 15.5–18 km in CALIOP data. Young and Vaughan (2009) noted for the CALIOP measurements, "The usual method of increasing the SNR (signal-to-noise ratio) is to average many profiles. However, along-track inhomogeneities in the atmospheric features, combined with the high speed (typically 7.5 km s^{-1}) of the satellite across these features and the relatively low firing rate of the laser (~20 s^{-1}), lead to situations where it is simply not possible to acquire a sufficient number of profiles before the subsatellite atmosphere changes significantly." Note also that the ground-based lidar data from Tsukuba (Fukuoka) have been averaged for 3 (4) hours in this study. We think that appropriate quality control (e.g., taking only high-quality nighttime measurements) and spatio-temporal averaging for CALIOP data might give us ATAL eastward extension signals over Japan in a Hovmöller diagram like Figures 7 and 8, but this would be a potential future work.

L317:

For ATAL studies, the applied CALIOP filter on cirrus clouds has been a depolarization ratio threshold of 5% (e.g. Vernier et al., 2015): (1) why has a different limit been applied for the present ground based observations? (2) could you discuss which effect the finding of this work indicating 5% depolarization and more for ATAL particles would have on the CALIOP data analysis?

Regarding (1), Vernier et al. (2009) masked ice clouds by using their total depolarization ratio (TDR'), defined by the perpendicular to total (particular plus molecular) backscatter signal, and not by using PDR. In that case, TDR' values would be small if BSR values of cirrus are small. Theoretically, for example, TDR' would be less than 5% if BSR values are smaller than 1.2 for cirrus for the case that the PDR value is 35% (see Figure R1-5 below). In addition, averaging the data for a large grid volume (2º longitude × 1º latitude × 200 m height) could reduce BSR and TDR' values if cirrus clouds are partially present in the volume. Thus, we presume that they removed the data even if it contained some cirrus clouds.

Reference:

Vernier, J. P., Pommereau, J. P., Garnier, A., Pelon, J., Larsen, N., Nielsen, J., Christensen, T., Cairo, F., Thomason, L. W., Leblanc, T., and McDermid, I. S.: Tropical stratospheric aerosol layer from CALIPSO lidar observations, J.

Geophys. Res., 114, https://doi.org/10.1029/2009jd011946, 2009.

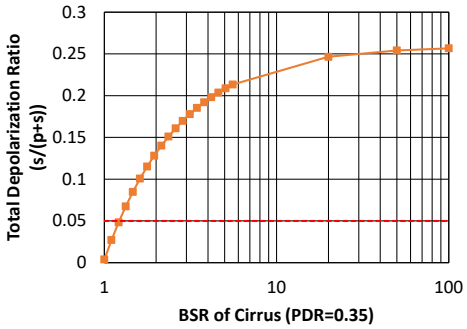

Figure R1-5. A theoretical total depolarization ratio (TDR') curve as a function of BSR for cirrus cloud particles with the PDR value of 35%. The horizontal dotted red line shows the threshold value of TDR' (5%) used in the papers by Vernier et al. (2009, 2015).

Regarding (2), we do not argue that future ATAL studies using CALIOP data should always use smaller threshold values. The choice of the threshold would depend on the purpose of each study. It is also possible that appropriate threshold numbers differ for different regions, e.g., either over the Tibetan Plateau or over Japan, in part because the chemical composition and crystal shape (if they are solid particles) may differ for different regions due to different life stages of the ATAL particles.

L327, 'with an average BSR value of 1.05 being a systematic feature':
Is there any information on the depolarization available from the OHP-lidar?

Unfortunately, the lidar at OHP has no capability of measuring the depolarization.

L337:
One may add the information from Fig. 2 in Wagner et al., 2020a, that the depolarization ratio obtained in the laboratory for solid ammonium nitrate particles was around 9%. Further, in Wagner et al., 2020b, from electron microscope images of ammonium nitrate particles Fig. 2c reveals 'that the crystalline AN particles are of rather compact shape with aspect ratios predominantly in the range from 0.80 to 1.25.'

Thank you very much for the information of these very important and relevant papers. We have modified the relevant part of the text. The revised, whole paragraph will be as follows:
"The PDR values obtained at Tsukuba, i.e., ~5% (3%–10%) suggest that these enhanced particles are solid particles, rather than spherical, liquid H_2SO_4 particles (PDR ~0%) or cirrus ice particles (PDR > 25%–30%). A recent laboratory experiment by Wagner et al. (2020a) showed the PDR values of ~9.5% for solid NH_4NO_3 particles at 488 nm. (Also, Wagner et al. (2020b) showed electron microscope images of solid NH_4NO_3 particles, which are "of rather compact shape with aspect ratios predominantly in the range from 0.80 to 1.25.") Thus, the values obtained with our lidars in Japan might be consistent

with those of solid NH_4NO_3 particles suggested by Höpfner et al. (2019). (Note that Sakai et al. (2010) investigated PDR values of other particle types at 532 nm in laboratory experiments; among these particles, sub-micrometre sea-salt and ammonium sulphate crystals (e.g., Plate 9 (pages 237–239) of Pruppacher and Klett, 1997) were found to have PDR values of ~8% PDR and ~4% PDR, respectively.) Small non-zero PDR values can occur if enhanced liquid H_2SO_4 particles and fresh ash particles from volcanic eruptions are mixed, although satellite data indicate this is less plausible (Sect. 3.3). Lidar measurements at Mauna Loa, Hawaii, indicated no signals from volcanic eruptions during the summer of 2018 (Chouza et al., 2020). Also, at the OHP lidar site in France, no enhancement in the lower stratospheric aerosol abundance was observed during the summer of 2018."

Technical corrections

Figure 4:
The CO isolines for different months cannot be distinguished easily. Perhaps use different line styles.

We have revised this figure as suggested.

L223:
Please add in this sentence the information 'from the CAMS reanalysis data'.

We have added this information.

L224, 'A potential temperature of 400 K corresponds to altitudes of 17.1 km at Tsukuba and 17.3 km at Fukuoka, on average, during July–September 2018':
This information should be provided before, e.g. where the trajectories are discussed.

This information has been moved to the first paragraph of Section 3.2.

L286, 'not have reached':
'have not reached'

Corrected.

L298, '. Rectangular':
'. The rectangular'

Corrected.

L341, ‘France, any enhancement’:
‘France, no enhancement’

Corrected.

References

Vernier, J.-P., Fairlie, T. D., Natarajan, M., Wienhold, F. G., Bian, J., Martinsson, B. G., Crumeyrolle, S., Thomason, L. W., and Bedka, K. M.: Increase in upper tropospheric and lower stratospheric aerosol levels and its potential connection with Asian pollution, Journal of geophysical research. Atmospheres JGR, 120, 1608–1619, https://doi.org/10.1002/2014JD022372, 2015.

Wagner, R., Bertozzi, B., Höpfner, M., Höhler, K., Möhler, O., Saathoff, H., and Leisner, T.: Solid Ammonium Nitrate Aerosols as Efficient Ice Nucleating Particles at Cirrus Temperatures, J. Geophys. Res., 125, e2019JD032248, https://doi.org/10.1029/2019JD032248, 2020a.

Wagner, R., Testa, B., Höpfner, M., Kiselev, A., Möhler, O., Saathoff, H., Ungermann, J., and Leisner, T.: High-resolution optical constants of crystalline ammonium nitrate for infrared remote sensing of the Asian Tropopause Aerosol Layer, Atmos. Meas. Tech. Discuss., https://doi.org/10.5194/amt-2020-262, 2020b.

The two papers by Wagner et al. have been cited in the revised manuscript. The paper by Vernier et al. had already been cited.

Finally, we have also made the following further revisions.

1. Tomohiro Nagai of MRI/JMA, Japan has been added as a coauthor due to his contributions to the lidar observations at Tsukuba.

2. The location of the "box" in Figure 9 (OMPS LP) has been corrected.

3. The colour code for Figure 10 (CALIOP) has been revised.

Response to comments by Referee #2 (Dr. Michelle Santee)

Thank you very much for your review.

Review of "Lower-stratospheric aerosol measurements in eastward shedding vortices over Japan from the Asian summer monsoon anticyclone during the summer of 2018" by Fujiwara et al.

Ground-based lidar measurements obtained at two stations in Japan during July to September 2018 are analyzed to look for signatures of the transport of aerosols from the Asian summer monsoon (ASM). Particle enhancements were observed in the lower stratosphere in August and September; back trajectories and satellite and reanalysis data are used to show that those air masses originated within the ASM anticyclone and were not influenced by volcanic or biomass burning emissions, and thus they likely reflect extension of the Asian Tropopause Aerosol Layer (ATAL) associated with eastward eddy shedding events. The analysis presented is sound, the manuscript is well written and well organized, and the topic is timely and of interest to the ACP readership. Although I do have some substantive issues that I would like to see considered before the paper is accepted for publication, most of my comments are minor wording suggestions.

Thank you very much for your evaluation.

Specific comments and questions (major substantive issues and minor points of clarification, wording suggestions, and grammar / typo corrections are listed together for each Section in sequential order through the manuscript):

Introduction

- L41-42: It would be better to add "e.g." in front of the list of references for aerosols and water vapor, as is done for trace gases.

Added.

- L53: was believed --> is believed

Changed.

- L57-59: The way this sentence is constructed – first talking about the behavior observed during a specific week in August 1997 and then stating that the peak in NH_4NO_3 occurs around August – may be slightly confusing for readers, especially those who are not familiar with Höpfner et al.'s paper and the particular satellite data they analyzed. I can understand that the authors do not wish to add extraneous detail to the Introduction, but I think it would be better to break this sentence in two and make it more clear that the findings reported by Höpfner et al. were based on different satellite data sets. As it is now, the week of 8–16 August 1997 appears to hold some special significance, rather than just being when CRISTA data were taken.

We have revised this sentence as:
"Their satellite data analysis using Cryogenic Infrared Spectrometers and Telescopes for the Atmosphere (CRISTA) data indicates enhanced NH_4NO_3 signals around the tropopause, both in the ASM region and the western Pacific (including Japan) during 8–16 August 1997 (with the western Pacific signals suggestive of shedding vortices); also, their analysis of satellite Michelson Interferometer for Passive Atmospheric Sounding (MIPAS) data together with CRISTA data show that the mass of NH_4NO_3 in the ASM region at 13–17 km peaks around August."

- L70: data --> the data

Corrected.

Section 2

- L86: made --> done

Changed.

- L97: The uncertainties of lidar data are discussed here, which are applied to the both systems --> The uncertainties of lidar data discussed here are applicable to both systems

Changed.

- L121: Since "PV" is used below, "(PV)" should be added here after "potential vorticity".

Added.

- L122 and L126: on to --> onto

Corrected.

- L124: Delete the comma after "but".

Deleted.

- L126-127: PV … are --> PV … is

Corrected.

- L136-137: Young and Vaughan (2009) does not appear in the reference list.

Thank you for pointing this out. We have added it.

Section 3

- L157: mixture --> a mixture

Added.

- Figure 1: The color bar, particularly for the PDR panel, could be improved. The pink color denoting the highest values is somewhat difficult to distinguish from the light purple used at the bottom of the PDR range; this would not really be a problem if more were filled in, but it complicates interpretation of such a sparse plot.

We have changed the color bar, by making the pink darker, and by removing light purple from the PDR (and TDR) figure.

- L179: Delete the comma after "2018".

Deleted.

- L191: For clarity, it might be good to repeat verbatim the description in the Figure 1 caption: "the daily (first) lapse-rate tropopause".

Added.

- L192: with --> at

Corrected.

- L199: at a 400 K --> at 400 K

Removed.

- L200: of boundaries --> of the boundary

Added.

- L201: The value for the CO concentration (65 ppbv) selected to identify the ASM anticyclone boundary seems reasonable, but nevertheless it would be appropriate to cite a reference to justify this choice.

We have revised this sentence as:
"By comparing the results from Santee et al. (2017) with our own analysis, the 65 ppbv contours . . . are chosen . . . "

- L210: Although it's implicit, rather than stating "during July–September 2018", it would be better to say "on all days during July–September 2018 on which measurements were made".

Corrected as suggested.

- Figures 4 and 5:
  - The vast majority of back trajectories launched from Tsukuba indicate that the air parcels had been transported from altitudes above about 10–12 km over the preceding 10 days (and even slightly higher than that for trajectories run back from Fukuoka). It therefore seemed a bit odd to me that the color bar extends down to Z = 4 km. I had to look closely to spot the single trajectory that appears to originate in the middle of the North Pacific at that altitude (Figure 4, bottom panel). Some explanation for this apparently anomalous parcel should be given.
  - The greens in these color bars are impossible to distinguish, so if the authors feel that the trajectory geopotential height information is important, then they need to use a different color palette. Also, the color bar increments (0.8 km) are awkward.
  - Perhaps both of the above issues could be addressed by reformulating the plots. The existence of the outlier parcel could simply be mentioned in the text and not shown, allowing the geopotential height range to be decreased so fewer colors are needed.

The coloured geopotential height range of Figures 4 and 5 has been changed (narrowed).

Regarding the trajectory originating in the middle of the North Pacific at that altitude (Figure 4, bottom panel), we have added the following note in the text:
"Note that there is a trajectory that originates in the Pacific south of Japan as low as 4 km (Figure 4, bottom, a small-scale spiral in purple); this is associated with upward transport in the typhoon Soulik."

- L230-232: I don't find the discussion of PV very illuminating. First, for clarity it would be better to say "with lower values inside than outside the ASM anticyclone at the same latitude (e.g., 30°N)". More importantly, I'm puzzled by the lack of a clear signature of anticyclonic flow in the PV field. Previous studies have diagnosed eddy shedding through examination of PV maps. In particular, Garny and Randel [JGR, 2013] (a paper that I am surprised to see is not cited in this manuscript) reported an episode of eastward eddy shedding in June 2006 not unlike the one depicted here, and they showed that the contours of CO (from MLS) and PV (from MERRA) follow very similar patterns (although they focused on a lower theta level, 360 K). Perhaps the authors should explore using different PV contours or applying some smoothing to the PV fields to see if a clearer signal emerges. In any case, more discussion of the behavior of PV associated with this event is warranted.

The paper by Garny and Randel (2013) has been cited in the Introduction.

Following the suggestion by Referee #3 (i.e., at and above 400 K, PV is not very useful to see the boundary of the ASM anticyclone), we have changed from PV to Montgomery streamfunction (MSF). Please see the response to Referee #3 for detailed revisions.

- L236: It seems to me that, in addition to Figure 7, the results of Figure 6 also suggest that the 60-ppbv CO contour is indicative of eastward eddy shedding vortices.

This sentence is specifically for Figure 7 in which we take a latitudinal average. We have revised this sentence as:
"In Fig.7, the 60-ppbv CO contour may be a good indicator of eastward shedding vortices."

- L237-238: It is difficult for the reader to judge the timing of these events from Figure 7, especially given that some y-axis tick marks appear to be absent. For example, for the first episode listed, the 60-ppbv CO contour seems to be present at the longitudes of the lidar sites a couple of days before 5 August. Are the 20-25 and 27-31 August events really separable? It might be helpful to guide the eye by overlaying colored horizontal lines to mark each event's start and end dates or perhaps pale (transparent) colored bands spanning the intervals.

We have added coloured line segments for the periods when CO concentration was ≥~60 ppbv along the longitude of Tsukuba. (The same line segments will also be added to the MLS water vapour figure.) Furthermore, the text describing these periods has been corrected as: 3–15, 20–24, and 28–31 August, and 3–8, 14–17, and 28–29 September.

- L223-240: Since previous studies have used MLS CO to look for evidence of eddy shedding (e.g., Garny and Randel [2013], Honomichl and Pan [2020]), and since MLS water vapor is shown in Figure 8, I am curious why only CO from the CAMS reanalysis – and not from MLS – is used here. Is it because the necessary longitudinal and temporal binning would smear out finer-scale structures too much? Clearly, despite such smoothing, the MLS H_2O data provide valuable information. On the flip side, the authors should probably offer an explanation of why water vapor from MLS was used but not that from CAMS.

Figures R2-1 and R2-2 below show the comparisons of CAMS data and MLS data for CO and for water vapor. As we can see, for both CO and water vapor, CAMS and MLS show qualitatively and broadly similar eastward extension signals over Japan; however, CAMS CO is greater than MLS CO (e.g., the differences are ~10 ppbv around the longitudes of Japan through August–September 2018), and CAMS water vapor mixing ratios are greater than MLS water vapor (e.g., the differences are roughly ~2 ppmv for the wet signals around the longitudes of Japan in August 2018). In this paper, we primarily use CAMS CO data as a high-resolution tracer of the ASM anticyclone. Figure 7 is a companion one for Figure 6. For water vapor, however, we use MLS data because MLS water vapor measurements in the lower stratosphere have been well validated with e.g., balloon measurements (e.g., Hurst et al., 2016; Fujiwara et al., 2010; Vömel et al., 2007), while reanalysis water vapor data in the lower stratosphere are in general less reliable (e.g., Davis et al., 2017).

Thus, we have made the following revisions:

In Section 2.2, in the second paragraph, we have added the following sentences:

"CAMS CO data are originally provided in mass mixing ratio, kg kg^{-1}, which are converted to volume mixing ratio, ppbv, for this study. It is noted that a quick comparison with MLS Version 4.2 Level 2 CO data (Santee et al., 2017; Livesey et al., 2020) at 400 K isentropic surface (in the form of longitude-time diagram like the one in Section 3.2) shows that CAMS CO data are roughly ~10 ppbv greater than MLS CO over Japan during August–September 2018, but also shows that eastward extension signals coming over Japan agree fairly well qualitatively within the differences in spatio-temporal sampling of the two data sets."

In Section 2.2, we have written the following new (third) paragraph for MLS water vapor data:
"MLS Version 4.2 Level 2 water-vapour data (Santee et al., 2017; Livesey et al., 2020) are analysed because water vapour is also a good tracer of the ASM anticyclone. We use MLS data rather than CAMS data for lower stratospheric water vapour because MLS data have been well validated with e.g., balloon-borne frost-point hygrometers (e.g., Hurst et al., 2016; Fujiwara et al., 2010; Vömel et al., 2007), while reanalysis water vapor data are in general less reliable in the lower stratosphere (e.g., Davis et al., 2017). We found that CAMS water vapour volume mixing ratio data (converted from the original specific humidity data) are greater than MLS data at 400 K isentropic surface over Japan during July–September 2018 (e.g., the differences are roughly ~2 ppmv for the wet signals around the longitudes of Japan in August 2018)."

References:

Davis, S. M., Hegglin, M. I., Fujiwara, M., Dragani, R., Harada, Y., Kobayashi, C., Long, C., Manney, G. L., Nash, E. R., Potter, G. L., Tegtmeier, S., Wang, T., Wargan, K., and Wright, J. S.: Assessment of upper tropospheric and stratospheric water vapor and ozone in reanalyses as part of S-RIP, Atmos. Chem. Phys., 17, 12743–12778, https://doi.org/10.5194/acp-17-12743-2017, 2017.

Fujiwara, M., Vömel, H., Hasebe, F., Shiotani, M., Ogino, S.-Y., Iwasaki, S., Nishi, N., Shibata, T., Shimizu, K., Nishimoto, E., Valverde-Canossa, J. M., Selkirk, H. B., and Oltmans, S. J.: Seasonal to decadal variations of water vapor in the tropical lower stratosphere observed with balloon-borne cryogenic frostpoint hygrometers, J. Geophys. Res., 115, D18304, https://doi.org/10.1029/2010JD014179, 2010.

Hurst, D. F., Read, W. G., Vömel, H., Selkirk, H. B., Rosenlof, K. H., Davis, S. M., Hall, E. G., Jordan, A. F., and Oltmans, S. J.: Recent divergences in stratospheric water vapor measurements by frost point hygrometers and the Aura Microwave Limb Sounder, Atmos. Meas. Tech., 9, 4447–4457, https://doi.org/10.5194/amt-9-4447-2016, 2016.

Vömel, H., Barnes, J. E., Forno, R. N., Fujiwara, M., Hasebe, F., Iwasaki, S., Kivi, R., Komala, N., Kyrö, E., Leblanc, T., Morel, B., Ogino, S.-Y., Read, W. G., Ryan, S. C., Saraspriya, S., Selkirk, H., Shiotani, M., Valverde Canossa, J., and Whiteman, D. N.: Validation of Aura MLS water vapor by balloonborne Cryogenic Frostpoint Hygrometer measurements, J. Geophys. Res., 112, D24S37, https://doi.org/10.1029/2007JD008698, 2007.

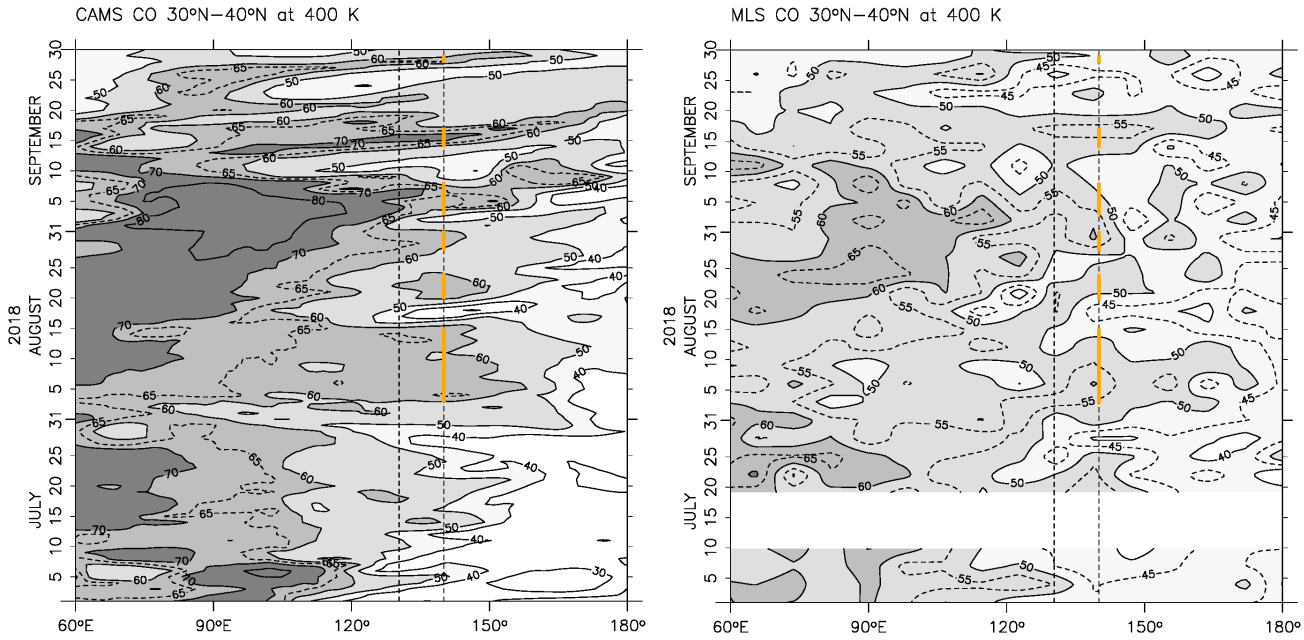

Figure R2-1. (Left) Same as Figure 7 (the revised version). (Right) Same as left but for MLS CO data. Data for the 30°N–40°N region have been aggregated into 3-day and 8°-longitude bins, each constituting about 10 individual data points. The contours for 45 ppbv and 55 ppbv as well as 65 ppbv are added as dotted lines.

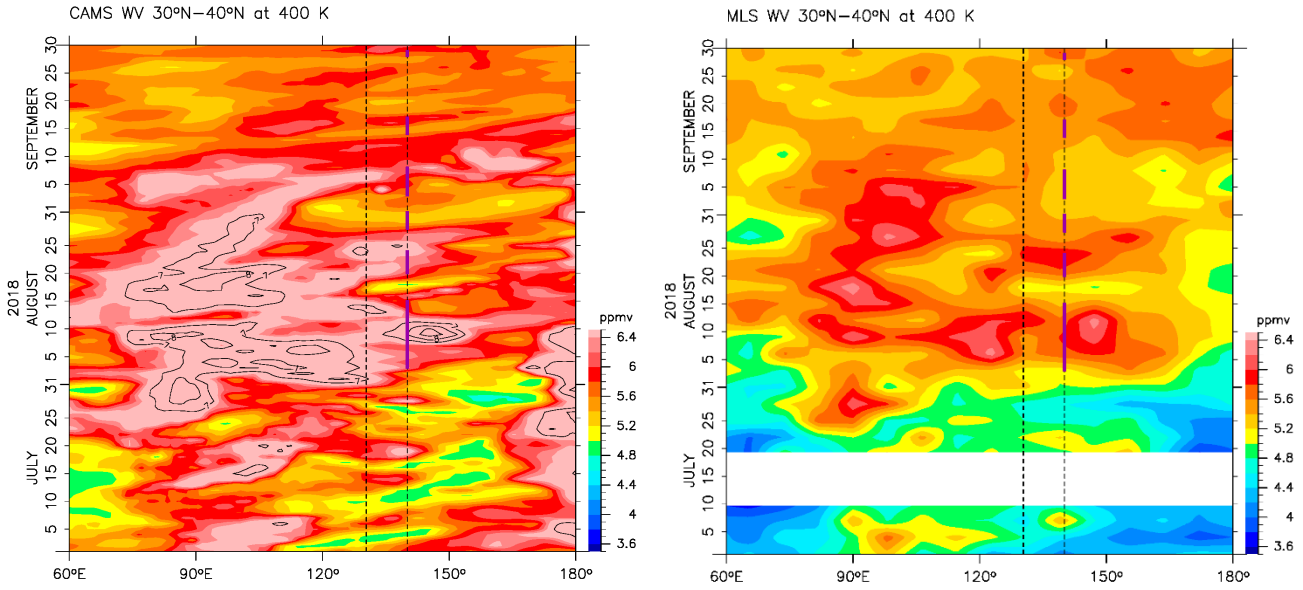

Figure R2-2. (Left) Longitude–time distribution of daily averaged water vapor volume mixing ratio at 400 K potential temperature averaged over 30°N–40°N, using CAMS reanalysis specific humidity data. The contour lines for 7, 8, 9, 10, 11 ppmv have been added. (Right) Same as Figure 8 (the revised version).

- L268-269: types of particle and gas --> types of particles and gases

Corrected.

- L286: but not have --> but had not

Corrected.

- L287: I think it would be appropriate to add “at least not in a monthly mean view” at the end of this sentence (mirroring the zonal mean caveat in L282).

Added.

- L288: unlikely due to --> unlikely to be due to

Corrected.

Section 4

- L311: measurements at --> measurements made at; also, delete the comma after “2018”

Corrected.

- L314: the BSR --> BSR

Deleted.

- L315-316: The authors might want to specifically note that none of the 11 nights on which data were taken at Fukuoka fell during the intervals of strong enhancement observed at Tsukuba.

We have added to this sentence,
“and due to the fact that the dates of lidar operation at Fukuoka did not overlap those at Tsukuba when strong enhancement was observed”

- L318: are of a few --> are a few

Corrected.

- L319: originate in the ASM anticyclone in association with eastward shedding vortices --> originate in the ASM anticyclone and are transported over these sites in association with eastward shedding vortices

Added.

- L320: eruptions and extensive --> eruptions or extensive

Corrected.

- L325-330: I'm not convinced that this is the best place for the discussion of the OHP measurements. I think it is generally inappropriate to introduce new aspects in the "Summary and Conclusions" section. In fact, these lines might belong in the Introduction.

This sentence has been moved to the Introduction.

- L332: Add a comma after "(3%–10%)".

Added.

- L337: Is it necessary to repeat "PDR" 3 times in this line (i.e., is it needed after "8%" and "4%")?

Deleted.

- L340-342: It seems to me that here again the Moana Loa and OHP information in these lines is out of place. Since these data add to the evidence that the signals observed at Tsukuba and Fukuoka must have arisen from the ATAL, this discussion could be moved to Section 3.3, which could then be renamed to reflect its exploration of other potential causes of the observed enhancements and not just focus on "Satellite aerosol data".

We have moved these sentences to the end of Section 3.3, whose title has been changed to "Investigation of other potential causes".

- L341: any enhancement --> no enhancement

Corrected.

- L360: Delete the comma after "extent"; also, is --> are

Corrected.

References

- L440: The paper by Hanumanthu et al. has now been accepted for publication in ACP.

Updated.

- L473: The reference for the MLS Data Quality Document (Livesey et al.) is missing the year.

The year 2020 has been added.

Finally, we have also made the following further revisions.

1. Tomohiro Nagai of MRI/JMA, Japan has been added as a coauthor due to his contributions to the lidar observations at Tsukuba.

2. The location of the "box" in Figure 9 (OMPS LP) has been corrected.

3. The colour code for Figure 10 (CALIOP) has been revised.

Response to comments by Anonymous Referee #3

Thank you very much for your review.

Comments on Manuscript No. ACP-2020-980

In the last decade the Asian Tropopause Aerosol Layer (ATAL) becomes in the focus of attention. This study shows that the transport of aerosol out of the ATAL by eastward shedding vortices were measured over Japan by two lidar systems during summer 2018. Several eddy shedding events were observed and backward trajectory calculations indicate that eddies including air masses with enhanced aerosol particles originate in the Asian monsoon anticyclone. The analysis of satellite observations and meteorological reanalysis confirm the eddy events and further show that the considered time period was free of the impact of volcanic eruptions and high forest fires.

This is a very interesting study, which merits its publication in ACP. The scientific content, the quality of the study and its presentation is good. Therefore, I suggest only some minor revisions before publication by ACP

Thank you very much for your evaluation.

1) P2/L51: 'The enhanced aerosol particle signature in the ASM anticyclone at 14–18 km altitude is known as the Asian Tropopause Aerosol Layer (ATAL), which was believed to consist of carbonaceous and sulphate materials, mineral dust, and nitrate particles (Vernier et al., 2015, 2018; Brunamonti et al., 2018; Bossolasco et al., 2020; Hanumanthu et al., 2020).'

From this statement it is not clear if the knowledge about the chemical composition of the the ATAL particles is based on in situ measurements, remotes sensing observations or model simulations. The discussion about the chemical composition of the ATAL should be much more improved and clarified. I recommend to add a short summery about the current knowledge of ATAL particle characteristics (e.g. chemical composition, particle size distribution, particle form, possible sources etc.). This would help to better bring the results of the lidar measurements presented in this study into the context of previous publications.

We would like to point out that one of the latest ATAL studies by Bossolasco et al. (2020) (a modeling study under review) discuss in the Introduction that "The sources, chemical composition and spatial and temporal variability of the ATAL are not yet well understood." Also, Hanumanth et al. (2020) (a study using balloon borne backscatter sondes) discuss in the Introduction that "The source regions of ATAL aerosols and their chemical precursors on the Earth's surface (origin) as well as the transport pathways from the surface to ATAL altitudes are poorly understood." Note also that Referee #2 suggested us to change from "was believed" to "is believed" in this sentence. Furthermore, in the text, in the following sentences, we introduce the recent study by Höpfner et al. (2019) rather extensively. We believe that this is the current status of our knowledge regarding the chemical composition of ATAL. Thus, we believe

that the current text is not inappropriate for the introduction to a study primarily using ground-based lidar systems.

2) P4/L114: ERA5 is a very new product from ECMWF, therefore I think it is worth to add a few references demonstrating the quality of ERA5 compared to the former ERA-Interim reanalysis.

We have added the following sentences:
"ERA5 temperature data in the tropical tropopause layer have been evaluated by Tegtmeier et al. (2020). Lagrangian transport calculations using ERA5 and its predecessor ERA-Interim have been compared by Hoffmann et al. (2019) and Li et al. (2020)."

Tegtmeier, S., Anstey, J., Davis, S., Dragani, R., Harada, Y., Ivanciu, I., Pilch Kedzierski, R., Krüger, K., Legras, B., Long, C., Wang, J. S., Wargan, K., and Wright, J. S.: Temperature and tropopause characteristics from reanalyses data in the tropical tropopause layer, Atmos. Chem. Phys., 20, 753–770, https://doi.org/10.5194/acp-20-753-2020, 2020.

Hoffmann, L., Günther, G., Li, D., Stein, O., Wu, X., Griessbach, S., Heng, Y., Konopka, P., Müller, R., Vogel, B., and Wright, J. S.: From ERA-Interim to ERA5: the considerable impact of ECMWFs next -generation reanalysis on Lagrangian transport simulations, Atmos. Chem. Phys., 19, 3097–3124, https://doi.org/10.5194/acp-19-3097-2019, 2019.

Li, D., Vogel, B., Müller, R., Bian, J., Günther, G., Ploeger, F., Li, Q., Zhang, J., Bai, Z., Vömel, H., and Riese, M.: Dehydration and low ozone in the tropopause layer over the Asian monsoon caused by tropical cyclones: Lagrangian transport calculations using ERA-Interim and ERA5 reanalysis data, Atmos. Chem. Phys., 20, 4133–4152, https://doi.org/10.5194/acp-20-4133-2020, 2020.

3) P4/L122: Please add a statement like this: 'CO and the ATAL have not necessarily the same emission sources, however CO is a good chemical tracer to indicated the location of the Asian monsoon anticyclone.'

We have added the following sentence:
"Although CO and ATAL aerosol particles do not necessarily have the same emission sources, CO is a good chemical tracer to indicate the location of the ASM anticyclone."

4) P5/L152: Is it possible that cirrus signal overlays the aerosol signal, so that cirrus and aerosol can coexist simultaneously? Or can you exclude this with your method?

Yes, it is always possible that cirrus signal overlays the aerosol signal if they coexist because of the larger backscattering cross section of cirrus particles. In that case, the BSR and PDR values would become those for cirrus particles.

5) P9/Fig.3: You could add a BSR profile from pre- or post-monsoon to show the difference. The difference can be

use to better highlight the signal in BSR from the ATAL.

Figures R3-1 and R3-2 below show the lidar profiles at Tsukuba on some days in May 2018 and in October 2018, respectively. These figures show that BSR in these months did not show enhancements of >1.1 like those found in August and September (Figs. 2c, e). However, we note that TDR slightly increased below 20 km, suggesting a possibility of presence of minute amount of non-spherical particles. The origins of the particles are unknown and a subject of our future study.

Figure R3-3 below shows the lidar profiles at Fukuoka on some days in May-June 2018 and in October-November 2018. Again, we did not detect depolarization enhanced layers (with depolarization ratio higher than 2%) in these months.

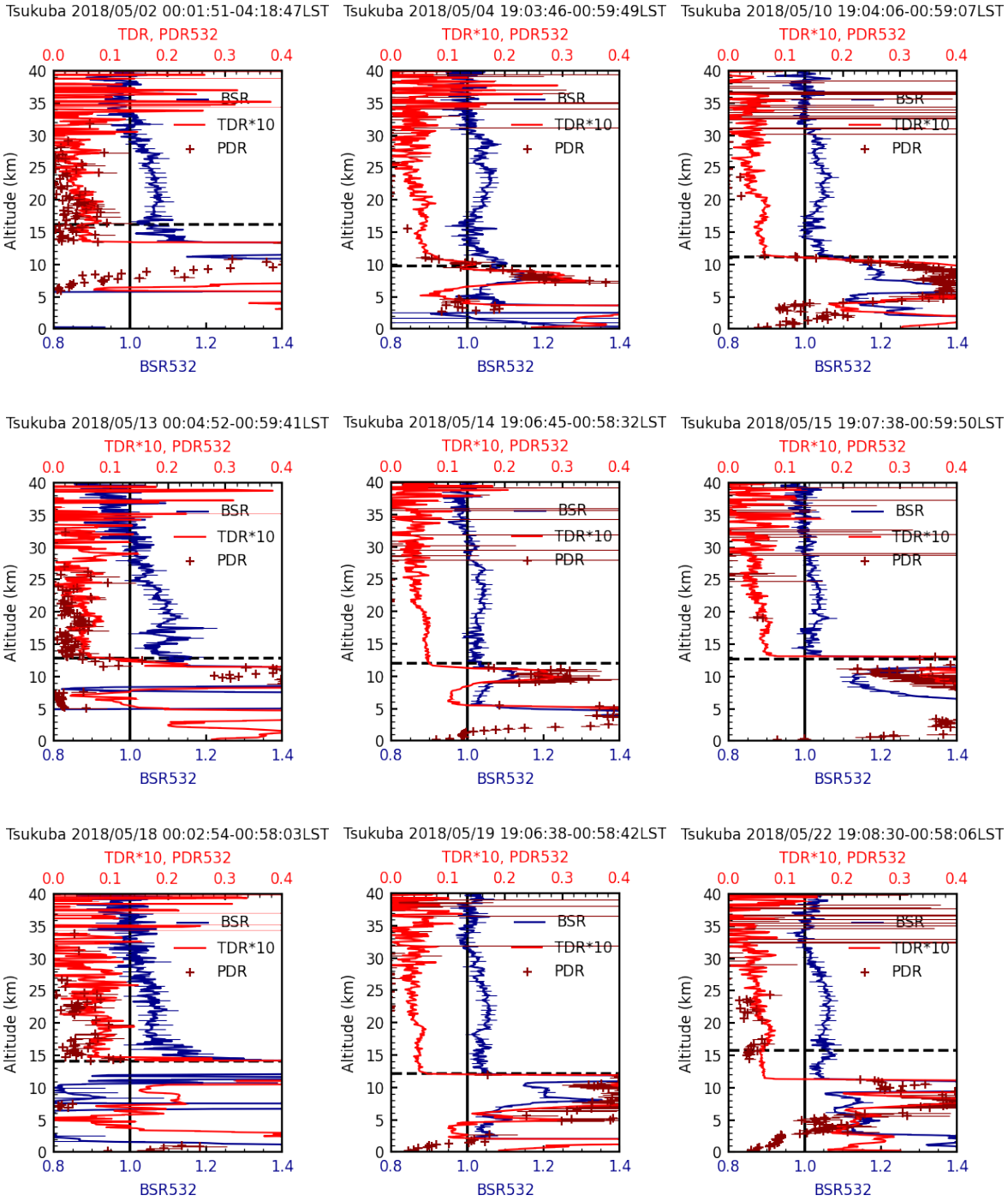
Tsukuba 2018/05/02 00:01:51-04:18:47LST
Tsukuba 2018/05/04 19:03:46-00:59:49LST
Tsukuba 2018/05/10 19:04:06-00:59:07LST
Tsukuba 2018/05/13 00:04:52-00:59:41LST
Tsukuba 2018/05/14 19:06:45-00:58:32LST
Tsukuba 2018/05/15 19:07:38-00:59:50LST
Tsukuba 2018/05/18 00:02:54-00:58:03LST
Tsukuba 2018/05/19 19:06:38-00:58:42LST
Tsukuba 2018/05/22 19:08:30-00:58:06LST
TDR, PDR532
TDR*10, PDR532
BSR
TDR*10
PDR
Altitude (km)
BSR532

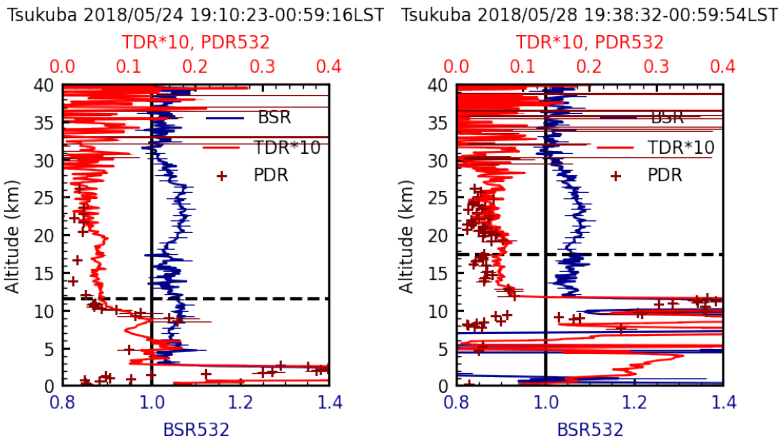

Figure R3-1. Lidar profiles taken at Tsukuba on May 2, 4, 10, 13, 14, 15, 18, 19, 22, 24, and 28, 2018. The horizontal dashed line in each panel indicates the location of the first lapse rate tropopause. It is noted that for "TDR*10" = 0.05 means TDR = 0.05/10 = 0.005, i.e., 0.5%TDR. This is close to the depolarization ratio value, 0.366% for air molecules.

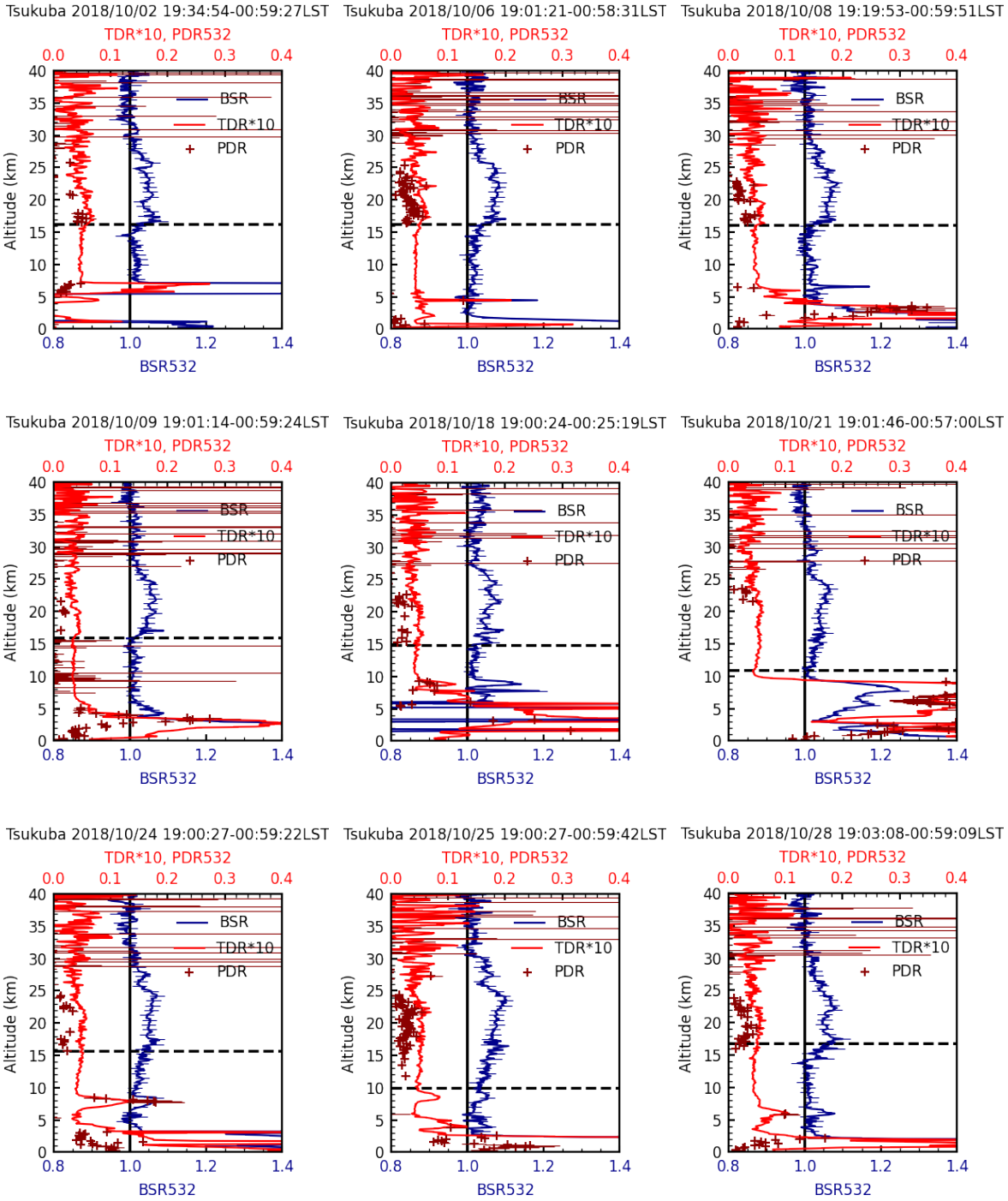
Tsukuba 2018/10/02 19:34:54-00:59:27LST
Tsukuba 2018/10/06 19:01:21-00:58:31LST
Tsukuba 2018/10/08 19:19:53-00:59:51LST
Tsukuba 2018/10/09 19:01:14-00:59:24LST
Tsukuba 2018/10/18 19:00:24-00:25:19LST
Tsukuba 2018/10/21 19:01:46-00:57:00LST
Tsukuba 2018/10/24 19:00:27-00:59:22LST
Tsukuba 2018/10/25 19:00:27-00:59:42LST
Tsukuba 2018/10/28 19:03:08-00:59:09LST
TDR*10, PDR532
BSR
TDR*10
PDR
Altitude (km)
BSR532

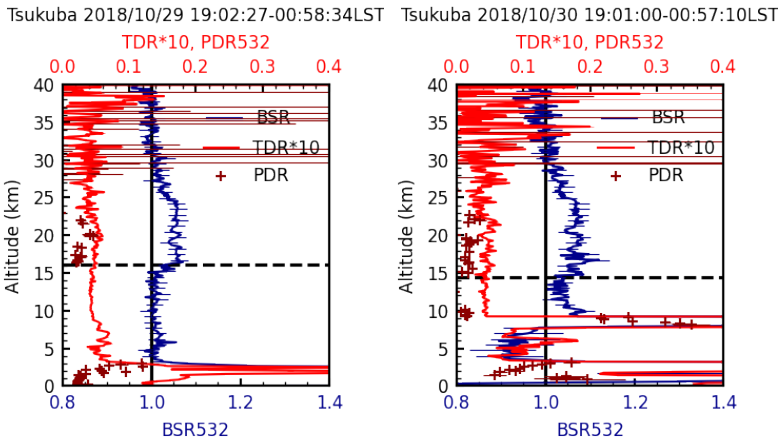

Figure R3-2. As for Figure R1-1, but for October 2, 6, 8, 9, 18, 21, 24, 25, 28, 29, and 30, 2018.

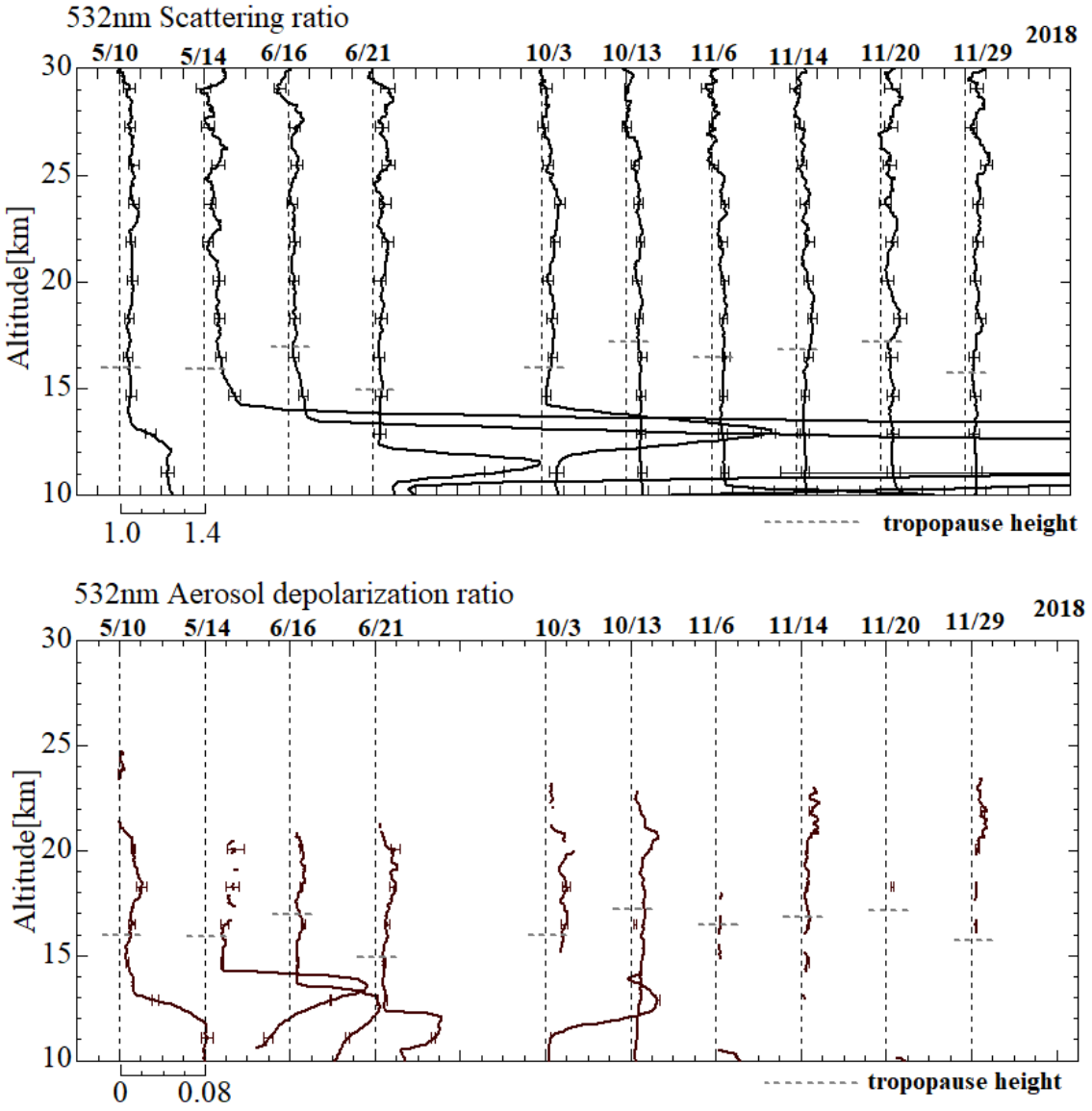

Figure R3-3. Lidar profiles taken at Fukuoka on the days in May-June 2018 and in October-November 2018 when the lidar was operated.

6) P10/L204: '... whereas those without enhanced aerosol particles tend to originate from edge regions surrounding the anticyclone.' and from the extratropical lower stratosphere. Right?

At the northern edge regions, yes. But, at the southern edge regions, they are from tropical lower stratosphere.

Why do you use only ten-days backward trajectories? What about 15- or 20-day backward calculations? In somewhat

longer trajectories, the difference between air masses from the core the anticyclone or from the edge (or outside from the anticyclone) should be more pronounced.

Figure R3-4 below shows the 15-day backward trajectories. We had found that if we plot longer trajectories, we have more trajectories within the ASM anticyclone, although the density is still lower for the cases without enhanced aerosols measured at Tsukuba/Fukuoka. Also, we had received a comment before the paper submission that longer trajectories are less reliable. Thus, we decided to show the results from 10-day backward trajectories which better shows the differences.

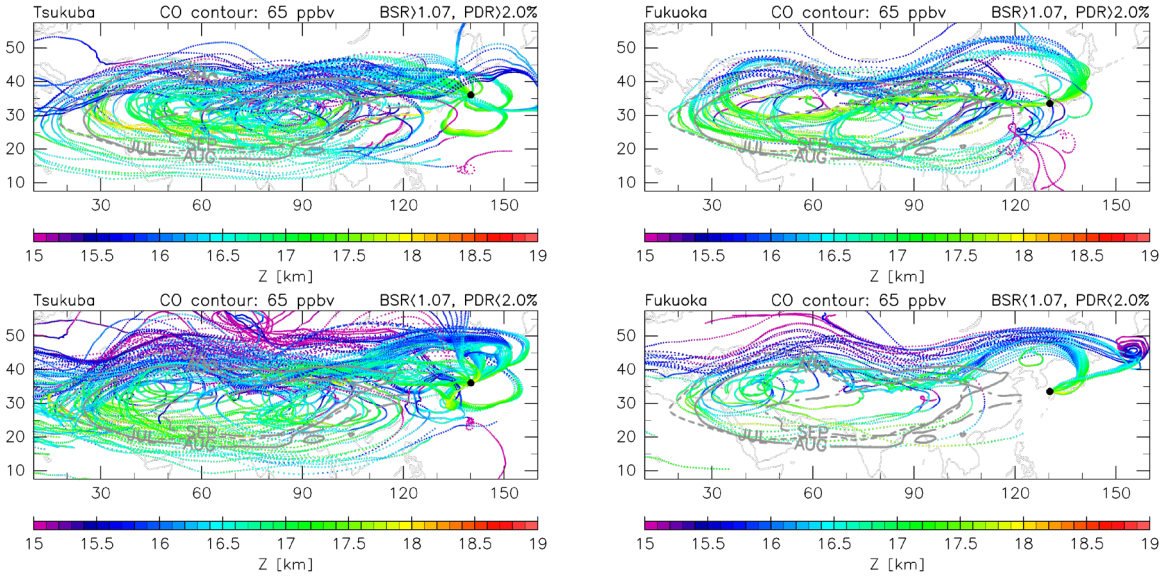

Figure R3-4. As for Figures 4 (for Tsukuba, for the left two panels) and 5 (for Fukuoka, for the right two panels), but for 15-day backward trajectories. (Note that the colour code for the geopotential height has been revised (to narrow the range of Z); please see the next QA.)

7) P11/Fig.4: Is it possible to adjust the color bar more to the Z range of the trajectories to better highlight the gradients along the trajectories. The bluish colors are only used for one trajectory over the Pacific in Fig. 4b. It looks like that this trajectory is influenced by a tropical cyclone. If that is true that could be mentioned as a side remark.

The colored geopotential height range of Figures 4 and 5 has been changed (narrowed).

Regarding the trajectory originating in the middle of the North Pacific at that altitude (Figure 4, bottom panel), we have added the following note in the text:
"Note that there is a trajectory that originates in the Pacific south of Japan as low as 4 km (Figure 4, bottom, a small-scale spiral in purple); this is associated with upward transport in the typhoon Soulik."

8) P13/L230 : 'PV can be regarded as a dynamical tracer, with lower values in the ASM anticyclone along the same latitudes (e.g., 30◦N), although background positive gradients in latitude and its noisier nature give more complicated features.'

PV can be very useful to see the edge of the Asian monsoon anticyclone at around 380K (e.g. Ploeger et al., 2015), above around 400K as shown in Fig. 6, the PV is not so useful. Instead you could try to use the (Montgomery) stream function or the geopotential height.

Ploeger, F., Gottschling, C., Grießbach, S., Grooß, J.-U., Günther, G., Konopka, P., Müller, R., Riese, M., Stroh, F.,

Tao, M., Ungermann, J., Vogel, B., and von Hobe, M.: A potential vorticity-based determination of the transport barrier in the Asian summer monsoon anticyclone, Atmos. Chem. Phys., 15, 13 145–13 159, https://doi.org/doi:10.5194/acp-15-13145-2015, 2015.

Thank you very much for your comment and suggestion. We have changed from PV to Montgomery streamfunction in Figure 6. We have added the following sentences in the second paragraph of Section 2.2:

"Carbon monoxide (CO), temperature (T), and geopotential (Φ) data are analysed in this paper."

"Montgomery streamfunction (MSF), defined as MSF = $c_p\ T + \Phi$, where c_p is specific heat of dry air at constant pressure, in isentropic coordinates corresponds to geopotential (height) in pressure coordinates (e.g., Amemiya and Sato, 2018) , and thus is a good dynamical indicator of the ASM anticyclone. Potential vorticity (PV) on isentropic surfaces (e.g., at 360–380 K) is often used as a dynamical tracer in studies of the ASM anticyclone (e.g., Popovic and Plumb, 2001; Garny and Randel, 2013; Ploeger et al., 2015; Amemiya and Sato, 2018); however, PV at and above 400 K (this isentropic surface will be focused in Section 3.2) is not very useful to analyse the ASM anticyclone boundary. Thus, we will analyse MSF at 400 K surface calculated from CAMS data."

Also, we have revised the second paragraph of Section 3.2 accordingly.

9) P16/Fig.8: Why do you show H2O from MLS and not CO from MLS? CO would be a better chemical tracer for transport as H2O which is in addition affected by microphysics. You could also use MLS O3 which should be anticorrelated to CO (low O3 in the anticyclone and high O3 in the lower stratosphere).

Figures R3-5 and R3-6 below show the comparisons of CAMS data and MLS data for CO and for water vapor. As we can see, for both CO and water vapor, CAMS and MLS show qualitatively and broadly similar eastward extension signals over Japan; however, CAMS CO is greater than MLS CO (e.g., the differences are ~10 ppbv around the longitudes of Japan through August–September 2018), and CAMS water vapor mixing ratios are greater than MLS water vapor (e.g., the differences are roughly ~2 ppmv for the wet signals around the longitudes of Japan in August 2018). In this paper, we primarily use CAMS CO data as a high-resolution tracer of the ASM anticyclone. Figure 7 is a companion one for Figure 6. For water vapor, however, we use MLS data because MLS water vapor measurements in the lower stratosphere have been well validated with e.g., balloon measurements (e.g., Hurst et al., 2016; Fujiwara et al., 2010; Vömel et al., 2007), while reanalysis water vapor data in the lower stratosphere are in general less reliable (e.g., Davis et al., 2017).

Thus, we have made the following revisions:

In Section 2.2, in the second paragraph, we have added the following sentences:
"CAMS CO data are originally provided in mass mixing ratio, kg kg^{-1}, which are converted to volume mixing ratio,

ppbv, for this study. It is noted that a quick comparison with MLS Version 4.2 Level 2 CO data (Santee et al., 2017; Livesey et al., 2020) at 400 K isentropic surface (in the form of longitude-time diagram like the one in Section 3.2) shows that CAMS CO data are roughly ~10 ppbv greater than MLS CO over Japan during August–September 2018, but also shows that eastward extension signals coming over Japan agree fairly well qualitatively within the differences in spatio-temporal sampling of the two data sets."

In Section 2.2, we have written the following new (third) paragraph for MLS water vapor data:
"MLS Version 4.2 Level 2 water-vapour data (Santee et al., 2017; Livesey et al., 2020) are analysed because water vapour is also a good tracer of the ASM anticyclone. We use MLS data rather than CAMS data for lower stratospheric water vapour because MLS data have been well validated with e.g., balloon-borne frost-point hygrometers (e.g., Hurst et al., 2016; Fujiwara et al., 2010; Vömel et al., 2007), while reanalysis water vapor data are in general less reliable in the lower stratosphere (e.g., Davis et al., 2017). We found that CAMS water vapour volume mixing ratio data (converted from the original specific humidity data) are greater than MLS data at 400 K isentropic surface over Japan during July–September 2018 (e.g., the differences are roughly ~2 ppmv for the wet signals around the longitudes of Japan in August 2018)."

References:

Davis, S. M., Hegglin, M. I., Fujiwara, M., Dragani, R., Harada, Y., Kobayashi, C., Long, C., Manney, G. L., Nash, E. R., Potter, G. L., Tegtmeier, S., Wang, T., Wargan, K., and Wright, J. S.: Assessment of upper tropospheric and stratospheric water vapor and ozone in reanalyses as part of S-RIP, Atmos. Chem. Phys., 17, 12743–12778, https://doi.org/10.5194/acp-17-12743-2017, 2017.

Fujiwara, M., Vömel, H., Hasebe, F., Shiotani, M., Ogino, S.-Y., Iwasaki, S., Nishi, N., Shibata, T., Shimizu, K., Nishimoto, E., Valverde-Canossa, J. M., Selkirk, H. B., and Oltmans, S. J.: Seasonal to decadal variations of water vapor in the tropical lower stratosphere observed with balloon-borne cryogenic frostpoint hygrometers, J. Geophys. Res., 115, D18304, https://doi.org/10.1029/2010JD014179, 2010.

Hurst, D. F., Read, W. G., Vömel, H., Selkirk, H. B., Rosenlof, K. H., Davis, S. M., Hall, E. G., Jordan, A. F., and Oltmans, S. J.: Recent divergences in stratospheric water vapor measurements by frost point hygrometers and the Aura Microwave Limb Sounder, Atmos. Meas. Tech., 9, 4447–4457, https://doi.org/10.5194/amt-9-4447-2016, 2016.

Vömel, H., Barnes, J. E., Forno, R. N., Fujiwara, M., Hasebe, F., Iwasaki, S., Kivi, R., Komala, N., Kyrö, E., Leblanc, T., Morel, B., Ogino, S.-Y., Read, W. G., Ryan, S. C., Saraspriya, S., Selkirk, H., Shiotani, M., Valverde Canossa, J., and Whiteman, D. N.: Validation of Aura MLS water vapor by balloonborne Cryogenic Frostpoint Hygrometer measurements, J. Geophys. Res., 112, D24S37, https://doi.org/10.1029/2007JD008698, 2007.

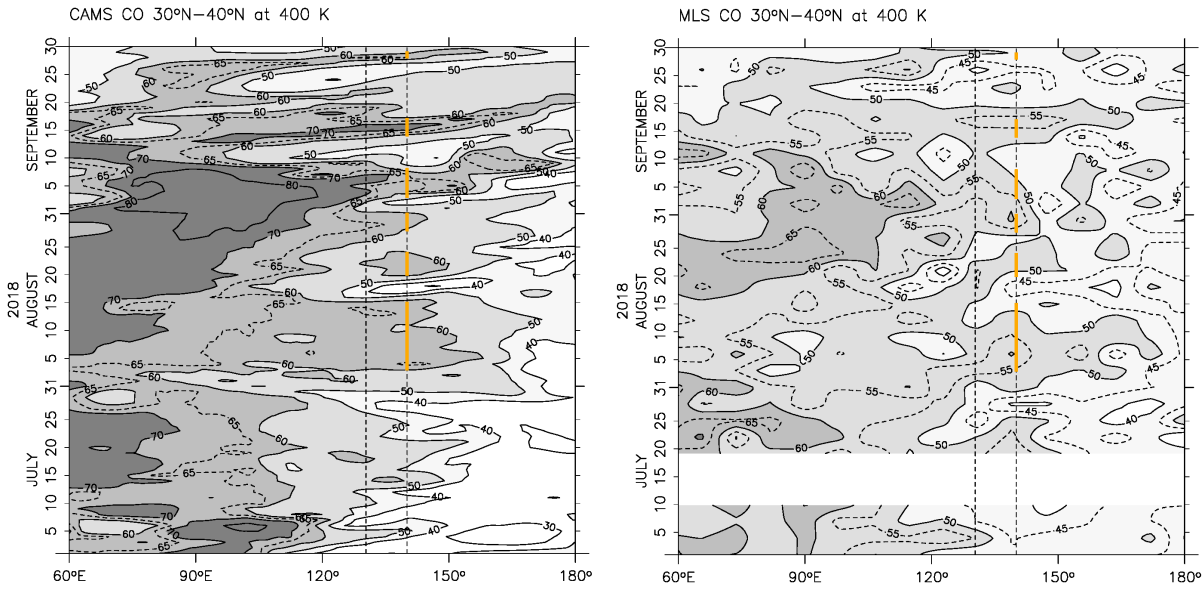

Figure R3-5. (Left) Same as Figure 7 (the revised version). (Right) Same as left but for MLS CO data. Data for the 30°N–40°N region have been aggregated into 3-day and 8°-longitude bins, each constituting about 10 individual data points. The contours for 45 ppbv and 55 ppbv as well as 65 ppbv are added as dotted lines.

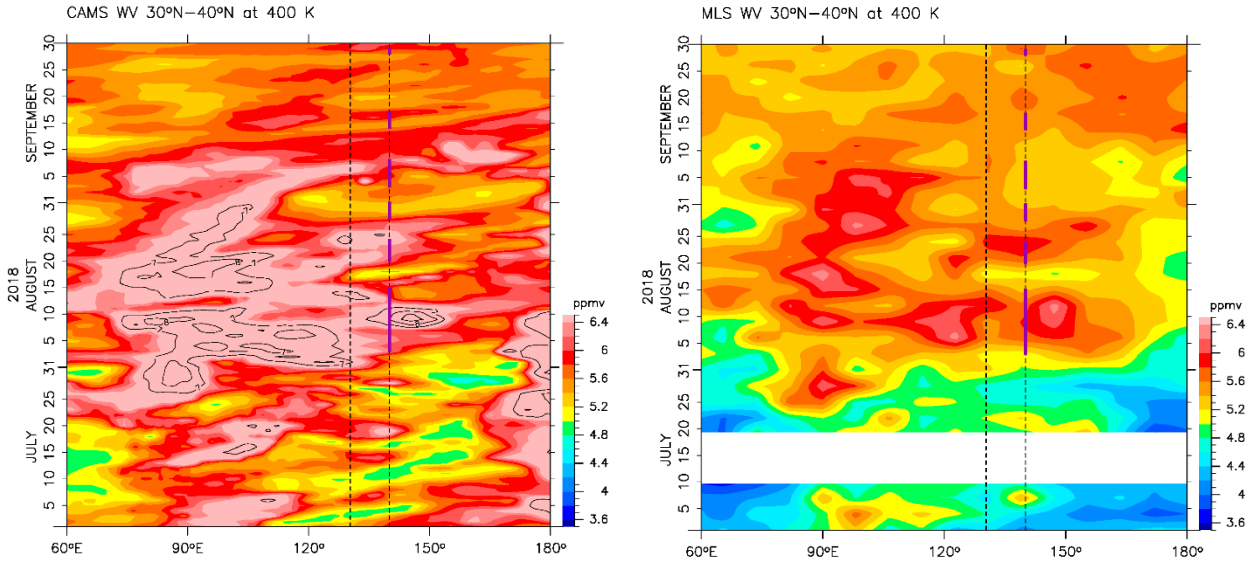

Figure R3-6. (Left) Longitude–time distribution of daily averaged water vapor volume mixing ratio at 400 K potential temperature averaged over 30°N–40°N, using CAMS reanalysis specific humidity data. The contour lines for 7, 8, 9, 10, 11 ppmv have been added. (Right) Same as Figure 8 (the revised version).

Two figures for ozone from CAMS and MLS are shown below. Figure R3-7 shows horizontal distributions of daily ozone at 400 K during 18–23 August 2018 using CAMS reanalysis data, similar to Figure 6. Figure R3-8 shows

longitude–time distribution (Hovmöller diagram) of ozone at 400 K averaged over 30°N–40°N using CAMS reanalysis and MLS data. We see that ozone and CO are anticorrelated around the northern edge of the ASM anticyclone (in other words, along the westerly jet stream). In particular, around 16–19 August, a strong stratosphere-to-troposphere intrusion occurred over Japan, which are clearly observed as a strong ozone enhancement event. Around the southeastern and southern part of the ASM anticyclone, however, the relationship between ozone and CO becomes less clear (i.e., not always clearly anticorrelated); ozone concentration is often still relatively high in CO enhanced regions there. This is probably in part due to the transport from the north (i.e., ozone of stratospheric origin) and in part due to upward transport from Asian countries where ozone is photochemically produced (i.e., ozone of tropospheric origin). Thus, in this paper, we decided not to show ozone results as the interpretation is more complicated than CO and water vapour.

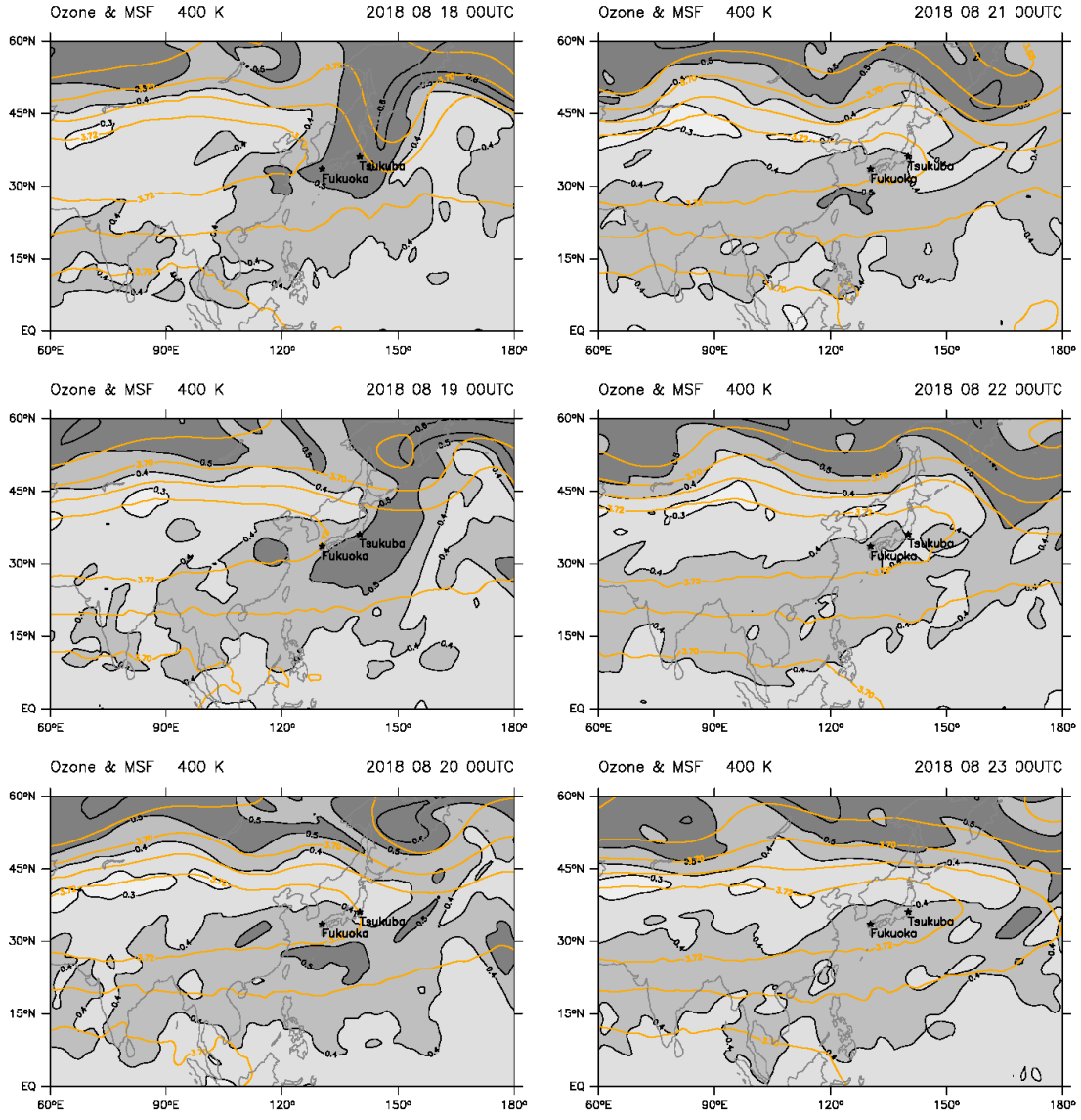

Figure R3-7. As for the revised Figure 6, but for ozone volume mixing ratio (black contours with grey tone, with

intervals of 0.1 ppmv) from CAMS reanalysis data. CAMS ozone data are originally provided in mass mixing ratio, kg kg^{-1}, which are converted to volume mixing ratio, ppmv, for this response letter.

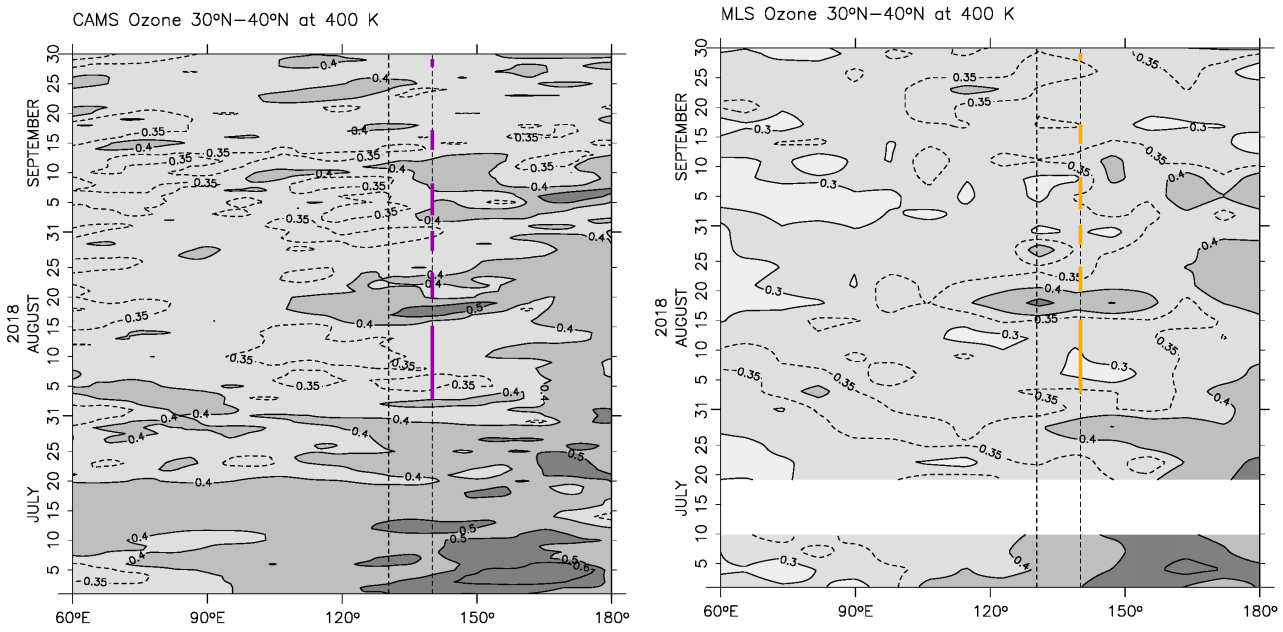

Figure R3-8. (Left) Same as Figure 7 (the revised version), but for CAMS ozone in ppmv. The contour interval is 0.1 ppmv, with 0.35 ppmv contours added (dotted). (Right) Same as left but for MLS ozone data. Data for the 30°N–40°N region have been aggregated into 3-day and 8°-longitude bins, each constituting about 10 individual data points.

10) P20/L331: 'The PDR values obtained at Tsukuba, i.e., ~5% (3%–10%) suggest that these enhanced particles are solid particles, rather than spherical, liquid H2SO4 particles (PDR ~0%) or cirrus ice particles (PDR > 25%–30%). The observed values may be consistent with those of solid NH4NO3 particles recently suggested by Höpfner et al. (2019).'

Using the particle depolarization ratio, the study shows that the aerosol particles are most likely solid and it is concluded that the aerosol particles possibly contain NH4NO3. In the literature it is discussed that also carbonaceous aerosols, dust, nitrate-containing aerosol, black carbon and organic carbon could contribute to the chemical composition of the ATAL. Can you exclude with your measurements such types of aerosol particles? Please clarify this point.

The lidar measurements cannot exclude the co-existence/existence of other types of aerosol particles. We have added the following sentence:

"However, it should be noted that the lidar BSR and PDR measurements cannot exclude the possibility of co-existence of other types of solid aerosol particles such as mineral dust, black carbon, and some types of carbonaceous

aerosols which are solid."

Minor comments:

1) P3/L84: (senkrecht in German) –> (= "senkrecht" in German) ?

Added.

2) P5/L37: remove large white spaces

This will be handled at the type-setting phase (if this paper is accepted).

3) P13/L223: 'Horizontal distributions of CO and PV' add 'from CAMS'

Added.

4) P13/L233: 'are shown in Figure 7' -> 'are shown as Hovmöller diagrams in Fig. 7'

We chose not to use the term "Hovmöller diagram" because this may not be understandable for some of the readers of the journal Atmospheric Chemistry and Physics. But, we are happy to make the change if the editor recommends to do so.

5) Fig.7/8: You could say that the Figures are 'Hovmöller diagrams'

Please see above.

Finally, we have also made the following further revisions.

1. Tomohiro Nagai of MRI/JMA, Japan has been added as a coauthor due to his contributions to the lidar observations at Tsukuba.

2. The location of the "box" in Figure 9 (OMPS LP) has been corrected.

3. The colour code for Figure 10 (CALIOP) has been revised.

Lower-stratospheric aerosol measurements in eastward shedding vortices over Japan from the Asian summer monsoon anticyclone during the summer of 2018

Masatomo Fujiwara[1], Tetsu Sakai[2], Tomohiro Nagai[2], Koichi Shiraishi[3], Yoichi Inai[4,5], Sergey Khaykin[6], Haosen Xi[7], Takashi Shibata[8], Masato Shiotani[9], and Laura L. Pan[10]

[1] Faculty of Environmental Earth Science, Hokkaido University, Sapporo, 060-0810, Japan
[2] Meteorological Research Institute, Japan Meteorological Agency, Tsukuba, 305-0052, Japan
[3] Faculty of Science, Fukuoka University, Fukuoka, 814-0180, Japan
[4] Graduate School of Science, Tohoku University, Sendai, 980-8578, Japan
[5] Now at Japan Meteorological Agency, Sapporo, 060-0002, Japan
[6] LATMOS/IPSL, UVSQ, Sorbonne Université, CNRS, Guyancourt, 78280, France
[7] Graduate School of Environmental Science, Hokkaido University, Sapporo, 060-0810, Japan
[8] Graduate School of Environmental Studies, Nagoya University, Nagoya, 464-8601, Japan
[9] Research Institute for Sustainable Humanosphere, Kyoto University, Uji, 611-0011, Japan
[10] National Center for Atmospheric Research, Boulder, CO 80301, USA

Correspondence to: Masatomo Fujiwara (fuji@ees.hokudai.ac.jp)

Abstract

Eastward airmass transport from the Asian summer monsoon (ASM) anticyclone in the upper troposphere and lower stratosphere (UTLS) often involves eastward shedding vortices, which can cover most of the Japanese archipelago. We investigated the aerosol characteristics of these vortices by analysing data from two lidar systems in Japan, at Tsukuba (36.1°N, 140.1°E) and Fukuoka (33.55°N, 130.36°E), during the summer of 2018. We observed several events with enhanced particle signals at Tsukuba at 15.5–18 km altitude (at or above the local tropopause) during August–September 2018, with a backscattering ratio of ~1.10 and particle depolarization of ~5% (i.e., not spherical, but more spherical than ice crystals). These particle characteristics may be consistent with those of solid aerosol particles, such as ammonium nitrate. Each event had a timescale of a few days. During the same study period, we also observed similar enhanced particle signals in the lower stratosphere at Fukuoka. The upper troposphere is often covered by cirrus clouds at both lidar sites. Backward trajectory calculations for these sites for days with enhanced particle signals in the lower stratosphere and days without indicate that the former airmasses originated within the ASM anticyclone, and the latter more from edge regions. Reanalysis carbon-monoxide and satellite water-vapour data indicate that eastward shedding vortices were involved in the observed aerosol enhancements. Satellite aerosol data confirm that the period and latitudinal region were free from the direct influence of documented volcanic eruptions and high latitude forest fires. Our results indicate that the Asian Tropopause Aerosol Layer (ATAL) over the ASM

region extends east towards Japan in association with the eastward shedding vortices, and that lidar systems in Japan can detect at least the lower stratospheric portion of the ATAL during periods when the lower stratosphere is undisturbed by volcanic eruptions and forest fires. The upper tropospheric portion of the ATAL is either depleted by tropospheric processes (convection and wet scavenging) during eastward transport or is obscured by much stronger cirrus cloud signals.

1 Introduction

The Asian Summer Monsoon (ASM) circulation includes a continental-scale anticyclone centred over the Tibetan Plateau, spanning from the Middle East to East Asia in the upper troposphere and lower stratosphere (UTLS). Satellite observations show elevated levels of trace gases of surface origin (e.g., Randel et al., 2010; Santee et al., 2017), aerosol particles (e.g., Vernier et al., 2015, 2018), and water vapour (e.g., Randel et al., 2015; Santee et al., 2017) within the ASM anticyclone due to active convection in this region and season. The ASM anticyclone exhibits distinct sub-seasonal variability due to westward and eastward shedding vortices (e.g., Popovic and Plumb, 2001; Amemiya and Sato, 2018), with the latter possibly being dynamically linked to the Bonin (or Ogasawara) High in the western Pacific (Enomoto et al., 2003) and constituting a major transport pathway of ASM airmasses to the whole Northern Hemisphere (NH) midlatitude UTLS through the westerly jet stream (e.g., Garny and Randel, 2013; Vogel et al., 2014, 2016; Ungermann et al., 2016; Pan et al., 2016; Fadnavis et al., 2018; Luo et al., 2018; Honomichl and Pan, 2020). Eastward shedding vortex events occur once in every 10–20 days during the NH summer, with a horizontal scale of 20°–30° longitude (2000–3000 km), and with a few days to one week of influence over the Japanese archipelago (e.g., Honomichl and Pan, 2020).

The enhanced aerosol particle signature in the ASM anticyclone at 14–18 km altitude is known as the Asian Tropopause Aerosol Layer (ATAL), which ~~was~~ is believed to consist of carbonaceous and sulphate materials, mineral dust, and nitrate particles (Vernier et al., 2015, 2018; Brunamonti et al., 2018; Bossolasco et al., 2020; Hanumanthu et al., 2020). Through analysis of satellite and high-altitude aircraft observations and laboratory experiments, Höpfner et al. (2019) provided evidence that a considerable part of the ATAL may contain solid ammonium nitrate (NH_4NO_3) particles. Their satellite data ~~analyses~~ analysis using Cryogenic Infrared Spectrometers and Telescopes for the Atmosphere (CRISTA) data indicates enhanced NH_4NO_3 signals around the tropopause, both in the ASM region and the western Pacific (including Japan) during 8–16 August 1997 (with the western Pacific signals suggestive of shedding vortices); also, their analysis of satellite Michelson Interferometer for Passive Atmospheric Sounding (MIPAS) data together with CRISTA data show that ~~with~~ the mass of NH_4NO_3 in the ASM region at 13–17 km peak~~sing~~ around August. It is also noted that Vernier et al. (2015, in their Figure 2b) showed mean eastward extension of the ATAL to the Japanese archipelago by averaging Cloud–Aerosol Lidar with Orthogonal Polarization (CALIOP) data for July–August 2006–2013, although the role of synoptic disturbances, such as eastward shedding vortices, in the ATAL eastward extension does not appear to have been investigated using CALIOP data.

~~It is also noted that the~~The "westward" extension of the ATAL to northern midlatitudes was reported by Khaykin et al. (2017), based on ground-based lidar at the Observatoire de Haute-Provence (OHP) in southern France (43.9°N, 5.7°E), with a layer of enhanced aerosol in the lower stratosphere with an average backscattering ratio (BSR; related to particle size and density) value of 1.05 being a systematic feature during August–October. This aerosol layer was shown to correlate with the seasonal water-vapour maximum, suggesting the influx of convectively moistened air from the ASM anticyclone, whose influence on the extratropical lower stratosphere in late summer to early winter is well known (e.g., Vogel et al., 2014; Müller et al., 2016; Rolf et al., 2018).

Some lidar systems currently in operation in Japan are capable of measuring UTLS aerosol characteristics, including those at the Meteorological Research Institute (MRI), Tsukuba (36.1°N, 140.1°E; Sakai et al., 2016) and Fukuoka University, Fukuoka (33.55°N, 130.36°E; Yasui et al., 1995). Both systems measure the ~~backscattering ratio (~~BSR~~; related to particle size and density)~~ and particle depolarization ratio (PDR; related to the degree of particle non-sphericity). Previous studies using data from these systems investigated the impacts of the large-scale tropical volcanic eruptions and other recent eruptions (Uchino et al. 1993; Sakai et al. 2016), and spring-time transport of dust particles from the Asian continent, "Kosa" events (yellow sand/dust events) (Sakai et al. 2003), amongst others; however, the data have not been investigated extensively for the possible detection of the ATAL from ASM circulation, i.e., its "eastward" extension, partly because extensive summer-time cloud cover often prevents lidar sensing of the UTLS region, and partly because ATAL signals are much weaker than volcanic signals. In this paper, focusing on the July–September 2018 period, we investigate whether these lidars are capable of measuring ATAL signals associated with eastward shedding vortices from the ASM anticyclone, with combined analyses of backward trajectories, chemical reanalysis data, and satellite data for full understanding of the lidar observations. The remainder of this paper is organised as follows. Section 2 describes the lidar and other data analysed in this paper. Section 3 presents the results and discussion, and Section 4 concludes the findings.

2 Data description

2.1 Lidar data

The lidar system at the MRI, Tsukuba (36.1°N, 140.1°E) used in this study is an Nd:YAG system operated at a wavelength of 532 nm, with a capability of both BSR and PDR measurements (Sakai et al., 2016), and which has been operating continuously since 2002. We define PDR as S/P, where S and P are the background-subtracted lidar photon counts of the perpendicular ("senkrecht" in German) and parallel components, respectively, with respect to the polarization plane of the emitted laser light. The temporal and height resolutions of the original processed data are 5 min and 7.5 m, respectively. Quality control has been ~~made~~ done primarily to flag data points influenced by thick cloud layers. To obtain vertical profiles of BSR and PDR with high signal-to-noise ratios, data were averaged over 150 m and 3 h, with time intervals of 18–21, 21–00, 00–03, and 03–06

local time (LT) for the use in this paper. BSR data were normalised to unity at the 30–33 km altitude where aerosol backscattering is assumed to be negligible, and PDR values were obtained using the method of Adachi et al. (2001).

The lidar system at Fukuoka (33.55°N, 130.36°E) used in this study is also an Nd:YAG system operated at a wavelength of 532 nm, with PDR measurement capability. This system has been operated manually only during nights under clear-sky/non-rainy conditions; during July–September 2018, the system was operated on 11 nights. Vertical profiles were averaged over 900 m and 4 h for each night for the use in this paper. The PDR for Fukuoka is originally defined as *S/(P+S)*, which has been converted to *S/P* for this paper.

The uncertainties of lidar data ~~are~~ discussed here~~, which~~ are ~~applied~~ applicable to ~~the~~ both systems. The BSR uncertainties were estimated as follows. The random component was estimated from the photon counts of the backscatter signals at 532 nm after temporal and vertical averaging by assuming Poisson statistics. Other sources of BSR uncertainties (biases) were estimated by assuming the uncertainty of the normalization value of BSR with 8.5×10^{-3} (Russell et al., 1979, 1982) and that of the extinction-to-backscatter ratio with 30 sr (Jäger and Hofmann, 1991; Jäger et al., 1995). The total uncertainty of BSR were then estimated to be 2–3 % typically around the tropopause.~~The BSR uncertainties were estimated from the photon counts of the backscatter signals at 532 nm by assuming Poisson statistics to be 2–3 % typically around the tropopause.~~ The PDR uncertainties were estimated from the parallel and perpendicular components of backscatter signals at 532 nm. Other sources of PDR ~~uncertainty~~ uncertainties (biases) include (1) the uncertainty in calibration of the total depolarization ratio (TDR), due to both particles and air molecules, and (2) the BSR uncertainty. Uncertainty (1) was estimated as follows. In the TDR calibration (Adachi et al., 2001), we subtracted depolarization caused by the lidar system (DEPsys) estimated from the observed TDR and BSR obtained in the altitude region where aerosol backscattering is negligible (i.e., BSR equals unity, and TDR equals the molecular depolarization ratio), or where spherical particles predominate (i.e., in lower tropospheric water clouds). DEPsys errors result in PDR bias. For example, a DEPsys error of ±0.2% results in a ±2% bias in PDR where BSR = 1.1. Uncertainty (2) arises mainly from our assumption that aerosol backscattering is negligible at 30–33 km altitude. We also assumed an aerosol extinction-to-backscatter ratio of 50 sr over the whole measurement height range. These assumptions result in errors in BSR and thus PDR. For example, BSR errors of +0.05 and –0.05 result in a bias of –1% and +3% in PDR, respectively, where BSR = 1.1 and TDR = 0.7%. Based on these considerations, we estimate that the total PDR uncertainty (random plus bias errors) is ≤±5% PDR.

2.2 Other data

Backward trajectories are calculated using the trajectory model used by Inai (2018) and Inai et al. (2018) and the most recent global atmospheric reanalysis dataset by the European Centre for Medium-Range Weather Forecasts (ECMWF), ERA5 (Hersbach et al., 2020), with 37 pressure levels up to 1 hPa and horizontal and temporal resolutions of 0.25° × 0.25° and 1 h,

respectively. ERA5 temperature data in the tropical tropopause layer have been evaluated by Tegtmeier et al. (2020). Lagrangian transport calculations using ERA5 and its predecessor ERA-Interim have been compared by Hoffmann et al. (2019) and Li et al. (2020).

The Copernicus Atmosphere Monitoring Service (CAMS) atmospheric-composition reanalysis dataset produced by the ECMWF (Inness et al., 2019) is used to analyse signatures of the ASM anticyclone and its eastward shedding vortices, with 25 pressure levels up to 1 hPa and horizontal and temporal resolutions of 0.75° × 0.75° and 3 h, respectively. Carbon monoxide (CO), temperature (T), and ~~potential vorticity~~ geopotential (Φ) data are primarily analysed in this paper. CO is chosen because it is a good tracer for polluted air of surface origin (e.g., Luo et al., 2018). Although CO and ATAL aerosol particles do not necessarily have the same emission sources, CO is a good chemical tracer to indicate~~d~~ the location of the ASM anticyclone. CO data on pressure levels are projected on~~-~~to isentropic surfaces using temperature data. In the CAMS, the Measurement of Pollution in the Troposphere (MOPITT) thermal infrared (TIR) satellite total-column CO data are assimilated, but~~,~~ Microwave Limb Sounder (MLS) and Infrared Atmospheric Sounding Interferometer (IASI) CO data are not. CAMS CO data are originally provided in mass mixing ratio, kg kg^{-1}, which are converted to volume mixing ratio, ppbv, for this study. It is noted that a quick comparison with MLS Version 4.2 Level 2 CO data (Santee et al., 2017; Livesey et al., 2020) at 400 K isentropic surface (in the form of longitude-time diagram like the one in Section 3.2) shows that CAMS CO data are roughly ~10 ppbv greater than MLS CO over Japan during August–September 2018, but also shows that eastward extension signals coming over Japan agree fairly well qualitatively within the differences in spatio-temporal sampling of the two datasets. The CAMS dataset also includes different types of aerosol particles, but they are not included in this study because relevant variables such as aerosol BSR and NH_4NO_3 concentration are not included. Montgomery streamfunction (MSF), defined as MSF = $c_p T + \Phi$, where c_p is specific heat of dry air at constant pressure, in isentropic coordinates corresponds to geopotential (height) in ~~pressure~~isobaric coordinates (e.g., Amemiya and Sato, 2018; Salby, 1996), and thus is a good dynamical indicator of the ASM anticyclone. Potential vorticity (PV) on isentropic surfaces (e.g., at 360–380 K) is often used ~~projected on to isentropic surfaces calculated from CAMS data are also analysed because it is often used~~ as a dynamical tracer in studies of the ASM anticyclone (e.g., Popovic and Plumb, 2001; Garny and Randel, 2013; Ploeger et al., 2015; Amemiya and Sato, 2018); however, PV at and above 400 K (this isentropic surface will be focused in Section 3.2) is not very useful to analyse the ASM anticyclone boundary. Thus, we will analyse MSF at~~on~~ 400 K surface calculated from CAMS data. ~~In addition,~~

MLS Version 4.2 Level 2 water-vapour data (Santee et al., 2017; Livesey et al., 2020) are analysed because water vapour is also a good tracer of the ASM anticyclone. We use MLS data rather than CAMS data for lower stratospheric water vapour because MLS data have been well validated with e.g., balloon-borne frost-point hygrometers (e.g., Hurst et al., 2016; Fujiwara et al., 2010; Vömel et al., 2007), while reanalysis water vapor data are in general less reliable in the lower stratosphere (e.g., Davis et al., 2017). We found that CAMS water vapour volume mixing ratio data (converted from the original specific humidity

data) are greater than MLS data at 400 K isentropic surface over Japan during July–September 2018 (e.g., the differences are roughly ~2 ppmv for the wet signals around the longitudes of Japan in August 2018).

The possible influence of volcanic eruptions and wildfire events is investigated using two satellite aerosol-particle datasets, one providing vertical extinction profile data at 675 nm from the Ozone Mapping and Profiler Suite (OMPS) Limb Profiler (LP), Level 2 Version 1.5 (Chen et al., 2018), and the other attenuated scattering-ratio data from the CALIOP onboard the Cloud–Aerosol Lidar and Infrared Pathfinder Satellite Observation (CALIPSO) satellite (Thomason et al., 2007; Winker et al., 2007, 2010). CALIOP Level 3 monthly-mean stratospheric aerosol data (CAL_LID_L3_Stratospheric_APro-Standard-V1-00) are used in this study; in this data product, clouds and Polar Stratospheric Clouds (PSCs) have been removed based on the information of particulate extinction-to-backscatter (lidar) ratio and the multiple-scattering factor profile (Young and Vaughan, 2009; Kim et al., 2018; https://www-calipso.larc.nasa.gov/resources/calipso_users_guide/data_summaries/l3/lid_l3_stratospheric_apro_v1-00_v01_desc.php).

3 Results and discussion

3.1 Lidar measurements

Time–height distributions of BSR and PDR observed in the UTLS at Tsukuba are shown in Figure 1, and the corresponding vertical profiles are shown in Figure 2. Because the PDR has more missing data points, the TDR time–height distribution is also shown in Figure A1. Days ~~that are~~with missing data (white regions; Fig. 1) are due to thick summer-time rain clouds in the lower-to-middle troposphere, which prevented the laser light reaching the middle stratosphere. However, some events with enhanced particle signals are evident just above the tropopause at 15.5–18 km, and last for a few days, mainly in August, but with some in September. In particular, the event peaking at around 21 August and spanning 18–26 August was the strongest one among those the lidar successfully measured during the three-month period. We also observe another strong event around 9 August at 15–17 km, although missing observations before and after this date prevent from characterizing the temporal scale of the event; furthermore, the tropopause height was highly variable around this date and was located at 17 km on that date, situating the aerosol enhanced layer temporarily in the troposphere. Fig. 2 shows that enhanced particle signals at 15.5–18 km were often observed in August, sometimes in September, but not in July. Typical BSR and PDR values of enhanced signals are ~1.10 (1.07–1.18) and ~5% (3%–10%), respectively (Figs. 1 and 2). Below the tropopause, strong signals were sometimes recorded with BSR values of >1.25 and with PDR values >>10%. In general, the PDR values are 0% for spherical particles (i.e., water clouds in the troposphere and liquid H_2SO_4 particles in the stratosphere) and are >25%–30% for ice cirrus particles (e.g., Sakai et al., 2003; Fujiwara et al., 2009). Strong signals in the upper troposphere are thus due to ice cirrus clouds. Enhanced signals in the lower stratosphere (15.5–18 km) may be due to solid particles, as indicated by the PDR values of ~5% (3%–10%). Taking PDR uncertainties (Sect. 2.1) into account, these

values can be considered as small, but non-zero, values. The PDR values of these signals, together with the region being above the local tropopause in most cases, strongly suggest that they are not ice cirrus particles. However, the possibility of a mixture of spherical H_2SO_4 particles (i.e., background stratospheric sulphate particles) and highly non-spherical particles, such as ice, volcanic ash (Prata et al., 2017), and wildfire smoke (Haarig et al., 2018), cannot be precluded only with our lidar data. We will come back to this issue in Sect. ~~4~~ 3.3 after investigating several other data. Before looking at the Fukuoka results, it is noted that for Tsukuba data we do not plot the data with "relative" uncertainty of PDR larger than 30%; this treatment resulted in removing data points with BSR values lower than ~1.05 where background spherical sulphate particles (with PDR values of <2%) were presumably predominant.

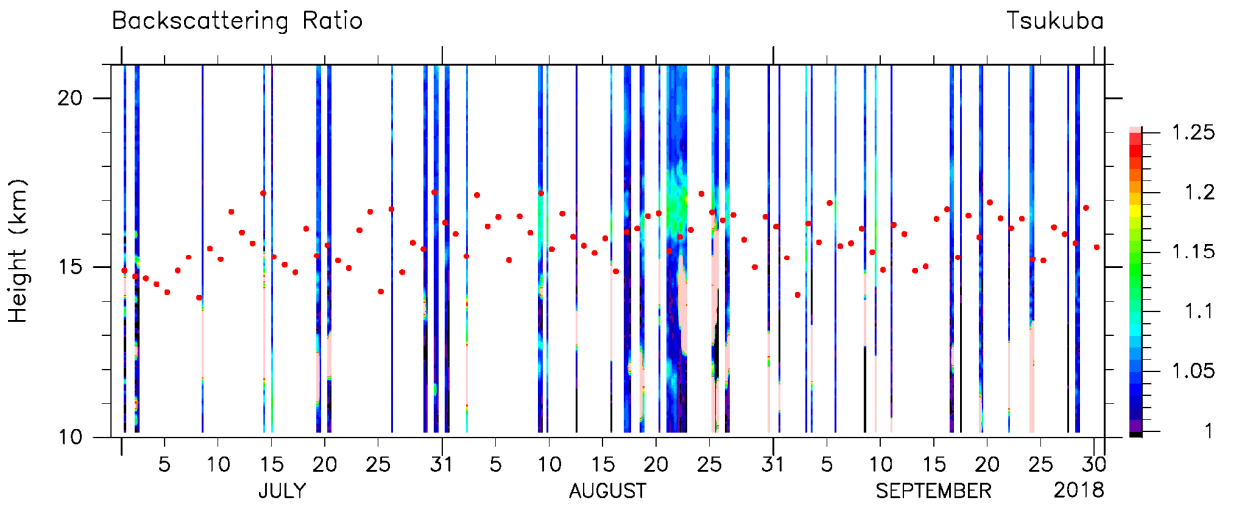
Backscattering Ratio
Tsukuba
Height (km)
20
15
10
1.25
1.2
1.15
1.1
1.05
1
5 10 15 20 25 31 5 10 15 20 25 31 5 10 15 20 25 30
JULY
AUGUST
SEPTEMBER
2018

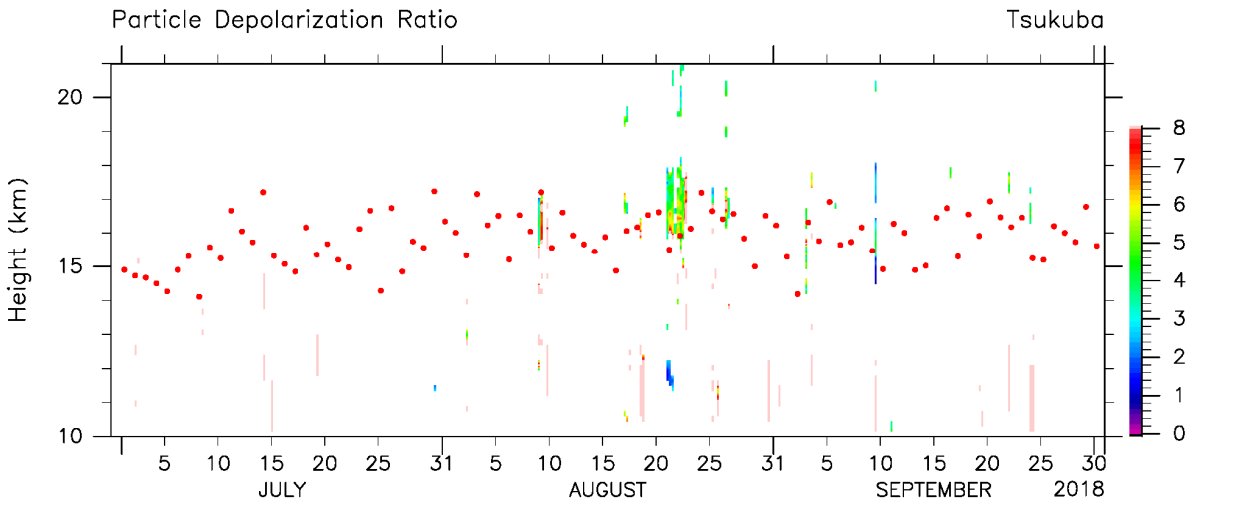
Particle Depolarization Ratio
Tsukuba
Height (km)
20
15
10
8
7
6
5
4
3
2
1
0
5 10 15 20 25 31 5 10 15 20 25 31 5 10 15 20 25 30
JULY
AUGUST
SEPTEMBER
2018

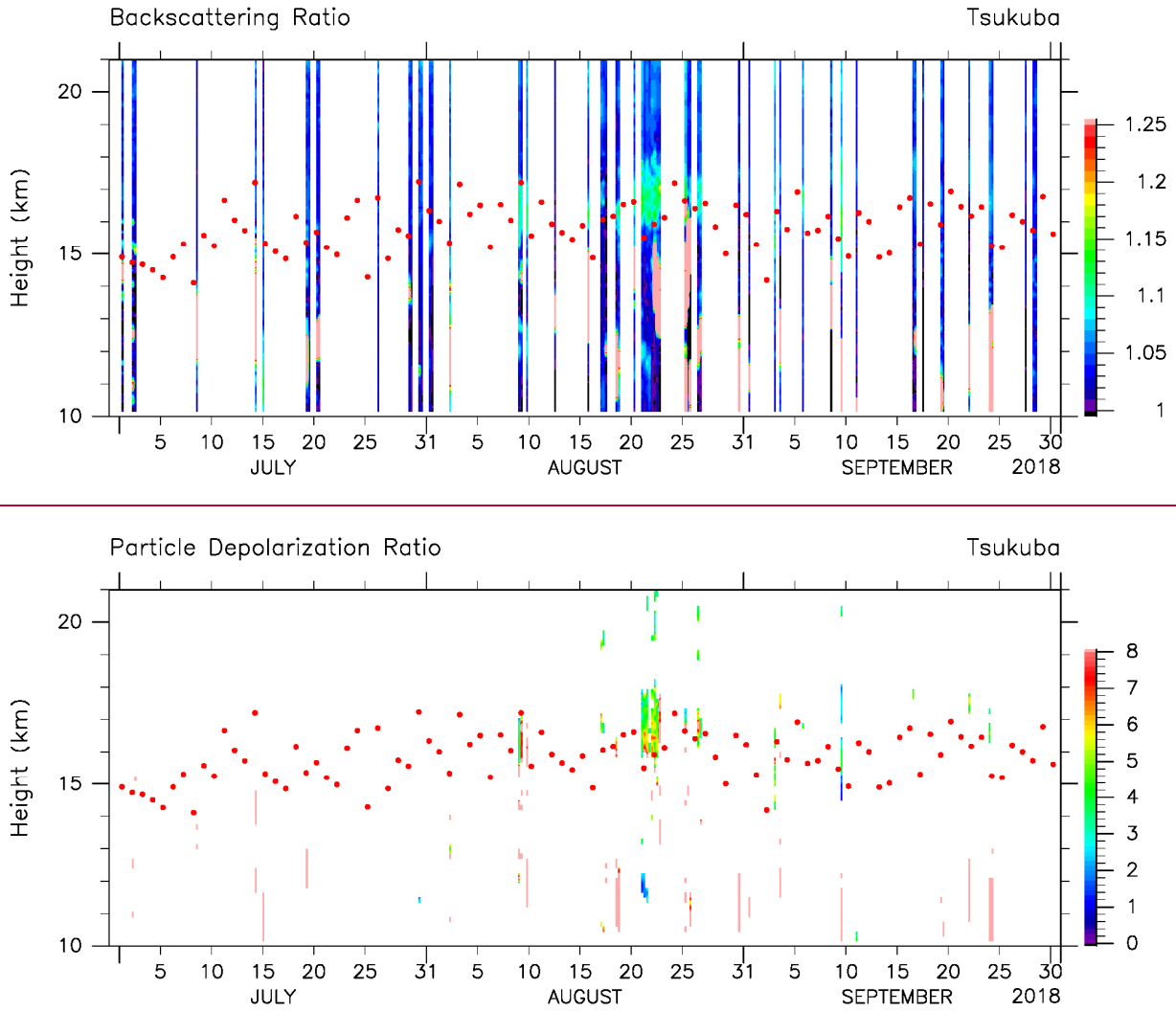

Figure 1 Time–height distributions of (top) backscattering ratio and (bottom) particle depolarization ratio (%) during July–September 2018, as measured using the lidar system at MRI, Tsukuba. For each day, four time slots (i.e., 18–21, 21–00, 00–03, and 03–06 LT) are prepared, with 3-h averaged data filling the slots where thick lower-to-middle tropospheric clouds do not exist. Red dots indicate the daily (first) lapse-rate tropopause locations determined by the Japan Meteorological Agency (JMA), based on 21 LT radiosonde data taken at the JMA "Tateno" site (which shares the same site as the MRI).

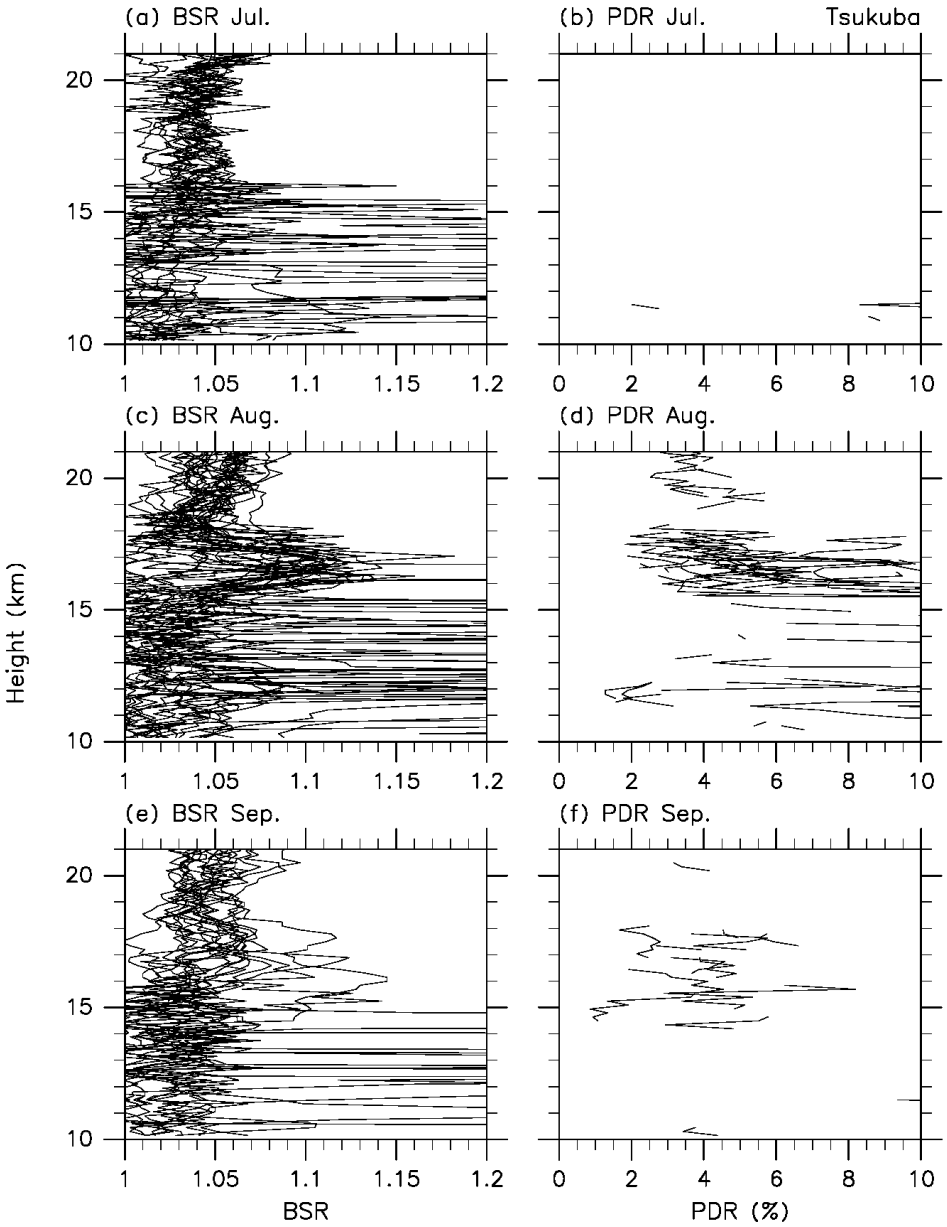

220 **Figure 2** Vertical profiles of (a, c, e) backscattering ratio (BSR) and (b, d, f) particle depolarization ratio (PDR, in %) in (a, b) July, (c, d) August, and (e, f) September 2018 obtained using the lidar system at MRI, Tsukuba. It is noted that strong and noisy signals in BSR below ~15.5 km are due to cirrus clouds.

Vertical profiles of BSR and PDR observed at Fukuoka for 11 clear-sky/non-rainy nights during July–September 2018~~,~~ are shown in Figure 3. Again, enhanced particle signals were observed mainly in August above the tropopause at 15.5–18 km. The BSR values were in the range 1.09–1.14, with PDR values of 1%–3% which are smaller than those observed at Tsukuba. It should be noted that the dates of lidar operation at Fukuoka did not overlap those at Tsukuba when strong enhancement was observed above the tropopause (e.g., 9 August, 18–26 August, and 9 September), perhaps partly explaining the differences between Figs. 2 and 3.

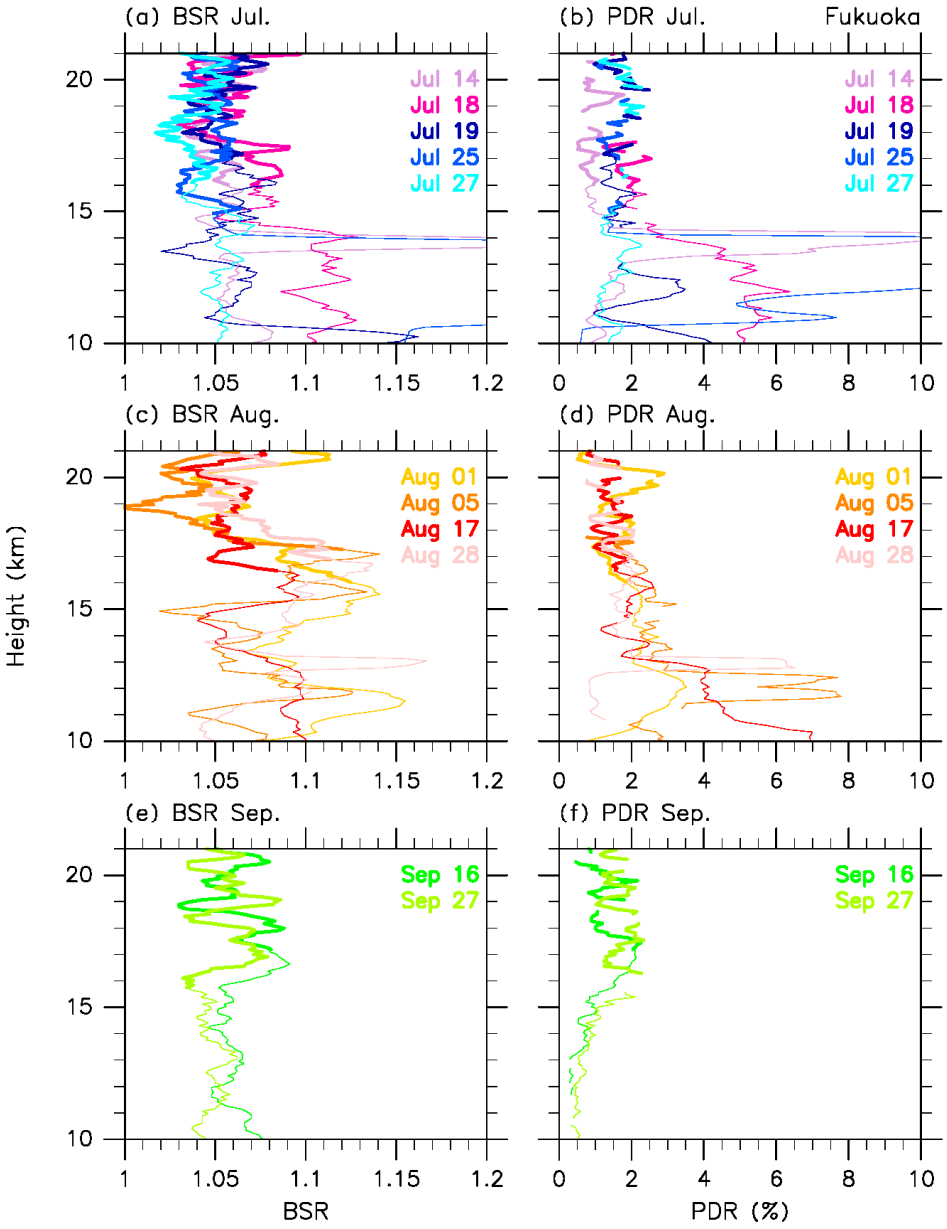

235 **Figure 3** Eleven vertical profiles of (a, c, e) backscattering ratio (BSR) and (b, d, f) particle depolarization ratio (PDR, in %) in (a, b) July, (c, d) August, and (e, f) September 2018 obtained using the lidar system at Fukuoka. Dates and colours are assigned in the legend where, for example, "Jul 14" refers to the night of July 14–15. Stratospheric portion of the profiles has been thickened using the daily (first) lapse-rate tropopause location information provided by the JMA, based on operational 21 LT radiosonde data taken at the JMA Fukuoka site (~~with~~ at a ~4 km distance from the lidar site).

240

3.2 Trajectories and airmasses

Ten-day kinematic backward trajectories (using vertical wind) from Tsukuba and Fukuoka are shown in Figures 4 and 5, respectively, with contrasting cases with or without aerosol particle enhancement in the 390–410 K potential-temperature range (around 16.5–17.5 km at these stations). A potential temperature of 400 K corresponds to altitudes of ~17.1 km at Tsukuba and ~17.3 km at Fukuoka, on average, during July–September 2018 (based on twice-daily radiosonde data at each site, taken from http://weather.uwyo.edu/upperair/sounding.html), i.e., near the centre of the lower stratospheric BSR enhancement. By comparing the results from Santee et al. (2017) with our own analysis, ~~The~~ the 65 ppbv contours of monthly mean CAMS CO data at ~~a~~ 400 K potential temperature are ~~shown~~ chosen as an index of the boundaries of the ASM anticyclone (i.e., within the anticyclone, CO concentration is >65 ppbv). These trajectories indicate that airmasses over both stations come mainly from the west, and sometimes via the north of Japan (indicative of the existence of vortices), and originated from the ASM anticyclone well within 10 days. They also indicate that airmasses with enhanced aerosol particles at this height tend to originate in regions within the ASM anticyclone at the altitudes 16.5–18 km, i.e., around or just below the tropopause, whereas those without enhanced aerosol particles tend to originate from edge regions surrounding the anticyclone. Note that there is a trajectory that originates in the Pacific south of Japan as low as 4 km (Figure 4, bottom, a small-scale spiral in purple); this is associated with upward transport in the typhoon Soulik.

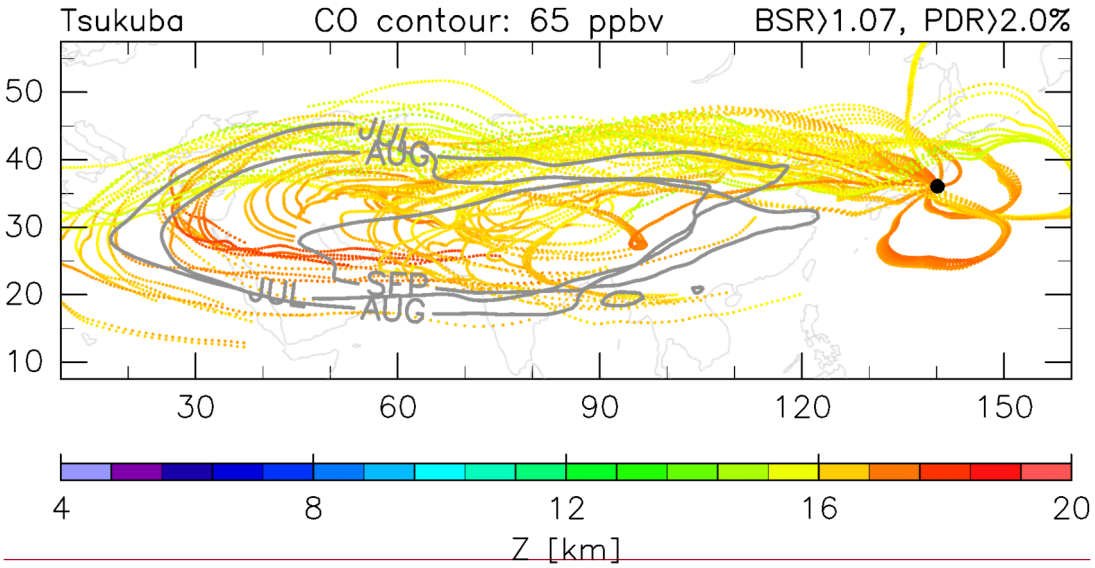
Tsukuba
CO contour: 65 ppbv
BSR>1.07, PDR>2.0%
50
40
30
20
10
30
60
90
120
150
JUL
AUG
JUL
SEP
AUG
4
8
12
16
20
Z [km]

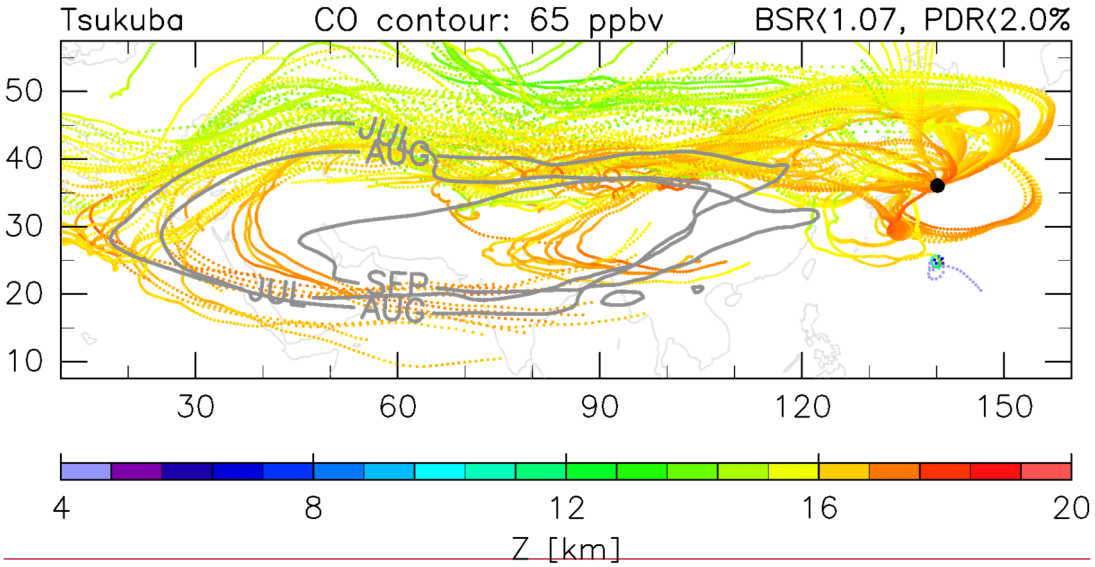
Tsukuba
CO contour: 65 ppbv
BSR<1.07, PDR<2.0%
50
40
30
20
10
30
60
90
120
150
JUL
AUG
JUL
SEP
AUG
4
8
12
16
20
Z [km]

260

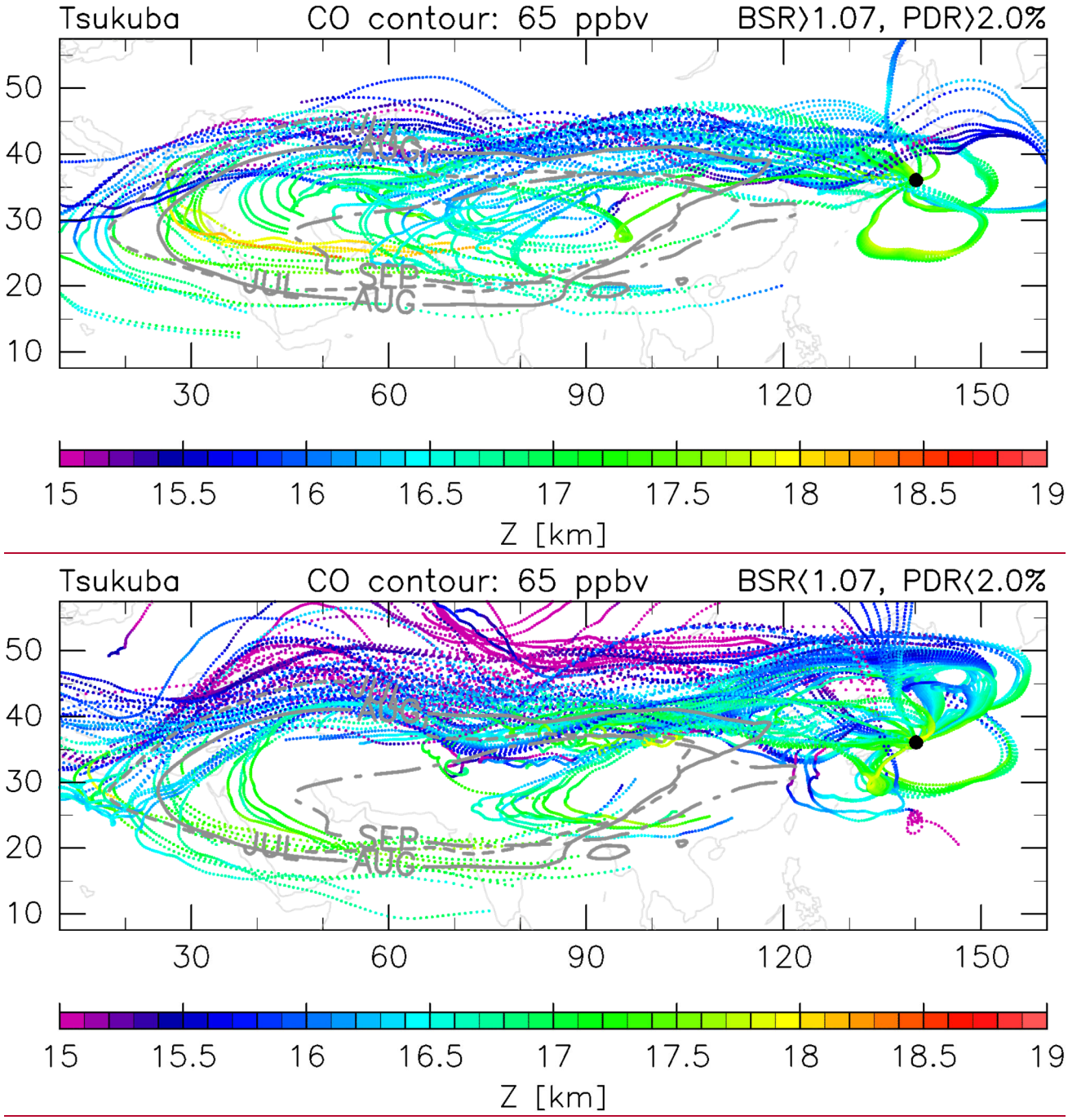

Figure 4 Kinematic backward trajectories for 10 days starting from Tsukuba in the 390–410 K potential temperature range at 100 m geopotential height intervals on all days during July–September 2018 on which measurements were made, using ERA5 reanalysis data. Cases are sorted into two categories: (top) with and (bottom) without enhanced aerosol signals observed by lidar at the trajectory starting points. The conditions and number of trajectories for the former and the latter cases are, respectively, BSR > 1.07; PDR > 2.0%; 78

trajectories and BSR < 1.07; PDR <2.0%; 136 trajectories. Colours indicate geopotential height (Z) values of the trajectories. Grey contours indicate 65 ppbv monthly mean CAMS CO levels at 400 K potential temperature, roughly indicating monthly mean boundaries of the ASM anticyclone (dotted for July, solid for August, and dash-dotted for September).

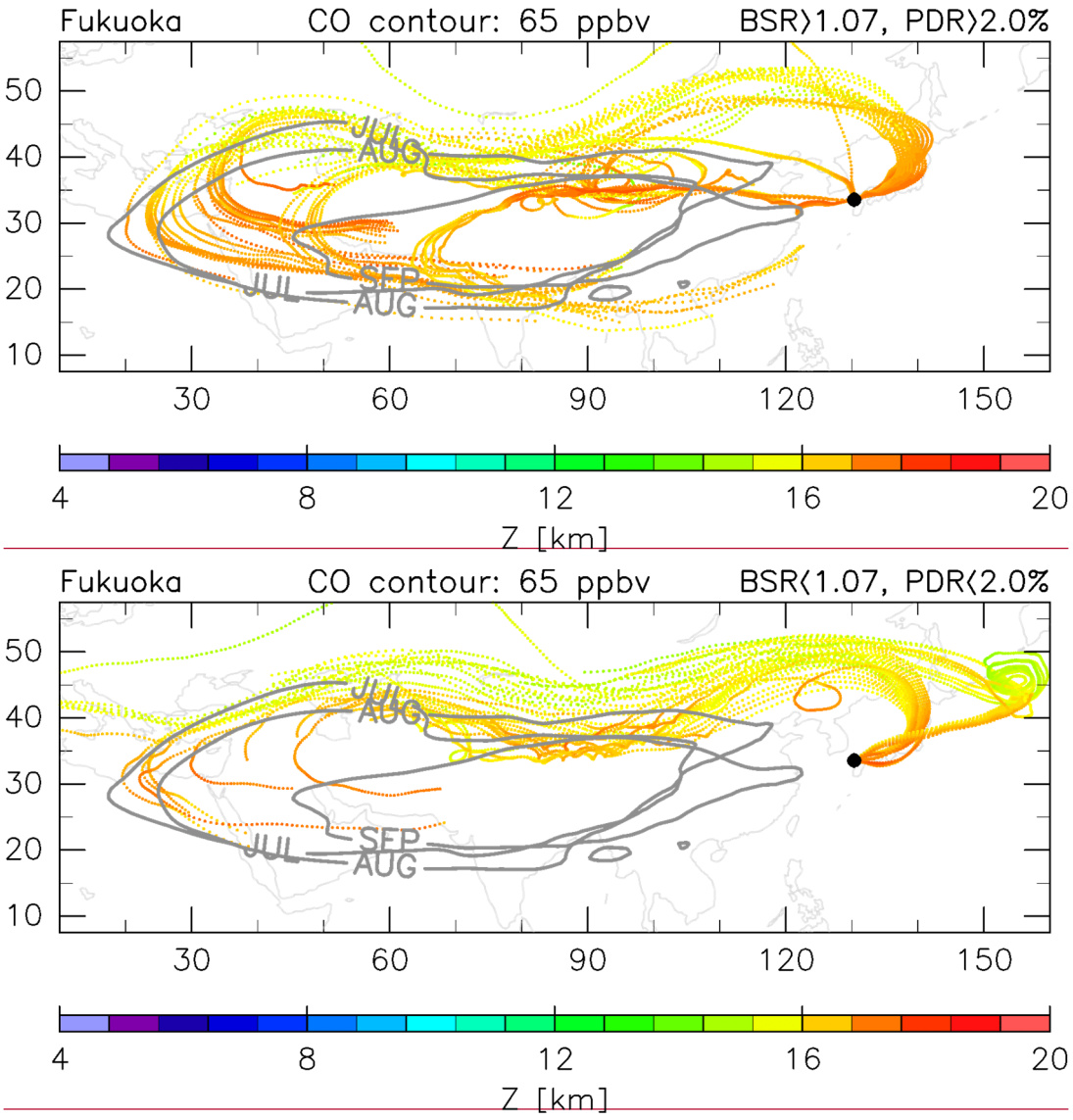

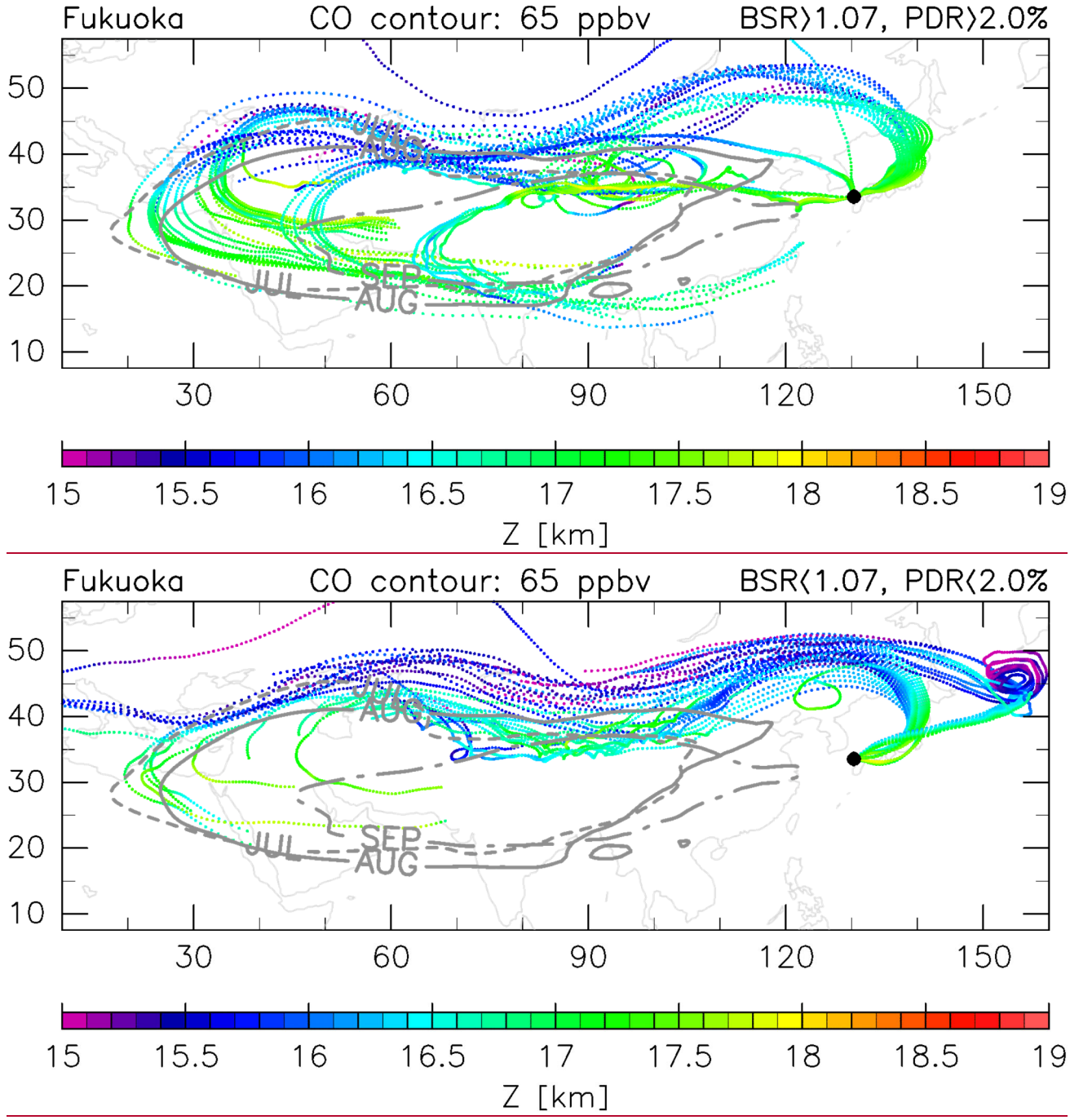

Figure 5 As for Fig. 4, but for trajectories from Fukuoka, with (top) 44 and (bottom) 37 trajectories.

Horizontal distributions of CO and ~~PV~~ MSF at the 400 K potential-temperature surface during 18–23 August 2018 from the CAMS reanalysis data are shown in Figure 6. Again, note that ~~A~~a potential temperature of 400 K corresponds to ~~altitudes of~~ ~17.1 km at Tsukuba and ~17.3 km at Fukuoka~~, on average,~~ during July–September 2018 ~~(based on twice-daily radiosonde data at each site, taken from http://weather.uwyo.edu/upperair/sounding.html), i.e., near the centre of the lower stratospheric BSR enhancement~~. The distribution of MSF indicates the location of the ASM anticyclone from the dynamical viewpoint. The strongest particle signals during the three months were observed on 21 August in the lower stratosphere over Tsukuba. The airmass with high CO concentrations was transported eastward from the ASM anticyclone centred over the Tibetan Plateau (Fig. 6), with an anticyclonic vortex of ~20° longitude scale reaching the Japanese archipelago on 21 August, providing a clear signature of eastward shedding vortices from the ASM anticyclone (e.g., Luo et al., 2018). ~~PV can be regarded as a dynamical tracer, with lower values in the ASM anticyclone along the same latitudes (e.g., 30°N), although background positive gradients in latitude and its noisier nature give more complicated features.~~ Daily averaged longitude–time CO distributions over 30°N–40°N are shown in Figure 7, with that latitude band chosen here because it includes the two lidar sites. The ASM anticyclone spans roughly 15°N–40°N, whereas the eastward shedding vortices are often located slightly to the north, at around 25°N–45°N, as indicated in Figs. 4–6; the latitude band must therefore be chosen carefully, depending on the research focus. In Fig.7, ~~The~~ the 60-ppbv CO contour may be a good indicator of eastward shedding vortices ~~(Fig. 7)~~. In July 2018, the eastward extension was weak, but in August there were three events that directly affected the two lidar sites, at ~~August 5~~3–15, 20–~~25~~ 24 (Fig. 6), and ~~27~~28–31 August. In September, there were three events, at ~~September~~ 3–8, 14–~~19~~ 17, and ~~27~~28–~~30~~ 29 September. A comparison with Fig. 1 indicates that aerosol-particle enhanced events correspond relatively well to CO-enhanced events, although missing lidar data points (due to low-level clouds) result in the fact that only the ~~August~~ 20–25 August event was relatively well observed, with the ~~5~~3–15 August event being captured only on 9 August. The ASM anticyclone is also characterised as an airmass hydrated by active convection from below (e.g., Santee et al., 2017). The longitude–time distribution of MLS water vapour at 400 K, averaged over 30°N–40°N with 8°-longitude and 3-day bins, is shown in Figure 8. The water-vapour-enhanced events over Japan correspond well with the CO-enhanced events over the same region shown in Fig. 7.

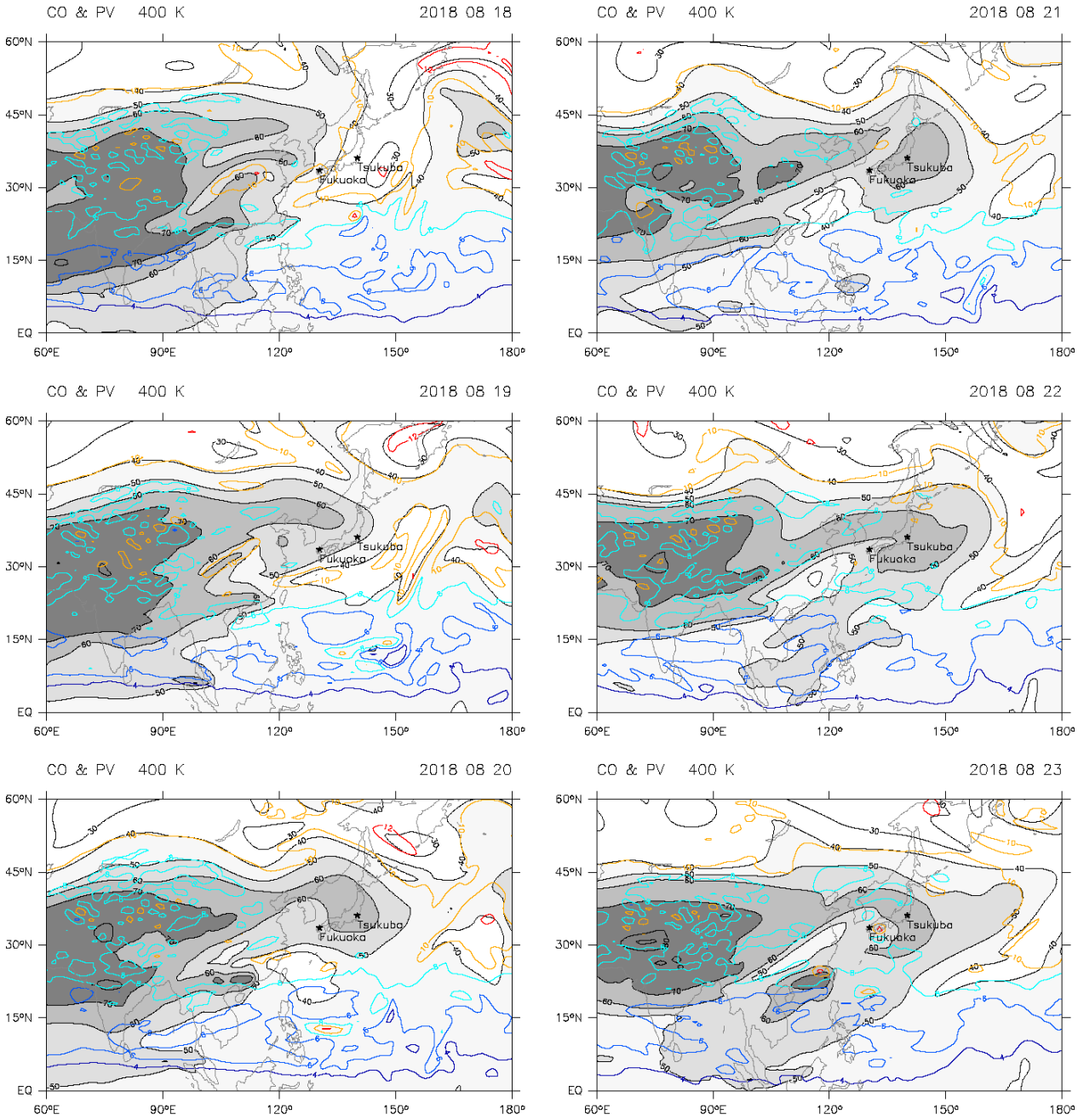
CO & PV 400 K 2018 08 18
CO & PV 400 K 2018 08 21
CO & PV 400 K 2018 08 19
CO & PV 400 K 2018 08 22
CO & PV 400 K 2018 08 20
CO & PV 400 K 2018 08 23
60°N
45°N
30°N
15°N
EQ
60°E
90°E
120°
150°
180°
Tsukuba
Fukuoka

305

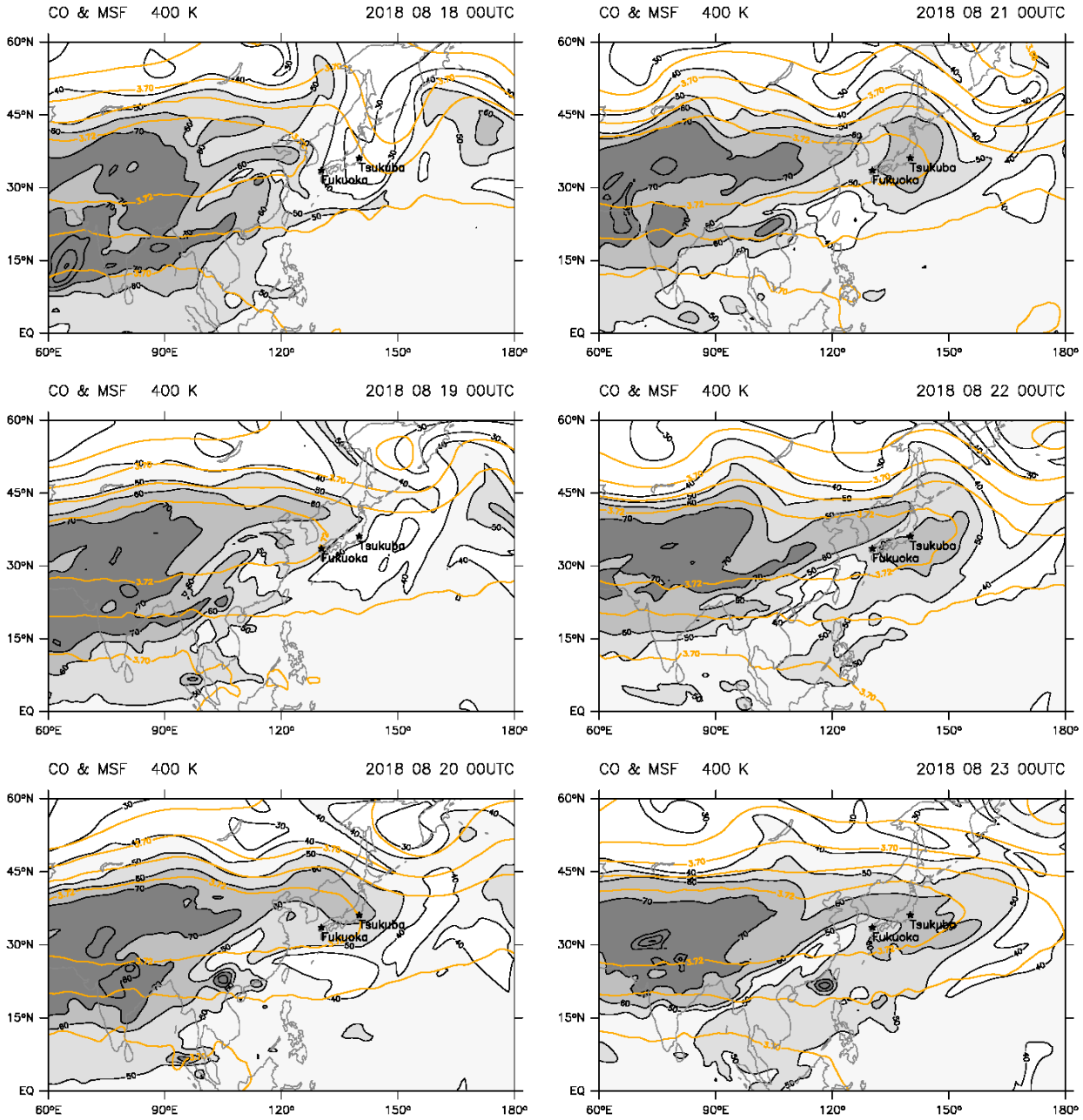

Figure 6 Horizontal distribution of daily, instantaneous (00 UTC) ~~averaged~~ CO (black contours with grey tone, with intervals of 10 ppbv) and ~~potential vorticity~~Montgomery streamfunction (~~PV~~MSF; coloured contours at intervals of ~~2 PV Unit where 1 PV Unit equals to~~ 0.01 × 10^{-6} ~~$^{.5}$K~~ m^2 ~~kg^{-1}~~·s^{-2}~~^{1}~~) at the 400 K potential-temperature level during 18–23 August 2018 (dates indicated at top right of each plot), using CAMS reanalysis data.

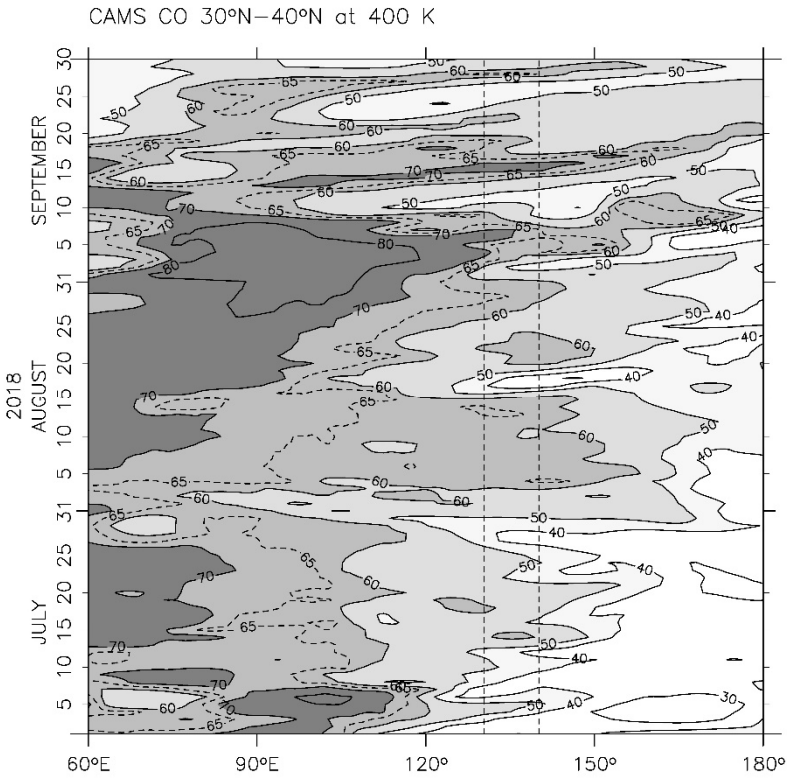
CAMS CO 30°N–40°N at 400 K
2018
JULY
AUGUST
SEPTEMBER
5 10 15 20 25 31 5 10 15 20 25 30
60°E
90°E
120°
150°
180°

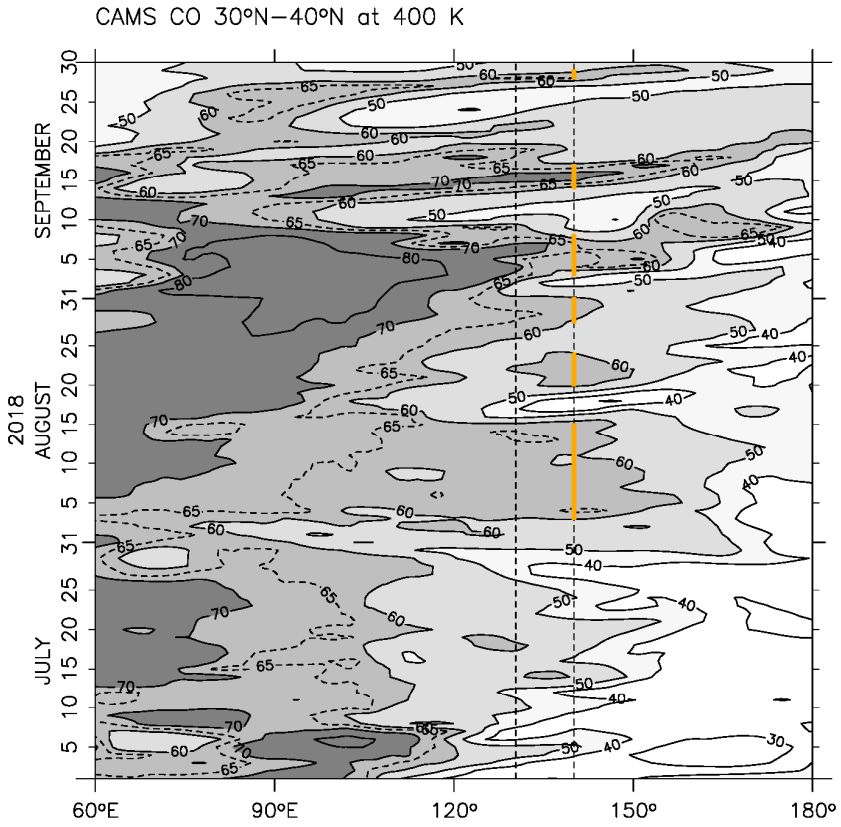

315

Figure 7 Longitude–time distribution of daily averaged CO concentration at 400 K potential temperature averaged over 30°N–40°N, using CAMS reanalysis data. The contour interval is 10 ppbv, with 65 ppbv contours added (dotted). Vertical dotted lines indicate the locations of the two lidar sites, Fukuoka (130.36°E) and Tsukuba (140.1°E)~~,~~; furthermore, the periods along the longitude of Tsukuba when CO concentration was ≥~60 ppbv (i.e., 3–15, 20–24, and 28–31 August, and 3–8, 14–17, and 28–29 September) are shown as orange line segments.

320

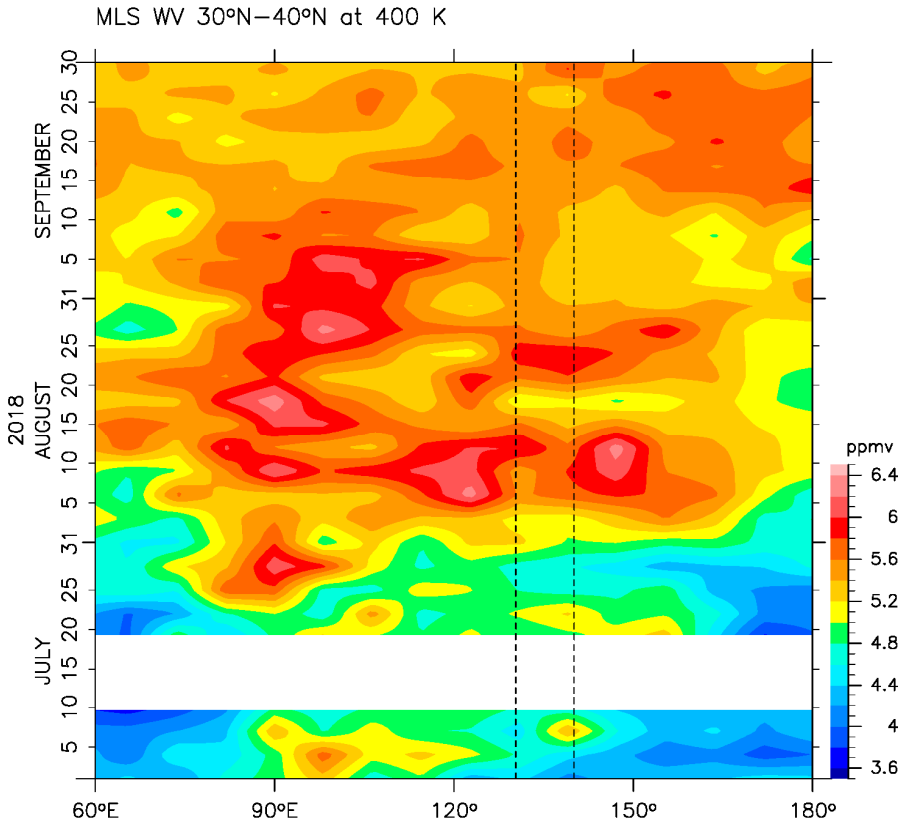
MLS WV 30°N–40°N at 400 K
2018
JULY
AUGUST
SEPTEMBER
5 10 15 20 25 31 5 10 15 20 25 31 5 10 15 20 25 30
60°E
90°E
120°
150°
180°
ppmv
6.4
6
5.6
5.2
4.8
4.4
4
3.6

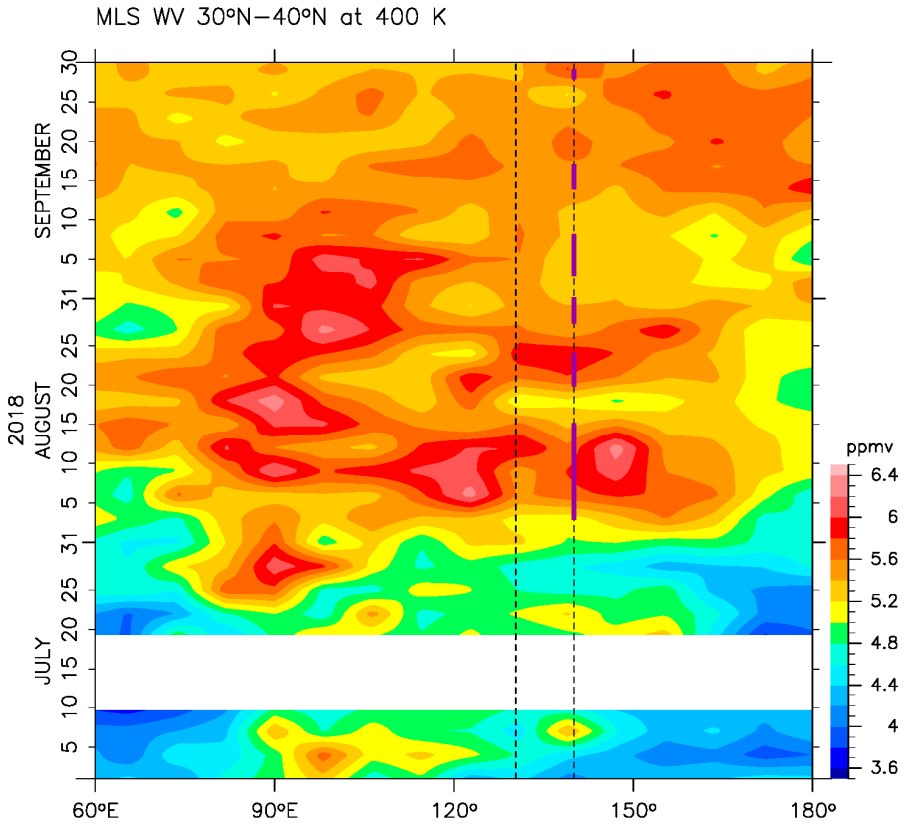

Figure 8 As for Fig. 7, but for water vapour (in ppmv) at 400 K measured with the satellite MLS instrument. Data for the 30°N–40°N region have been aggregated into 3-day and 8°-longitude bins, each constituting about 10 individual data points. The white region indicates missing measurements. The purple line segments are the same ones but in orange in Fig. 7.

3.3 ~~Satellite aerosol data~~Investigation of other potential causes

Lidar is sensitive to various types of volcanic aerosol (e.g., Yasui et al., 1996; Sakai et al., 2016; Khaykin et al., 2017). The lower stratosphere is continuously influenced by volcanic eruptions (GVP, 2013), which inject various types of particles and gases into the atmosphere (e.g., Robock, 2000). Among them, solid ash particles may remain in the stratosphere for up to a few months, while liquid H_2SO_4 particles resulting from reaction of volcanic SO_2 and H_2S gases with OH and H_2O may remain for a year or more. Aerosol particles are also emitted from biomass burning and forest fires and, although these particles rarely reach the stratosphere, extensive fire events can influence the stratospheric aerosol loading (e.g., Khaykin et al., 2018; Peterson et al., 2018). In this section, the global lower-stratospheric aerosol loading during the summer of 2018 is investigated by the analysis of satellite aerosol data.

The time–latitude distribution of zonal-mean lower-stratospheric aerosol optical depth (AOD) at 675 nm from the OMPS LP satellite instrument is shown in Figure 9. At high NH latitudes, the lower-stratospheric AOD increased in the summer of 2017 due to extensive wildfires in Canada (Khaykin et al., 2018; Peterson et al., 2018), but their influence ~~was~~ became negligible by early 2018. In July 2018, the eruption of Ambae (or Aoba; 15.389°S, 167.835°E; GVP, 2019), Vanuatu, in the tropical western Pacific, caused increasing stratospheric AOD in the tropics. We also observed very weak signals around the same latitude from the beginning of April 2018, possibly due to the eruption of the same Ambae during March–April 2018 (GVP, 2018). However, the lower stratospheric AOD at 25°N–40°N was relatively low during July–September 2018, at least on a zonal-mean scale. The monthly mean CALIOP attenuated scattering-ratio distribution due to aerosol particles at 17 km in July and August 2018 is shown in Figure 10 where the ATAL is evident, with enhanced aerosol signals over the ASM region. In August there was also a hint of eastward extension of the ATAL to Japan, with a slight increase in the scattering ratio. By August, effects of the Ambae eruption had extended to about half of the tropics, but ~~not have~~ had not reached Japan directly, at least not in a monthly mean view (see also the 10-day backward trajectories; Figs. 4 and 5).

Finally, Chouza et al. (2020) showed that lidar measurements at Mauna Loa, Hawaii, indicated no signals from volcanic eruptions during the summer of 2018. Also, at the OHP lidar site in France (43.9°N, 5.7°E), no enhancement in the lower stratospheric aerosol abundance was observed during the summer of 2018. In summary, enhanced aerosol particle signals observed at Tsukuba (36.1°N) and Fukuoka (33.55°N) were thus unlikely to be due to volcanic eruptions or northern wildfires.

360

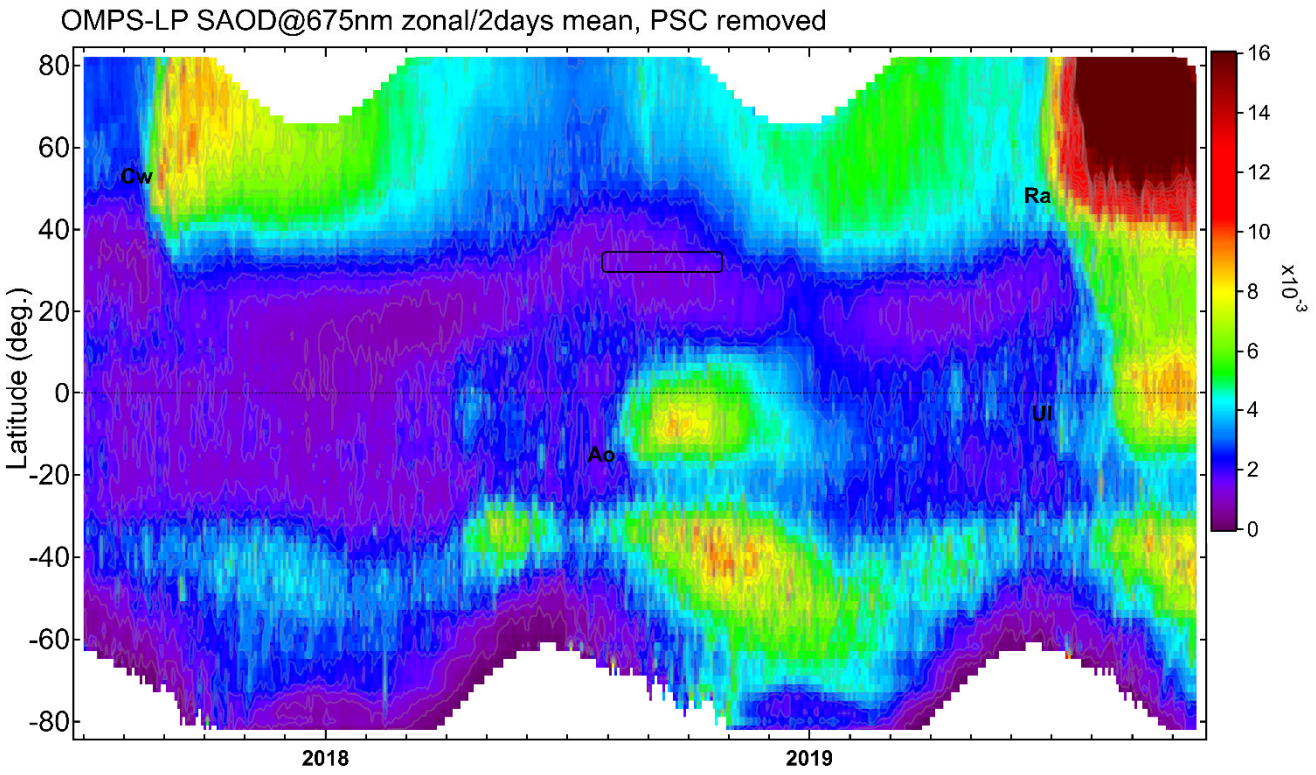
OMPS-LP SAOD@675nm zonal/2days mean, PSC removed
Latitude (deg.)
80
60
40
20
0
-20
-40
-60
-80
2018
2019
Cw
Ra
Ao
Ul
16
14
12
10
8
6
4
2
0
x10-3

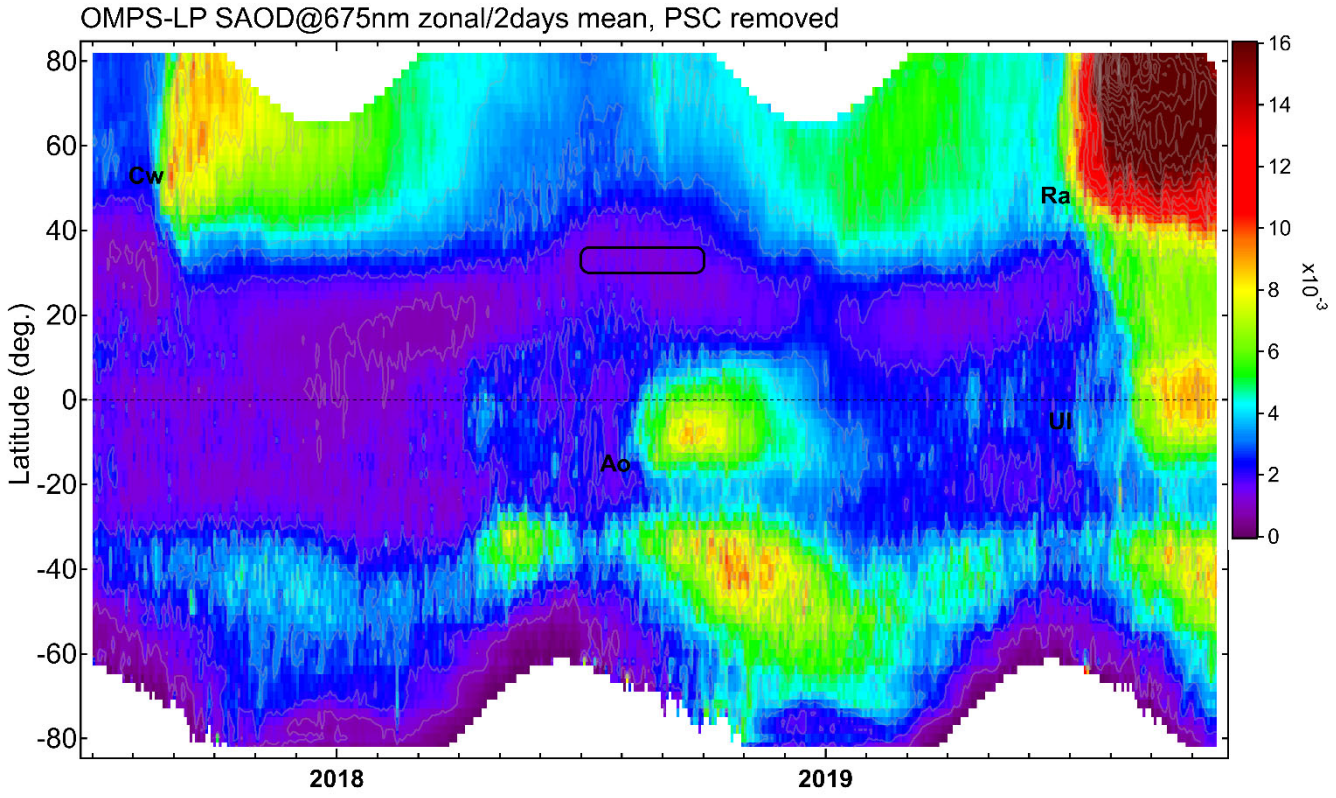

Figure 9 Time–latitude distribution of zonal- and 2-day-mean lower-stratospheric aerosol optical depth at 675 nm between the tropopause and 21 km altitude, from July 2017 to October 2019, as calculated from OMPS LP satellite data. The tropopause altitude for each OMPS LP profile was provided within the OMPS LP dataset. Signals due to Polar Stratospheric Clouds (PSCs) have been removed. Major events that significantly enhanced NH stratospheric aerosol loading are labelled: Cw, Canadian wildfires in the summer of 2017; Ao, Ambae (Aoba) eruption, Vanuatu (July 2018); Ra, Raikoke eruption, Kuril Islands, Russia (June 2019); Ul, Ulawun eruption, Papua New Guinea (July, August, and October 2019) (GVP, 2013). The ~~R~~rectangular box indicates the period and location of the lidar measurements; white regions indicate missing measurements.

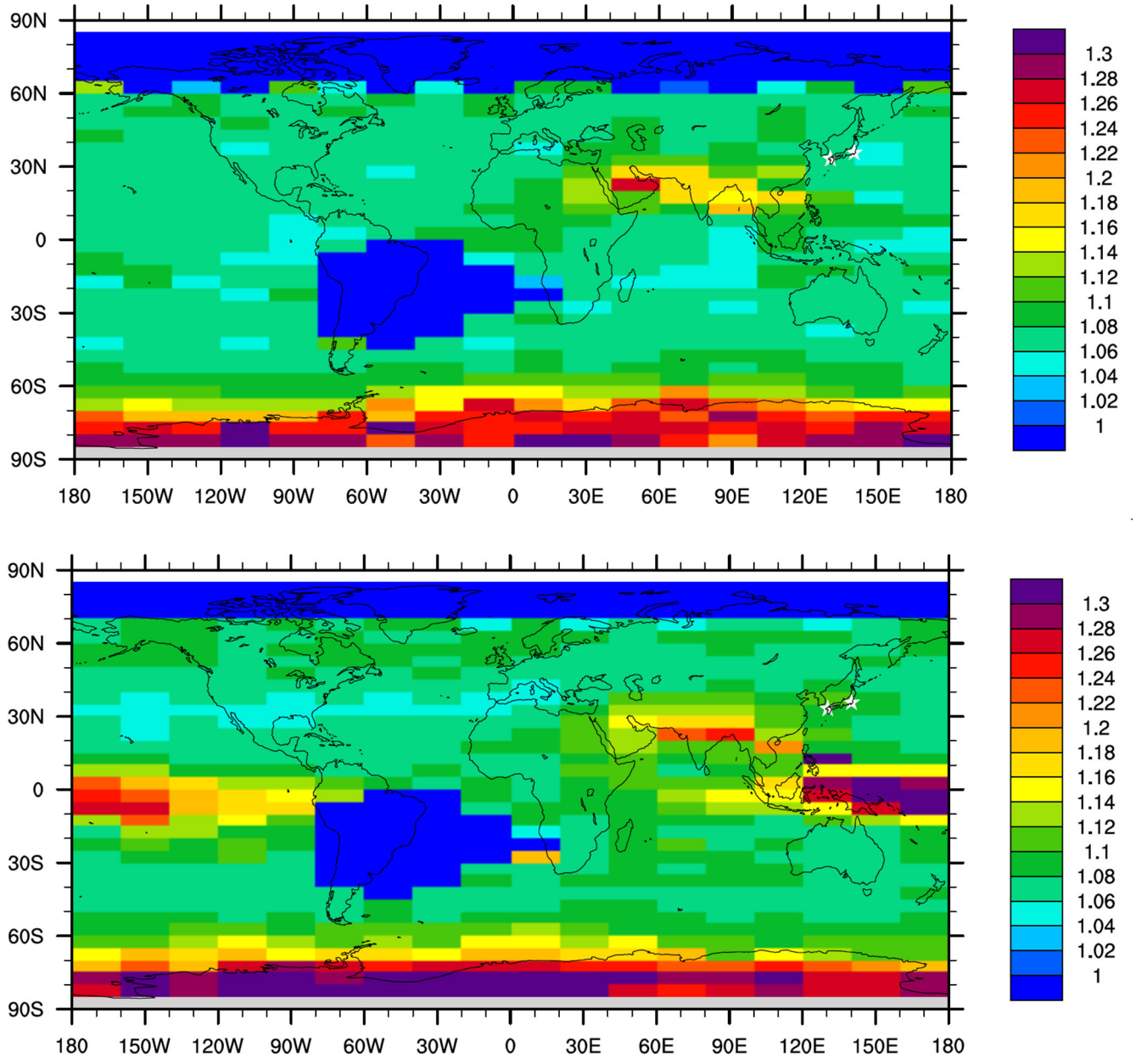
90N
60N
30N
0
30S
60S
90S
180
150W
120W
90W
60W
30W
0
30E
60E
90E
120E
150E
180
1.3
1.28
1.26
1.24
1.22
1.2
1.18
1.16
1.14
1.12
1.1
1.08
1.06
1.04
1.02
1

375

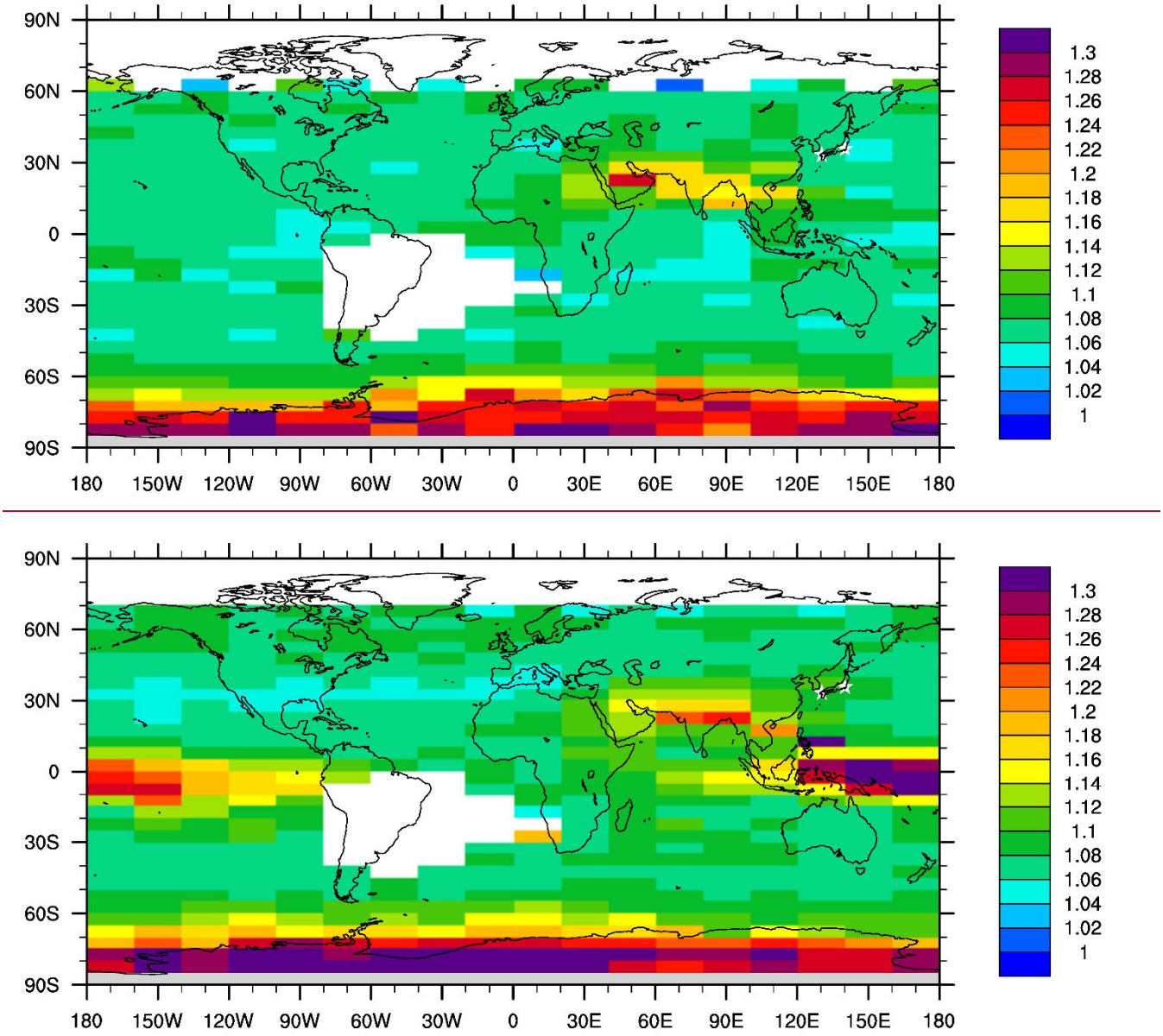

Figure 10 Monthly mean horizontal distribution of attenuated scattering ratio at 17.042 km observed with the CALIOP satellite instrument in (top) July 2018 and (bottom) August 2018. Spatial bins are 5° in latitude, 20° in longitude, and 900 m in altitude. Clouds and PSCs have been removed (Sect. 2.2). It is noted that the CALIOP attenuated scattering ratio is defined as the ratio of the measured attenuated backscatter coefficients and the attenuated backscatter coefficients calculated from the molecular model, and its valid range is from 0.60 and 25.00. The two lidar station locations are marked with white stars. White regions indicate missing measurements. (See Noel et al. (2014) for the data missing over the South Atlantic region).

4 Summary and conclusions

Lidar aerosol-particle measurements made at Tsukuba and Fukuoka, Japan, during the summer of 2018~~,~~ were investigated to determine whether these lidars are capable of detecting the eastward extension of the ATAL from the ASM anticyclone in the UTLS. Both lidars observed enhanced aerosol-particle signals between the local tropopause and up to a few km above it, with ~~the~~ BSR values of ~1.10 (1.07–1.18) and PDR values of ~5% (3%–10%) at Tsukuba and with similar BSR but lower PDR values at Fukuoka. The PDR difference between the two sites may be due to the Fukuoka lidar operating on only 11 nights during the three-month period and due to the fact that the dates of lidar operation at Fukuoka did not overlap those at Tsukuba when strong enhancement was observed. The lidars often detected strong signals (BSR values of >1.25 and with PDR values >>10%) due to ice cirrus clouds below the tropopause. The Tsukuba measurements indicated that timescales of lower-stratospheric enhancements are ~~of~~ a few days. Backward trajectory calculations and reanalysis CO data support the hypothesis that airmasses with enhanced aerosol signals originate in the ASM anticyclone and are transported over these sites in association with eastward shedding vortices. OMPS LP and CALIOP satellite data indicated that the 25°N–40°N region was not influenced by volcanic eruptions ~~and~~ or extensive biomass burning events during July–September 2018. Our results indicate that the enhanced aerosol particle levels measured at Tsukuba and Fukuoka are due to eastward shedding vortices of the ATAL from the ASM anticyclone; i.e., they originated from pollutants emitted from Asian countries and transported vertically by convection in the ASM region.

~~It is also noted that the "westward" extension of the ATAL to northern midlatitudes was reported by Khaykin et al. (2017), based on ground-based lidar at the Observatoire de Haute-Provence (OHP) in southern France (43.9°N, 5.7°E), with a layer of enhanced aerosol in the lower stratosphere with an average BSR value of 1.05 being a systematic feature during August–October. This aerosol layer was shown to correlate with the seasonal water-vapour maximum, suggesting the influx of convectively moistened air from the ASM anticyclone, whose influence on the extratropical lower stratosphere in late summer to early winter is well known (e.g., Vogel et al., 2014; Müller et al., 2016; Rolf et al., 2018).~~

The PDR values obtained at Tsukuba, i.e., ~5% (3%–10%), suggest that these enhanced particles are solid particles, rather than spherical, liquid H_2SO_4 particles (PDR ~0%) or cirrus ice particles (PDR > 25%–30%). A recent laboratory experiment by Wagner et al. (2020a) showed the PDR values of ~9.5% for solid NH_4NO_3 particles at 488 nm. (Also, Wagner et al. (2020b) showed electron microscope images of solid NH_4NO_3 particles, which are "of rather compact shape with aspect ratios predominantly in the range from 0.80 to 1.25.") ~~The~~ Thus, the ~~observed~~ values obtained with our lidars in Japan might~~ay~~ be consistent with those of solid NH_4NO_3 particles ~~recently~~ suggested by Höpfner et al. (2019). ~~There seem to have been no previous studies of lidar PDR values for solid NH_4NO_3 particles.~~ (Note that Sakai et al. (2010) investigated PDR values of other particle types at 532 nm in laboratory experiments; among these particles, sub-micrometre sea-salt and ammonium

sulphate crystals (e.g., Plate 9 (pages 237–239) of Pruppacher and Klett, 1997) were found to have PDR values of ~8% ~~PDR~~ and ~4% ~~PDR~~, respectively.) ~~Solid NH_4NO_3 particles may have similar PDR values as their crystal structures could be similar.~~ Small non-zero PDR values can occur if enhanced liquid H_2SO_4 particles and fresh ash particles from volcanic eruptions are mixed, although satellite data indicate this is less plausible (Sect. 3.3). ~~Lidar measurements at Mauna Loa, Hawaii, indicated no signals from volcanic eruptions during the summer of 2018 (Chouza et al., 2020). Also, at the OHP lidar site in France, any enhancement in the lower stratospheric aerosol abundance was observed during the summer of 2018.~~However, it should be noted that the lidar BSR and PDR measurements cannot exclude the possibility of co-existence of other types of solid aerosol particles such as mineral dust, black carbon, and some types of carbonaceous aerosols which are solid.

Lower-stratospheric aerosol enhancement over Japan was observed mainly during August–September, and seldom in July. This may be partly explained by the seasonality of the concentration of solid NH_4NO_3 particles in the ASM anticyclone (Höpfner et al., 2019), peaking in August with significant year-to-year variations. Furthermore, June and July are in the rainy season for most of Japan, in association with the "Baiu" frontal system (e.g., Ninomiya and Shibagaki, 2007). In July 2018, severe rainfall and flood events occurred early in the month (Shimpo et al., 2019), after which many parts of Japan experienced high surface temperatures with cumulonimbus clouds in several areas. Typhoons, synoptic low systems, and frontal systems affected Japan through to the end of September 2018, with these rainfall and thick-cloud events preventing the lidars from sensing the lower stratosphere, causing many of the missed-data slots in Fig. 1.

In summary, part of the ATAL in the ASM anticyclone airmass is transported eastward and passes over Japan in the UTLS. Lidars in Japan can observe the lower stratospheric portion of these aerosol particles if conditions permit, with summer-time active convection and various weather systems often preventing their sensing of the lower stratosphere. Volcanic eruptions and extensive wildfires may complicate the detection of particles of ATAL origin over Japan. The upper tropospheric portion of these particles is either depleted by tropospheric processes (convection and wet scavenging) or obscured by much stronger cirrus-cloud signals. Despite the limited sampling, the lidar detection of ATAL particles verifies eastward UTLS transport associated with sub-seasonal-scale dynamics of the ASM anticyclone, a process observed by satellite instruments and predicted by models. The spatial extent~~,~~ and chemical and aerosol content of this transport process ~~is~~are the main focus of an upcoming airborne field campaign, the Asian summer monsoon Chemical and Climate Impact Project (ACCLIP; Pan et al., 2019), which is scheduled to take place over the western Pacific during July–August 2021.

Appendix A

The time–height distribution of TDR at Tsukuba is shown in Figure A1, complementing Fig. 1b (PDR distribution).

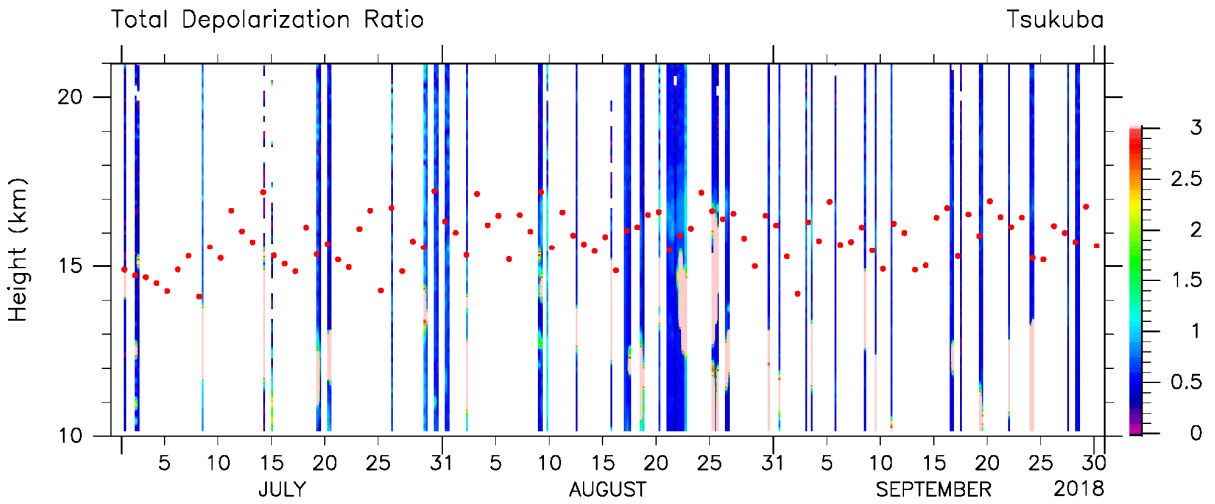

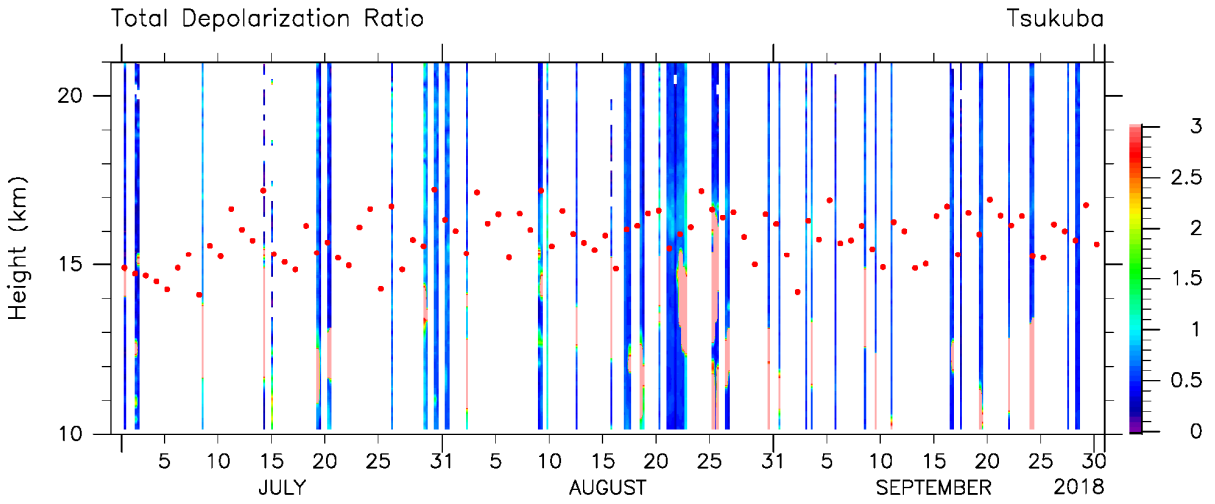

Figure A1 As for Fig. 1, but for the total depolarization ratio (TDR, %).

Data availability

Lidar data analysed in this study can be downloaded from the following websites: https://mri-2.mri-jma.go.jp/owncloud/s/GrNGNiGKzq8tjqH for Tsukuba; and https://www.cis.fukuoka-

u.ac.jp/~ksiraisi/LidarDataArchive/Fukuoka_2018summer.zip for Fukuoka. ERA5 and CAMS data can be downloaded from the Copernicus website, with the former from https://cds.climate.copernicus.eu and the latter from https://ads.atmosphere.copernicus.eu. MLS Version 4.2 Level 2 data can be downloaded from https://acdisc.gesdisc.eosdis.nasa.gov/data/Aura_MLS_Level2/. OMPS LP Level 2 Version 1.5 data can be downloaded from https://snpp-omps.gesdisc.eosdisc.eosdis.nasa.gov/data. CALIOP data can be downloaded from https://asdc.larc.nasa.gov/search.

Author contributions

MF, MS, and LLP designed the study. MF, T Sakai, and KS analysed lidar data and drafted the manuscript. YI calculated trajectories. MF and HX analysed CAMS data. SK and MF analysed MLS data. ~~and~~SK analysed OMPS LP data, while T Shibata analysed CALIOP data. All authors contributed to the interpretation, and reviewed and edited the manuscript.

Competing interests

The authors declare that they have no conflict of interest.

Acknowledgements

This study was financially supported by the research grant for Mission Research on Sustainable Humanosphere from Research Institute for Sustainable Humanosphere (RISH), Kyoto University, Japan, for the fiscal years 2019–2020. We thank the undergraduate students at Faculty of Science, Fukuoka University who operated the lidar system at Fukuoka. The GFD-DENNOU library was used for producing Figures 1–~~7~~ 8 and A1. We thank Nawo Eguchi and Suginori Iwasaki for valuable comments on draft manuscript. We also thank two anonymous reviewers and Michelle Santee for valuable comments and suggestions.

Financial support

This study was financially supported by the research grant for Mission Research on Sustainable Humanosphere from Research Institute for Sustainable Humanosphere (RISH), Kyoto University, Japan for the fiscal years 2019–2020.

References

Adachi, H., Shibata, T., Iwasaka, Y., and Fujiwara, M.: Calibration method for the lidar-observed stratospheric depolarization ratio in the presence of liquid aerosol particles, Appl. Opt., 40(36), 6587–6595, https://doi.org/10.1364/AO.40.006587, 2001.

Amemiya, A., and Sato, K.: A two-dimensional dynamical model for the subseasonal variability of the Asian monsoon anticyclone, J. Atmos. Sci., 75, 3597–3612, https://doi.org/10.1175/JAS-D-17-0208.1, 2018.

Bossolasco, A., Jegou, F., Sellitto, P., Berthet, G., Kloss, C., and Legras, B.: Global modelling studies of composition and decadal trends of the Asian Tropopause Aerosol Layer, Atmos. Chem. Phys. Discuss., https://doi.org/10.5194/acp-2020-677, in review, 2020.

Brunamonti, S., Jorge, T., Oelsner, P., Hanumanthu, S., Singh, B. B., Kumar, K. R., Sonbawne, S., Meier, S., Singh, D., Wienhold, F. G., Luo, B. P., Boettcher, M., Poltera, Y., Jauhiainen, H., Kayastha, R., Karmacharya, J., Dirksen, R., Naja, M., Rex, M., Fadnavis, S., and Peter, T.: Balloon-borne measurements of temperature, water vapor, ozone and aerosol backscatter on the southern slopes of the Himalayas during StratoClim 2016–2017, Atmos. Chem. Phys., 18, 15937–15957, https://doi.org/10.5194/acp-18-15937-2018, 2018.

Chen, Z., Bhartia, P. K., Loughman, R., Colarco, P., and DeLand, M.: Improvement of stratospheric aerosol extinction retrieval from OMPS/LP using a new aerosol model, Atmos. Meas. Tech., 11, 6495–6509, https://doi.org/10.5194/amt-11-6495-2018, 2018.

Chouza, F., Leblanc, T., Barnes, J., Brewer, M., Wang, P., and Koon, D.: Long-term (1999–2019) variability of stratospheric aerosol over Mauna Loa, Hawaii, as seen by two co-located lidars and satellite measurements, Atmos. Chem. Phys., 20, 6821–6839, https://doi.org/10.5194/acp-20-6821-2020, 2020.

Davis, S. M., Hegglin, M. I., Fujiwara, M., Dragani, R., Harada, Y., Kobayashi, C., Long, C., Manney, G. L., Nash, E. R., Potter, G. L., Tegtmeier, S., Wang, T., Wargan, K., and Wright, J. S.: Assessment of upper tropospheric and stratospheric water vapor and ozone in reanalyses as part of S-RIP, Atmos. Chem. Phys., 17, 12743–12778, https://doi.org/10.5194/acp-17-12743-2017, 2017.

Enomoto, T., Hoskins, B. J., and Matsuda, Y.: The formation mechanism of the Bonin high in August. Quart. J. Roy. Meteorol. Soc., 129, 157–178, https://doi.org/10.1256/qj.01.211, 2003.

Fadnavis, S., Roy, C., Chattopadhyay, R., Sioris, C. E., Rap, A., Müller, R., Kumar, K. R., and Krishnan, R.: Transport of trace gases via eddy shedding from the Asian summer monsoon anticyclone and associated impacts on ozone heating rates, Atmos. Chem. Phys., 18, 11493–11506, https://doi.org/10.5194/acp-18-11493-2018, 2018.

Fujiwara, M., Iwasaki, S., Shimizu, A., Inai, Y., Shiotani, M., Hasebe, F., Matsui, I., Sugimoto, N., Okamoto, H., Nishi, N., Hamada, A., Sakazaki, T., and Yoneyama, K.: Cirrus observations in the tropical tropopause layer over the western Pacific, J. Geophys. Res., 114(D9), D09304, https://doi.org/10.1029/2008JD011040, 2009.

Fujiwara, M., Vömel, H., Hasebe, F., Shiotani, M., Ogino, S.-Y., Iwasaki, S., Nishi, N., Shibata, T., Shimizu, K., Nishimoto, E., Valverde-Canossa, J. M., Selkirk, H. B., and Oltmans, S. J.: Seasonal to decadal variations of water vapor in the tropical

lower stratosphere observed with balloon-borne cryogenic frostpoint hygrometers, J. Geophys. Res., 115, D18304, https://doi.org/10.1029/2010JD014179, 2010.

Garny, H., and Randel, W. J.: Dynamic variability of the Asian monsoon anticyclone observed in potential vorticity and correlations with tracer distributions, J. Geophys. Res. Atmos., 118, 13,421–13,433, https://doi.org/10.1002/2013JD020908, 2013.

GVP (Global Volcanism Program): Volcanoes of the World, v. 4.9.0 (04 Jun 2020), Venzke, E (ed.), Smithsonian Institution, https://doi.org/10.5479/si.GVP.VOTW4-2013, 2013 (last accessed: 3 July 2020).

GVP (Global Volcanism Program): Report on Ambae (Vanuatu) (Crafford, A.E., and Venzke, E., eds.), Bulletin of the Global Volcanism Network, 43:7, Smithsonian Institution, https://doi.org/10.5479/si.GVP.BGVN201807-257030, 2018 (last accessed: 4 July 2020).

GVP (Global Volcanism Program): Report on Ambae (Vanuatu) (Krippner, J.B., and Venzke, E., eds.), Bulletin of the Global Volcanism Network, 44:2, Smithsonian Institution, https://doi.org/10.5479/si.GVP.BGVN201902-257030, 2019 (last accessed: 4 July 2020).

Haarig, M., Ansmann, A., Baars, H., Jimenez, C., Veselovskii, I., Engelmann, R., and Althausen, D.: Depolarization and lidar ratios at 355, 532, and 1064 nm and microphysical properties of aged tropospheric and stratospheric Canadian wildfire smoke, Atmos. Chem. Phys., 18, 11847–11861, https://doi.org/10.5194/acp-18-11847-2018, 2018.

Hanumanthu, S., Vogel, B., Müller, R., Brunamonti, S., Fadnavis, S., Li, D., Ölsner, P., Naja, M., Singh, B. B., Kumar, K. R., Sonbawne, S., Jauhiainen, H., Vömel, H., Luo, B., Jorge, T., Wienhold, F. G., Dirkson, R., and Peter, T.: Strong day-to-day variability of the Asian Tropopause Aerosol Layer (ATAL) in August 2016 at the Himalayan foothills, Atmos. Chem. Phys., 20, 14273–14302, https://doi.org/10.5194/acp-20-14273-2020, 2020.~~Hanumanthu, S., Vogel, B., Müller, R., Brunamonti, S., Fadnavis, S., Li, D., Ölsner, P., Naja, M., Singh, B. B., Kumar, K. R., Sonbawne, S., Jauhiainen, H., Vömel, H., Luo, B., Jorge, T., Wienhold, F. G., Dirkson, R., and Peter, T.: Strong variability of the Asian Tropopause Aerosol Layer (ATAL) in August 2016 at the Himalayan foothills, Atmos. Chem. Phys. Discuss., https://doi.org/10.5194/acp-2020-552, in review, 2020.~~

Hersbach, H., Bell, B., Berrisford, P., Hirahara, S., Horányi, A., Muñoz-Sabater, J., Nicolas, J., Peubey, C., Radu, R., Schepers, D., Simmons, A., Soci, C., Abdalla, S., Abellan, X., Balsamo, G., Bechtold, P., Biavati, G., Bidlot, J., Bonavita, M., Chiara, G., Dahlgren, P., Dee, D., Diamantakis, M., Dragani, R., Flemming, J., Forbes, R., Fuentes, M., Geer, A., Haimberger, L., Healy, S., Hogan, R. J., Hólm, E., Janisková, M., Keeley, S., Laloyaux, P., Lopez, P., Lupu, C., Radnoti, G., Rosnay, P., Rozum, I., Vamborg, F., Villaume, S., and Thépaut, J.: The ERA5 global reanalysis, Quart. J. Royal Meteorol. Soc., ~~in press~~146, 1999–2049, https://doi.org/10.1002/qj.3803, 2020.

Hoffmann, L., Günther, G., Li, D., Stein, O., Wu, X., Griessbach, S., Heng, Y., Konopka, P., Müller, R., Vogel, B., and Wright, J. S.: From ERA-Interim to ERA5: the considerable impact of ECMWF's next-generation reanalysis on Lagrangian transport simulations, Atmos. Chem. Phys., 19, 3097–3124, https://doi.org/10.5194/acp-19-3097-2019, 2019.

Honomichl, S. B., and Pan, L. L.: Transport from the Asian summer monsoon anticyclone over the western Pacific, J. Geophys. Res. Atmos., 125, e2019JD032094~~in press~~, https://doi.org/10.1029/2019JD032094, 2020.

Höpfner, M., Ungermann, J., Borrmann, S., Wagner, R., Spang, R., Riese, M., Stiller, G., Appel, O., Batenburg, A. M., Bucci, S., Cairo, F., Dragoneas, A., Friedl-Vallon, F., Hünig, A., Johansson, S., Krasauskas, L., Legras, B., Leisner, T., Mahnke, C., Möhler, O., Molleker, S., Müller, R., Neubert, T., Orphal, J., Preusse, P., Rex, M., Saathoff, H., Stroh, F., Weigel, R., and Wohltmann, I.: Ammonium nitrate particles formed in upper troposphere from ground ammonia sources during Asian monsoons, Nat. Geosci., 12(8), 608–612, https://doi.org/10.1038/s41561-019-0385-8, 2019.

Hurst, D. F., Read, W. G., Vömel, H., Selkirk, H. B., Rosenlof, K. H., Davis, S. M., Hall, E. G., Jordan, A. F., and Oltmans, S. J.: Recent divergences in stratospheric water vapor measurements by frost point hygrometers and the Aura Microwave Limb Sounder, Atmos. Meas. Tech., 9, 4447–4457, https://doi.org/10.5194/amt-9-4447-2016, 2016.

Inai, Y.: Long-term variation in the mixing fraction of tropospheric and stratospheric air masses in the upper tropical tropopause layer, J. Geophys. Res. Atmos., 123, 4890–4909, https://doi.org/10.1029/2018JD028300, 2018.

Inai, Y., Aoki, S., Honda, H., Furutani, H., Matsumi, Y., Ouchi, M., Sugawara, S., Hasebe, F., Uematsu, M., and Fujiwara, M.: Balloon-borne tropospheric CO_2 observations over the equatorial eastern and western Pacific, Atmos. Environ., 184, 24–36, https://doi.org/10.1016/j.atmosenv.2018.04.016, 2018.

Inness, A., Ades, M., Agustí-Panareda, A., Barré, J., Benedictow, A., Blechschmidt, A.-M., Dominguez, J. J., Engelen, R., Eskes, H., Flemming, J., Huijnen, V., Jones, L., Kipling, Z., Massart, S., Parrington, M., Peuch, V.-H., Razinger, M., Remy, S., Schulz, M., and Suttie, M.: The CAMS reanalysis of atmospheric composition, Atmos. Chem. Phys., 19, 3515–3556, https://doi.org/10.5194/acp-19-3515-2019, 2019.

Jäger, H., and Hofmann, D.: Midlatitude lidar backscatter to mass, area, and extinction conversion model based on in situ aerosol measurements from 1980 to 1987, Appl. Opt., 30(1), 127, https://doi.org/10.1364/ao.30.000127, 1991.

Jäger, H., Deshler, T., and Hofmann, D. J.: Midlatitude lidar backscatter conversions based on balloonborne aerosol measurements, Geophys. Res. Lett., 22(13), 1729–1732, https://doi.org/10.1029/95GL01521, 1995.

Khaykin, S. M., Godin-Beekmann, S., Keckhut, P., Hauchecorne, A., Jumelet, J., Vernier, J.-P., Bourassa, A., Degenstein, D. A., Rieger, L. A., Bingen, C., Vanhellemont, F., Robert, C., DeLand, M., and Bhartia, P. K.: Variability and evolution of the midlatitude stratospheric aerosol budget from 22 years of ground-based lidar and satellite observations, Atmos. Chem. Phys., 17, 1829–1845, https://doi.org/10.5194/acp-17-1829-2017, 2017.

Khaykin, S. M., Godin-Beekmann, S., Hauchecorne, A., Pelon, J., Ravetta, F., and Keckhut, P.: Stratospheric smoke with unprecedentedly high backscatter observed by lidars above southern France, Geophys. Res. Lett., 45(3), 1639–1646, https://doi.org/10.1002/2017GL076763, 2018.

Kim, M.-H., Omar, A. H., Tackett, J. L., Vaughan, M. A., Winker, D. M., Trepte, C. R., Hu, Y., Liu, Z., Poole, L. R., Pitts, M. C., Kar, J., and Magill, B. E.: The CALIPSO version 4 automated aerosol classification and lidar ratio selection algorithm, Atmos. Meas. Tech., 11, 6107–6135, https://doi.org/10.5194/amt-11-6107-2018, 2018.

Li, D., Vogel, B., Müller, R., Bian, J., Günther, G., Ploeger, F., Li, Q., Zhang, J., Bai, Z., Vömel, H., and Riese, M.: Dehydration and low ozone in the tropopause layer over the Asian monsoon caused by tropical cyclones: Lagrangian transport calculations using ERA-Interim and ERA5 reanalysis data, Atmos. Chem. Phys., 20, 4133–4152, https://doi.org/10.5194/acp-20-4133-2020, 2020.

Livesey, N. J., Read, W. G., Wagner, P. A., Froidevaux, L., Lambert, A., Manney, G. L., Millán Valle, L. F., Pumphrey, H. C., Santee, M. L., Schwartz, M. J., Wang, S., Fuller, R. A., Jarnot, R. F., Knosp, B. W., Martinez, E., and Lay, R. R.: Aura Microwave Limb Sounder (MLS) Version 4.2x Level 2 and 3 data quality and description document, Tech. Rep. JPL D-33509 Rev. E, 2020, available at: https://mls.jpl.nasa.gov/ (last accessed: 26 August 2020).

Luo, J., Pan, L. L., Honomichl, S. B., Bergman, J. W., Randel, W. J., Francis, G., Clerbaux, C., George, M., Liu, X., and Tian, W.: Space–time variability in UTLS chemical distribution in the Asian summer monsoon viewed by limb and nadir satellite sensors, Atmos. Chem. Phys., 18, 12511–12530, https://doi.org/10.5194/acp-18-12511-2018, 2018.

Müller, S., Hoor, P., Bozem, H., Gute, E., Vogel, B., Zahn, A., Bönisch, H., Keber, T., Krämer, M., Rolf, C., Riese, M., Schlager, H., and Engel, A.: Impact of the Asian monsoon on the extratropical lower stratosphere: trace gas observations during TACTS over Europe 2012, Atmos. Chem. Phys., 16, 10573–10589, https://doi.org/10.5194/acp-16-10573-2016, 2016.

Ninomiya, K., and Shibagaki, Y.: Multi-scale features of the Meiyu-Baiu front and associated precipitation systems, J. Meteorol. Soc. Japan, 85B, 103–122, https://doi.org/10.2151/jmsj.85B.103, 2007.

Noel, V., Chepfer, H., Hoareau, C., Reverdy, M., and Cesana, G.: Effects of solar activity on noise in CALIOP profiles above the South Atlantic Anomaly, Atmos. Meas. Tech., 7, 1597–1603, https://doi.org/10.5194/amt-7-1597-2014, 2014.

Pan, L. L., Honomichl, S. B., Kinnison, D. E., Abalos, M., Randel, W. J., Bergman, J. W., and Bian, J.: Transport of chemical tracers from the boundary layer to stratosphere associated with the dynamics of the Asian summer monsoon, J. Geophys. Res. Atmos., 121, 14,159–14,174, https://doi.org/10.1002/2016JD025616, 2016.

Pan, L., Kinnison, D., Liang, Q., Atlas, E., Bresch, J. Case, P., Fujiwara, M., Honomichl, S., Lait, L., Newman, P., Nishi, N., Randel, B., Smith, R., Tilmes, S., and Toon, B.: Progress in the Asian summer monsoon Chemical and Climate Impact Project (ACCLIP), presented at the AGU Fall Meeting 2019, American Geophysical Union, San Francisco, CA, USA, Abstract No. A51K-2788, https://agu.confex.com/agu/fm19/meetingapp.cgi/Paper/543867, 2019 (last accessed: 11 October 2020). (Poster pdf available at http://n2t.net/ark:/85065/d7m3301b, last accessed: 11 October 2020.)

Peterson, D. A., Campbell, J. R., Hyer, E. J., Fromm, M. D., Kablick, G. P., III, Cossuth, J. H., and DeLand, M. T.: Wildfire-driven thunderstorms cause a volcano-like stratospheric injection of smoke, npj Clim. Atmos. Sci., 1(1), https://doi.org/10.1038/s41612-018-0039-3, 2018.

Ploeger, F., Gottschling, C., Griessbach, S., Grooß, J.-U., Guenther, G., Konopka, P., Müller, R., Riese, M., Stroh, F., Tao, M., Ungermann, J., Vogel, B., and von Hobe, M.: A potential vorticity-based determination of the transport barrier in the Asian summer monsoon anticyclone, Atmos. Chem. Phys., 15, 13145–13159, https://doi.org/10.5194/acp-15-13145-2015, 2015.

Popovic, J. M., and Plumb, R. A.: Eddy shedding from the upper-tropospheric Asian monsoon anticyclone, J. Atmos. Sci., 58, 93–104, https://doi.org/10.1175/1520-0469(2001)058<0093:ESFTUT>2.0.CO;2, 2001.

Prata, A. T., Young, S. A., Siems, S. T., and Manton, M. J.: Lidar ratios of stratospheric volcanic ash and sulfate aerosols retrieved from CALIOP measurements, Atmos. Chem. Phys., 17, 8599–8618, https://doi.org/10.5194/acp-17-8599-2017, 2017.

Pruppacher, H. R., and Klett, J. D.: Microphysics and Clouds and Precipitation, Second Revised and Enlarged Edition, Kluwer Academic Pub., Dordrecht, 954 pp., 1996.

Randel, W. J., Park, M., Emmons, L., Kinnison, D., Bernath, P., Walker, K. A., Boone, C., and Pumphrey, H.: Asian monsoon transport of pollution to the stratosphere, Science, 328 (5978), 611–613, https://doi.org/10.1126/science.1182274, 2010.

Randel, W. J., Zhang, K., and Fu, R.: What controls stratospheric water vapor in the NH summer monsoon regions?, J. Geophys. Res. Atmos., 120, 7988–8001, https://doi.org/10.1002/2015JD023622, 2015.

Robock, A.: Volcanic eruptions and climate, Rev. Geophys., 38, 191–219, https://doi.org/10.1029/1998RG000054, 2000.

Rolf, C., Vogel, B., Hoor, P., Afchine, A., Günther, G., Krämer, M., Müller, R., Müller, S., Spelten, N., and Riese, M.: Water vapor increase in the lower stratosphere of the Northern Hemisphere due to the Asian monsoon anticyclone observed during the TACTS/ESMVal campaigns, Atmos. Chem. Phys., 18, 2973–2983, https://doi.org/10.5194/acp-18-2973-2018, 2018.

Russell, P. B., Swissler, T. J., and McCormick, M. P.: Methodology for error analysis and simulation of lidar aerosol measurements, Appl. Opt., 18(22), 3783, https://doi.org/10.1364/ao.18.003783, 1979.

Russell, P. B., Morley, B. M., Livingston, J. M., Grams, G. W., and Patterson, E. M.: Orbiting lidar simulations 1: Aerosol and cloud measurements by an independent-wavelength technique, Appl. Opt. 21(9), 1541, https://doi.org/10.1364/ao.21.001541, 1982.

Sakai, T., Nagai, T., Nakazato, M., Mano, Y., and Matsumura, T.: Ice clouds and Asian dust studied with lidar measurements of particle extinction-to-backscatter ratio, particle depolarization, and water-vapor mixing ratio over Tsukuba, Appl. Opt., 42, 7103-7116, https://doi.org/10.1364/AO.42.007103, 2003.

Sakai, T., Nagai, T., Zaizen, Y., and Mano, Y.: Backscattering linear depolarization ratio measurements of mineral, sea-salt, and ammonium sulfate particles simulated in a laboratory chamber, Appl. Opt., 49(23), 4441–4449, https://doi.org/10.1364/AO.49.004441, 2010.

Sakai, T., Uchino, O., Nagai, T., Liley, B., Morino, I., and Fujimoto, T.: Long-term variation of stratospheric aerosols observed with lidars over Tsukuba, Japan, from 1982 and Lauder, New Zealand, from 1992 to 2015, J. Geophys. Res. Atmos., 121, 10,283–10,293, https://doi.org/10.1002/2016JD025132, 2016.

Salby, M. L.: Fundamentals of Atmospheric Physics, Elsevier, 1996.

Santee, M. L., Manney, G. L., Livesey, N. J., Schwartz, M. J., Neu, J. L., and Read, W. G.: A comprehensive overview of the climatological composition of the Asian summer monsoon anticyclone based on 10 years of Aura Microwave Limb Sounder measurements, J. Geophys. Res. Atmos., 122, 5491–5514, https://doi.org/10.1002/2016JD026408, 2017.

Shimpo, A., Takemura, K., Wakamatsu, S., Togawa, H., Mochizuki, Y., Takekawa, M., Tanaka, S., Yamashita, K., Maeda, S., Kurora, R., Murai, H., Kitabatake, N., Tsuguti, H., Mukougawa, H., Iwasaki, T., Kawamura, R., Kimoto, M., Takayabu, I., Takayabu, Y.N., Tanimoto, Y., Hirooka, T., Masumoto, Y., Watanabe, M., Tsuboki, K., and Nakamura, H.: Primary Factors behind the Heavy Rain Event of July 2018 and the subsequent heat wave in Japan, Sci. Online Lett. Atmos., 15A, 13–18, https://doi.org/10.2151/sola.15A-003, 2019.

Tegtmeier, S., Anstey, J., Davis, S., Dragani, R., Harada, Y., Ivanciu, I., Pilch Kedzierski, R., Krüger, K., Legras, B., Long, C., Wang, J. S., Wargan, K., and Wright, J. S.: Temperature and tropopause characteristics from reanalyses data in the tropical tropopause layer, Atmos. Chem. Phys., 20, 753–770, https://doi.org/10.5194/acp-20-753-2020, 2020.

Thomason, L. W., Pitts, M. C., and Winker, D. M.: CALIPSO observations of stratospheric aerosols: a preliminary assessment, Atmos. Chem. Phys., 7, 5283–5290, https://doi.org/10.5194/acp-7-5283-2007, 2007.

Uchino, O., Nagai, T., Fujimoto, T., Fujiwara, M., Akiyoshi, H., Yasumatsu, S., Hayashida, S., Sasano, Y., Nakane, H., Iwasaka, Y., Hase, M., Shibata, T., Itabe, T., Asai, K., Nomura, A., Saito, Y., Kano, T., Sai, Y., Tamaki, K., Nomura, R., Sunagawa, T., Nagasawa, C., Abo, M., Idesako, Y., and Kai, K.: Observation of the Pinatubo volcanic cloud by lidar network in Japan, J. Meteorol. Soc. Jpn., 71, 285–296, https://doi.org/10.2151/jmsj1965.71.2_285, 1993.

Ungermann, J., Ern, M., Kaufmann, M., Müller, R., Spang, R., Ploeger, F., Vogel, B., and Riese, M.: Observations of PAN and its confinement in the Asian summer monsoon anticyclone in high spatial resolution, Atmos. Chem. Phys., 16, 8389–8403, https://doi.org/10.5194/acp-16-8389-2016, 2016.

Vernier, J.-P., Fairlie, T. D., Natarajan, M., Wienhold, F. G., Bian, J., Martinsson, B. G., Crumeyrolle, S., Thomason, L. W., and Bedka, K. M.: Increase in upper tropospheric and lower stratospheric aerosol levels and its potential connection with Asian pollution, J. Geophys. Res. Atmos., 120, 1608–1619, https://doi.org/10.1002/2014JD022372, 2015.

Vernier, J.-P., Fairlie, T. D., Deshler, T., Venkat Ratnam, M., Gadhavi, H., Kumar, B. S., Natarajan, M., Pandit, A. K., Akhil Raj, S. T., Hemanth Kumar, A., Jayaraman, A., Singh, A. K., Rastogi, N., Sinha, P. R., Kumar, S., Tiwari, S., Wegner, T., Baker, N., Vignelles, D., Stenchikov, G., Shevchenko, I., Smith, J., Bedka, K., Kesarkar, A., Singh, V., Bhate, J., Ravikiran, V., Durga Rao, M., Ravindrababu, S., Patel, A., Vernier, H., Wienhold, F. G., Liu, H., Knepp, T. N., Thomason, L., Crawford, J., Ziemba, L., Moore, J., Crumeyrolle, S., Williamson, M., Berthet, G., Jégou, F., and Renard, J.-B.: BATAL: The Balloon measurement campaigns of the Asian Tropopause Aerosol Layer, Bull. Amer. Meteorol. Soc., 99(5), 955–973, 2018.

Vogel, B., Günther, G., Müller, R., Grooß, J.-U., Hoor, P., Krämer, M., Müller, S., Zahn, A., and Riese, M.: Fast transport from Southeast Asia boundary layer sources to northern Europe: rapid uplift in typhoons and eastward eddy shedding of the Asian monsoon anticyclone, Atmos. Chem. Phys., 14, 12745–12762, https://doi.org/10.5194/acp-14-12745-2014, 2014.

Vogel, B., Günther, G., Müller, R., Grooß, J.-U., Afchine, A., Bozem, H., Hoor, P., Krämer, M., Müller, S., Riese, M., Rolf, C., Spelten, N., Stiller, G. P., Ungermann, J., and Zahn, A.: Long-range transport pathways of tropospheric source gases originating in Asia into the northern lower stratosphere during the Asian monsoon season 2012, Atmos. Chem. Phys., 16, 15301–15325, https://doi.org/10.5194/acp-16-15301-2016, 2016.

Vömel, H., Barnes, J. E., Forno, R. N., Fujiwara, M., Hasebe, F., Iwasaki, S., Kivi, R., Komala, N., Kyrö, E., Leblanc, T., Morel, B., Ogino, S.-Y., Read, W. G., Ryan, S. C., Saraspriya, S., Selkirk, H., Shiotani, M., Valverde Canossa, J., and Whiteman, D. N.: Validation of Aura MLS water vapor by balloonborne Cryogenic Frostpoint Hygrometer measurements, J. Geophys. Res., 112, D24S37, https://doi.org/10.1029/2007JD008698, 2007.

Wagner, R., Bertozzi, B., Höpfner, M., Höhler, K., Möhler, O., Saathoff, H., and Leisner, T.: Solid ammonium nitrate aerosols as efficient ice nucleating particles at cirrus temperatures, J. Geophys. Res. Atmos., 125, e2019JD032248, https://doi.org/10.1029/2019JD032248, 2020a.

Wagner, R., Testa, B., Höpfner, M., Kiselev, A., Möhler, O., Saathoff, H., Ungermann, J., and Leisner, T.: High-resolution optical constants of crystalline ammonium nitrate for infrared remote sensing of the Asian Tropopause Aerosol Layer, Atmos. Meas. Tech. Discuss., https://doi.org/10.5194/amt-2020-262, in review, 2020b.

Winker, D. M., Hunt, W. H., and McGill, M. J.: Initial performance assessment of CALIOP, Geophys. Res.Lett., 34(19), L19803, https://doi.org/10.1029/2007GL030135, 2007.

Winker, D. M., Pelon, J., Coakley, J. A., Jr., Ackerman, S. A., Charlson, R. J., Colarco, P. R., Flamant, P., Fu, Q., Hoff, R. M., Kittaka, C., Kubar, T. L., Le Treut, H., Mccormick, M. P., Mégie, G., Poole, L., Powell, K., Trepte, C., Vaughan, M. A., and Wielicki, B. A.: The CALIPSO mission: A global 3D view of aerosols and clouds, Bull. Amer. Meteorol. Soc., 91(9), 1211–1230, https://doi.org/10.1175/2010BAMS3009.1, 2010.

Yasui, M., Fujiwara, M., Akiyoshi, H., Ikawa, S., Nonaka, H., Shiraishi, K.: Seasonal variation of Pinatubo volcanic aerosols in the stratosphere observed by lidar in Fukuoka, J. Geomag. Geoelectr., 47, 989-998, https://doi.org/10.5636/jgg.47.989, 1995.

Yasui, M, Fujiwara, M., Shibata, T., Akiyoshi, H., Ikawa, S., Shiraishi, K., Nonaka, H.: Variations of volcanic aerosols observed in Fukuoka - A comparison of Mt El Chichon and Mt Pinatubo events, J. Geomag., Geoelectr., 48, 403-413, https://doi.org/10.5636/jgg.48.403, 1996.

Young, S. A., and Vaughan, M. A.: The retrieval of profiles of particulate extinction from Cloud-Aerosol Lidar Infrared Pathfinder Satellite Observations (CALIPSO) data: Algorithm description, J. Atmos. Oceanic Technol., 26 (6), 1105–1119, https://doi.org/10.1175/2008jtecha1221.1, 2009.